Design of a Pultrusion Die

Using a Design Optimization Technique

by

Teck Wah Awa

Thesis submitted to the Faculty of the

Virginia Polytechnic Institute and State University

in partial fulfillment of the requirements for the degree of

Master of Science

in

Mechanical Engineering

APPROVED:

Dr. Robert L. West, Chairman

Dr. Douglas J. Nelson

Dr. Curtis H. Stern

Dr. Brian Vick

February, 1991

Blacksburg, Virginia

Design of a Pultrusion Die

Using a Design Optimization Technique

by

Teck Wah Awa

Dr. Robert L. West, Chairman

Mechanical Engineering

(ABSTRACT)

The objective of this study is to design a pultrusion die with a desired temperature profile. Design optimization programs were developed to synthesize the number of cartridge heaters, power input and location of each cartridge heater for a laboratory-scale pultrusion die. This is the first step in developing a pultrusion control process. Before this can be done, a thorough understanding of the pultrusion process is required. The parameters investigated are fiber-resin mixture, degree of curing, production temperature profile and pulling speed. It was found that these parameters are interrelated.

For the pultrusion process, the die itself is the main component and is a curing reactor. Therefore, the production temperature profile was chosen to be the main parameter under study. The remaining parameters can be functionally related to the production temperature profile which then determines the mechanical properties of the material. The design optimization problem is narrowed down to determining the optimum heating configuration to produce the desired production temperature profile. A 2-D steady-state conduction heat transfer model was developed for a laboratory-scale pultrusion die. Two numerical solution methods were investigated, the finite difference and boundary element methods. Both methods successfully simulate the production temperature profile. The boundary element method was found to be more appropriate due to its flexibility and was chosen as the heat transfer analysis tool incorporated into the design optimization program. Two configurations of the die were investigated, a two-side-insulated and four-side-insulated model. This will provide a way of studying the power requirements for the die.

The die design methodology was formulated around a nonlinear programming technique to minimize the sum of square error between the desired and synthesized temperature profiles. The design variables were the number of cartridge heaters, power input and location of each cartridge heater along the length of the die. There are several design constraints imposed on the design problem to eliminate the overlapping and over crossing of the successive heater locations. The design optimization programs successfully synthesized the number of cartridge heaters, power input and location of each cartridge heater for the laboratory-scale pultrusion die. With a four-side-insulated model, the power consumption was reduced by a factor of 2 to 3 times the power required with a two-side-insulated die.

Acknowledgements

The deepest appreciation is due to the author's major professor, Dr. R. L. West for his valuable guidance and encouragement in dealing with problems during the past two years. Sincere appreciation is extended to Promatec Inc., especially to Dr. H. L. Price for supporting the study, both financially and technically. Many thanks to Dr. D. J. Nelson, Dr. C. H. Stern and Dr. B. Vick for serving on the graduate committee and for their respected reviews and consultations. The author is thankful to Mr. Jeffrey C. Collie for his previous work in developing the initial model. And finally, special thanks to all those who supported the author physically and spiritually throughout the graduate study.

The author is dedicating this thesis to his mother, for her love and support.

Table of Contents

List of Illustrations

List of Tables

Chapter I. Pultrusion Process

1.1. Introduction

Pultrusion is a continuous manufacturing technique for producing reinforced fiber composite materials with constant cross section profiles. In pultrusion, fiber is pulled through a resin bath and a heated die. The die itself is a shaping mold and a curing reactor. The temperature along the die is usually not constant, resulting in a temperature gradient. Generally, the temperature profiles are generated to obtain a desired curing. Due to the heat transfer from the die and the thermosetting resin, curing is initiated which causes the liquified resin to gel and solidify. The heat is usually provided by heater platens. The end product of this pultrusion process is a transformation of low strength fiber-resin mixture into a high strength and continuous solid composite material. Figure 1 shows a sketch of a typical pultrusion die.

The knowledge of the mechanics and chemical processes taking place in the pultrusion die is important in the development of a pultrusion process. This is especially true when using a thermosetting resin such as epoxy. The most important factor throughout the process is the production temperature profile. The reaction of a thermosetting resin is time dependent, and both

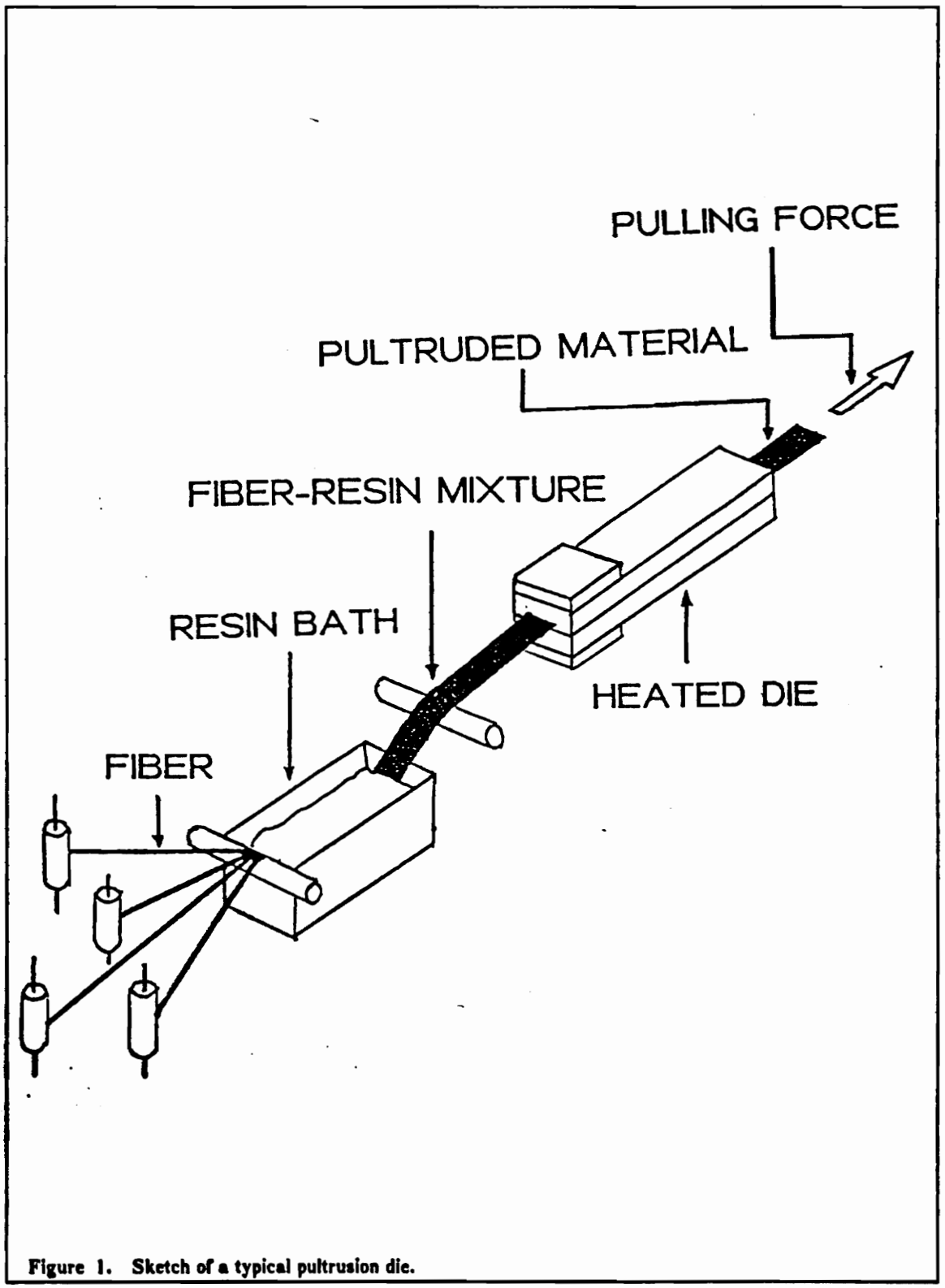

Figure 1. Sketch of a typical pultrusion die.

endothermic before the curing is initiated and exothermic. Therefore, the rate and the amount of heat added to and removed from the die is important. If not enough heat is added, the required exothermic temperature for the fiber-resin mixture cannot be reached. As a result, the pultruded materials are insufficiently cured and less desirable composite properties will be obtained. Conversely, if too much heat is added, thermal stress cracking will occur as the fiber-resin mixture cools. To ensure a solidified composite material, the curing process must take place for some minimum time and temperature before the fiber-resin mixture exits from the die. These factors will eventually determine the pulling speed required for a particular die's length and heating configuration.

In the epoxy pultrusion process, the production rate is determined by the pulling speed. The production rates for this type of continuous pultrusion process typically range from 1 inch per minute to 15 feet per minute. However, the more realistic rates are from 2 to 4 feet per minute [1]. In turn, the pulling speed is closely related to the pulling force. The pulling force is critical and restricted by the generation of large shear forces which will resist the fiber-resin motion and possibly lead to profile destruction due to resin adhered to the die wall.

A typical pultrusion control system should be able to be programmed to produce mechanical properties to within some prescribed margin of the desired composite properties. The desired composite properties such as specific gravity and hardness depend on the degree of curing, pulling speed, fiber-resin mixture formula and production temperature profile. These parameters are coupled to each other. A fundamental understanding of these interrelationships is required before a control process can be implemented on a selective pultrusion die.

1.2. Literature Review

Literature on the pultrusion process in the public domain is scarce. The pultrusion technique can be considered new and most of the developments are based on trial and error experimentation. This is mainly due to the lack of understanding of the process. Only recently have researchers in the pultrusion industries shown an interest in developing a fundamental understanding of the process.

1.2.1. Pultrusion History and Development

In 1951, the first patent was issued strictly for pultrusion. The early pultrusion processes produced simple geometries with minimum cross sections of round, square and rectangular sections. As the pultrusion technologies improved, the shape of the pultruded products became more complex such as I-beams, channels and tubes. The use of pultruded products is not restricted to the aerospace and automobile industries. Pultrusion products are penetrating almost every industry, especially the sporting industry.

Since pultrusion is a continuous manufacturing process, a long production with uniform shape up to 5000 feet or more can readily be produced. Contrarily, variable properties can also be obtained by varying the fiber orientations entering the die or varying the conditions in the intermediate steps of the pultrusion process. Because pultrusion is a continuous process, pultruded products usually have higher strength than those produced by extrusion. Developments in the pultrusion industry are in the direction of incorporating the latest reinforced fibers and newest resin formulations. The most commonly used materials for pultrusion are fiberglass and thermosetting polyester resins. High strength materials that require corrosion resistance, electrical resistance, and lightspaceweight can be produced by the pultrusion process especially with polyester resins.

1.2.2. Characteristics of the Pultrusion Process

Work on development of a new method of characterizing the pultrusion process can be found in Sumerak [2]. He measured the internal pressure, pulling force, internal product surface temperature, mold temperature profile, internal product exotherm, viscosity and line speed of a pultrusion process. His results show that as the resin heated up, the viscosity decreased and the internal pressure increased. The resin used in Sumerak's experiment was a styrene monomer. From the same experiment, he also observed that at the same pulling rate, the pulling force was reduced and suggested that a different coefficient of friction resulted for heated and unheated fiber-resin mixture. As the fiber began to cure, the reverse process took place. The internal pressure decreased and the viscosity increased, causing the pulling force to increase. Sumerak also measured the temperature profile of an non-thermosetting resin to eliminate the effect of heat transfer to the fiber from the exothermic reaction of the resin. The temperature of the fiber-resin mixture never reached the die temperature before exiting the die. With the thermosetting resin, the temperature of the mixture was above the die temperature as a result of the exothermic reaction, but the temperature dropped to the die temperature as the fiber exited the die. For both non-thermosetting and thermosetting resins, the entry temperature of the fiber-resin mixture was always below the die temperature. This lower entry temperature slowed down the curing rate. The idea of preheating the fiber-resin mixture before it entered the die was tested out by researchers in the 1950s' [3].

A preheating technique using radio-frequencies (RF) was developed to speed up the curing process especially with products having a larger cross-section [3]. However, there is a limitation on the pultrusion speed with this method. If the pultrusion rate is too slow, the pultruded products show internal thermo-cracking due to excess exothermic reaction. Conversely, if the pultrusion rate is too fast, external cracking results from not enough curing. McQuarrie [3] eliminated this problem by inventing a high-speed pultrusion process using polyester resins. The most commonly used thermosetting resins today are polyester resins, which comprise 85 to 90 % of the pultrusion product. The remaining pultrusion products are derived from epoxy resin. For this process,

McQuarrie was awarded a patent for the process which produces smoother surfaces without internal or external cracking in a shorter period of time.

Price and Cupschalk [4] performed some experimental work on the pulling force in the pultrusion process. Their study showed that the pulling force was affected by the volume of the fiber-resin mixture, die temperature and pulling speed. Their work was conducted on a laboratory-scale pultrusion die using carbon fiber preinpregnated tape with an epoxy resin.

1.2.3. Pultrusion Process Modeling

Tulig [5] developed a model for the heat transfer and chemical reaction occurring in a pultrusion die. His model was successful in predicting the temperature distribution and degree of resin cure through the die for a certain set of fiber-resin properties. The mathematical model was compared with a simple experimental technique for measuring the temperature distribution for both thermosetting epoxy resin and non-thermosetting models. Tulig's formulation was based on an assumption that the motion of the fibers and resin through the die can be modeled by a steady plug flow. With this assumption, the model was formulated as a plug flow reactor with conduction heat transfer in directions perpendicular to the direction of part flow. The ultimate goal of Tulig's research was to optimize the pultrusion process for particular resins.

An investigation to provide a better understanding of the pultrusion process was also carried out by Kershaw, Tulig and Yamashita [6]. Kershaw and his colleagues modeled the processes occurring in the die itself. They concentrated on developing epoxy resin systems that improved the processability and quality of the resulting composite materials. The mathematical model was developed from the plug flow reactor with a conduction heat transfer term, which was the same formulation used by Tulig in his earlier work. Using this model the relationships between the pulling speed, pulling force, degree of curing, resin formulation and preheating the fiber-resin

mixture before it entered the die were studied. Their results showed that it is possible to understand the pultrusion process by mathematical modeling of the die alone.

Chapter II. Problem Definition

2.1. General

The ultimate goal of the pultrusion process is to produce a composite material having the desired properties with minimal variation. This requires reliability, uniformity and consistency in production. These requirements can be achieved by die design and coupling a monitor and automated control system to the process. A consistent quality control system can result in greater confidence in the predicted composite properties of the products. The final state of an automated control system will be a feedback control system. The block diagram of a proposed feedback control system is shown in Figure 2.

The objective of this study is to design the pultrusion die. As described earlier, the desired composite properties are interrelated to the degree of curing, pulling speed, fiber-resin mixture formula and production temperature profile. In this study, a steady-state heat transfer model is developed to describe the relationships between these parameters. The heat transfer model will serve as the basis for the objective function and constraints used with the design optimization procedure.

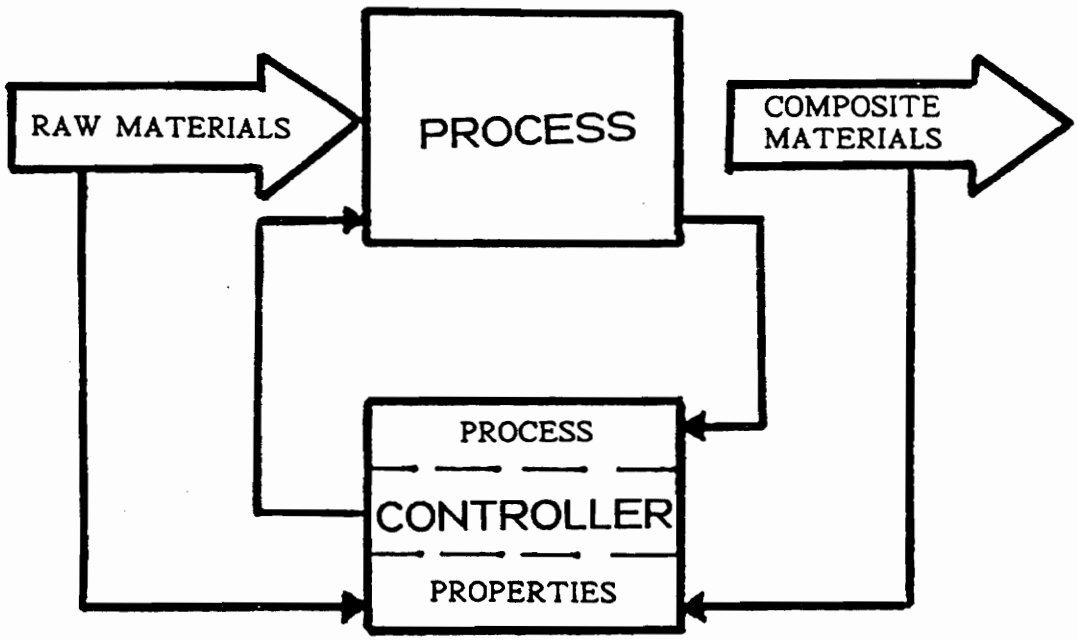

Figure 2. Block diagram of a proposed feedback control system.

2.2. *Understanding of Design Parameters*

The pultrusion process is based on resin curing which is a function of the production temperature profile. The degree of curing also depends on the fiber-resin mixture formula, which is the quantity and type of raw fiber, and the resin in use. The relation between the required temperature profile for a particular degree of curing with a certain kind of raw fiber and type of resin is usually available in the manufacturers' data sheets.

A thermosetting resin will respond with both endothermic and exothermic time dependent reactions. Because of this characteristic, heat will be transferred to the resin which will lower the production temperature profile. After the prescribed heat required to initiate the thermo-chemical reaction of the resin is attained, heat will be released which will shift the production temperature profile upward. During the endothermic and exothermic reaction periods, the production temperature profile developed in the die is a transient coupled heat transfer process. The actual production temperature profile is a result of the coupling between the heat generated by the heaters and the heat absorbed and released from the thermosetting resin. To simplify this study, the transient phase of the heat transfer cycle is ignored. This is equivalent to saying that the heat transfer model for this study is valid for non-thermosetting resins in a steady-state heat transfer phase or thermosetting resins in a steady-state heat transfer phase if the transient coupled heat transfer effect is insignificant to the heat transfer model. At this stage, the significance of the transient coupled heat transfer effect is unavailable for the die under consideration.

The degree of curing for the fiber-resin mixture is a time dependent process. This can be modeled spatially from a point on the materials perspective. As the point moves through the die it "sees" the thermal gradient along the cavity of the die.

The original production temperature profile produced in a pultrusion die is dependent on the heater configuration. The heating is described by the number of heaters, power input and location of each

heater with respect to the length of the die. The length of the die can indirectly affect the pultrusion process. For example, different length dies will require different heating configurations and different pulling speeds to produce the same properties for the same fiber-resin mixture formula. Since a laboratory-scale pultrusion die had already been built, the length of the die will be treated as a fixed parameter. The amount of heat released from each heater is controlled by the amount of power input to the heaters. The production temperature profile developed in the die can be altered by rearranging the heating configuration. The power input to the heaters can be used as a control parameter to maintain a desired production temperature profile along the length of the die. This temperature profile can be numerically computed using a steady-state conduction heat transfer formulation.

The scope of this study is to design the pultrusion die by determining the heating configuration which includes the number of heaters, power input and location of each heater for a given production temperature profile. The pulling speed, which is highly dependent on the production rate, will be included in the pultrusion process model as a fixed parameter.

2.3. Configuration of a Laboratory-Scale Die

A laboratory-scale pultrusion die is constructed of steel blocks [7]. The length of the die is 0.5 m and consists of two equal size blocks, each having cross-section dimensions of 76 x 60 mm (about a 1.3 : 1 aspect ratio). These two blocks are firmly attached to minimize the heat loss to the surroundings. There is an opening in the middle of the die. This opening is known as the die cavity and has cross-section dimensions of 12.5 x 2.4 mm (about a 5 : 1 aspect ratio). Figure 3 shows the physical dimensions of this laboratory-scale pultrusion die. The fiber-resin mixture will pass through this cavity for curing.

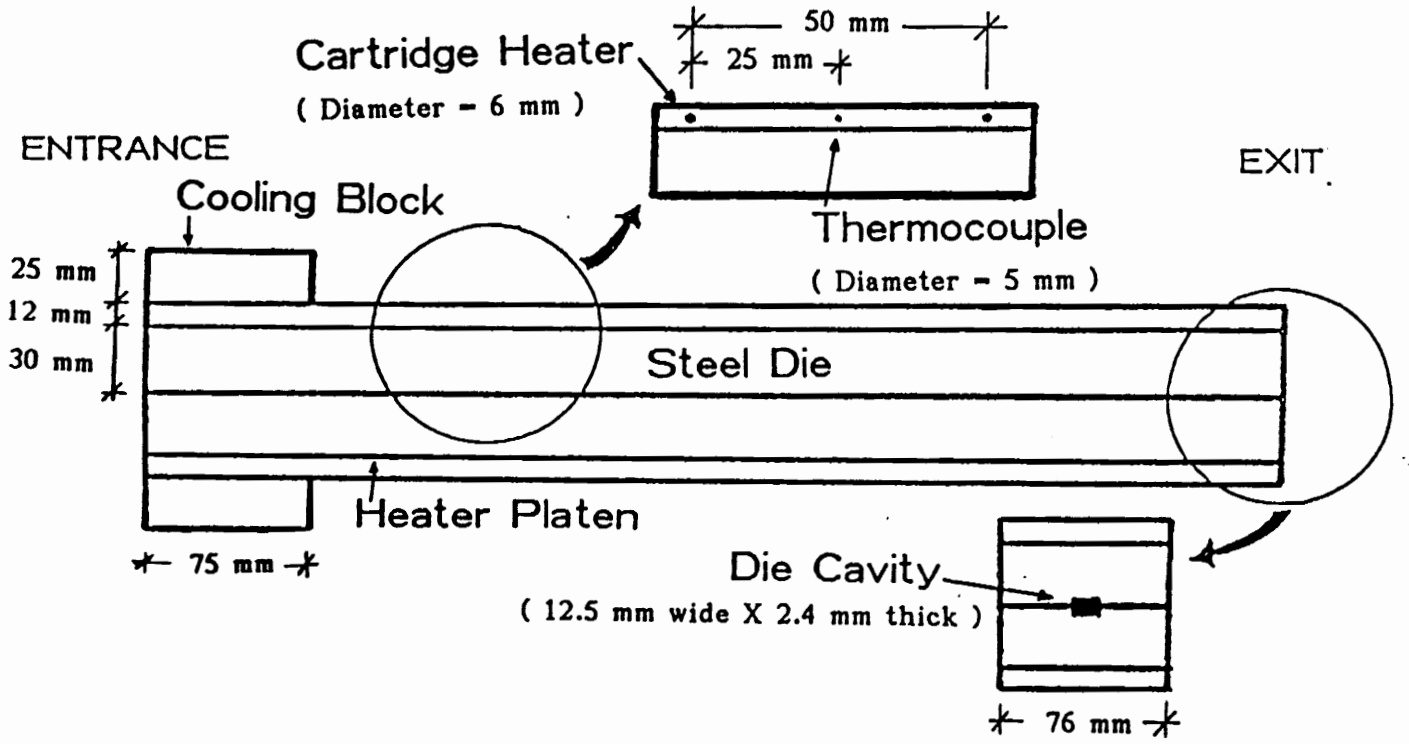

Figure 3. Physical dimensions of the laboratory-scale pultrusion die.

Heat is supplied to the die by two heater platens attached to the top and bottom of the die. The dimensions of these platens are 76 x 12 mm. These heater platens are attached to the die to ensure good heat transfer to the die blocks. There are ten predrilled holes of 6 mm diameter on both of the heater platens. Cartridge heaters (one top and one bottom) are inserted into these holes. Each cartridge heater has a maximum manufacturer rated power of 100 watts. From laboratory testing, it was found that each of these heaters has the capability of producing 85.4 watts.

There are also nine 5 mm diameter predrilled holes on both of the heater platens for inserting thermocouples. The thermocouple holes are alternatively arranged with the cartridge heater holes and they are evenly spaced. The spacing between holes is 25 mm. The clearances of the cartridge heaters in the predrilled holes and the thermocouples in the predrilled holes are assumed to be neglectable. The temperatures are measured using iron-constantan thermocouples.

There are two cooling blocks, each having a length of 75 mm and cross-section dimensions of 76 x 25 mm, firmly connected to the top and bottom of the die at the entrance end of the die. The entrance end of the die is the end where the fiber-resin mixture enters the die cavity for the curing process. With this short laboratory die, these cooling blocks will help to ensure a lower temperature at the entry point to prevent thermo-cracking of the fiber-resin mixture due to a sudden increase in temperature caused by the exothermal reaction of the resin. The cooling blocks will also provide a gradual increase in the temperature profile along the length of the cooling blocks.

2.4. Objectives

The main objective is to design the pultrusion die to obtain a desired temperature profile subject to design constraints. The main activity is the development of a mathematical model of a physical problem, which is the pultrusion process. With this mathematical model, a design optimization

model can be developed for the design of the pultrusion die. The first goal of this study is to develop a first order heat transfer model for predicting the temperature profile of the laboratory-scale pultrusion die. A design optimization problem can then be formulated against the heat transfer model to make design trade-offs for synthesizing the heating configuration. The design optimization problem formulated in this study is to synthesize the heating configuration to produce the desired production temperature profile. The heating configuration includes three variables: the number of heaters, the power input and location of the heaters. The final objective is to examine the power requirement by insulating the die completely except at the entrance and exit of the die. The specific objectives of this study are:

1. To develop a heat transfer model for a laboratory-scale pultrusion die.
2. To perform a design optimization on the die based on the heat transfer model, which also includes the sensitivity analysis.
3. To examine the effect of insulation in terms of power requirement.

2.5. Problem Solving Methodology

This section gives a brief description of methodology used to perform this pultrusion die design based on a heat transfer model. Detailed descriptions will be included in the following chapters. The problem solving approach is divided into five subsections. They are heat transfer formulation, die modeling, heat transfer model verification, design optimization, and power requirement examination.

2.5.1. Heat Transfer Formulation

A method of computing the temperature profile for this laboratory-scale pultrusion die is desired. A heat transfer model is required to predict the temperature of the die at any desired location. The dominant mode of heat transfer in the die is heat conduction. Free convection governs the heat transfer at the exposed surfaces.

In order to produce uniform and consistent continuous composite materials, the production temperature profile must be stable and maintained at a constant profile. Usually, the die is in use for long hours of operation. Therefore, a steady-state heat transfer solution of the die is appropriate. In addition, this heat transfer model neglected the effect of the heat transfer of the fiber-resin mixture flowing through the die cavity and also the effect of the exothermic reaction from the thermosetting resin. There are several methods available to solve this steady-state heat transfer problem. Two of these methods, the finite difference method and the boundary element method, will be investigated before a final solution method is selected. The selected solution method must be flexible and easy to incorporate into the design optimization procedures used to synthesize the design variables.

2.5.2. Die Modeling

The laboratory-scale pultrusion die was previously modeled as a 2-D steady-state conduction heat transfer model of unit depth with insulation at the top and bottom surfaces [7]. This means that both side surfaces of the die (in the depth direction) were subjected to free convection (see Figure 4a). This initial model is called a two-side-insulated heat transfer model. The model used in this study is a four-side-insulated heat transfer model with unit depth. This means that the die was insulated at 4 side surfaces except the entrance and exit ends. The only modification needed on the die to accommodate this change is to insulate both the front and back surfaces (see Figure 4b).

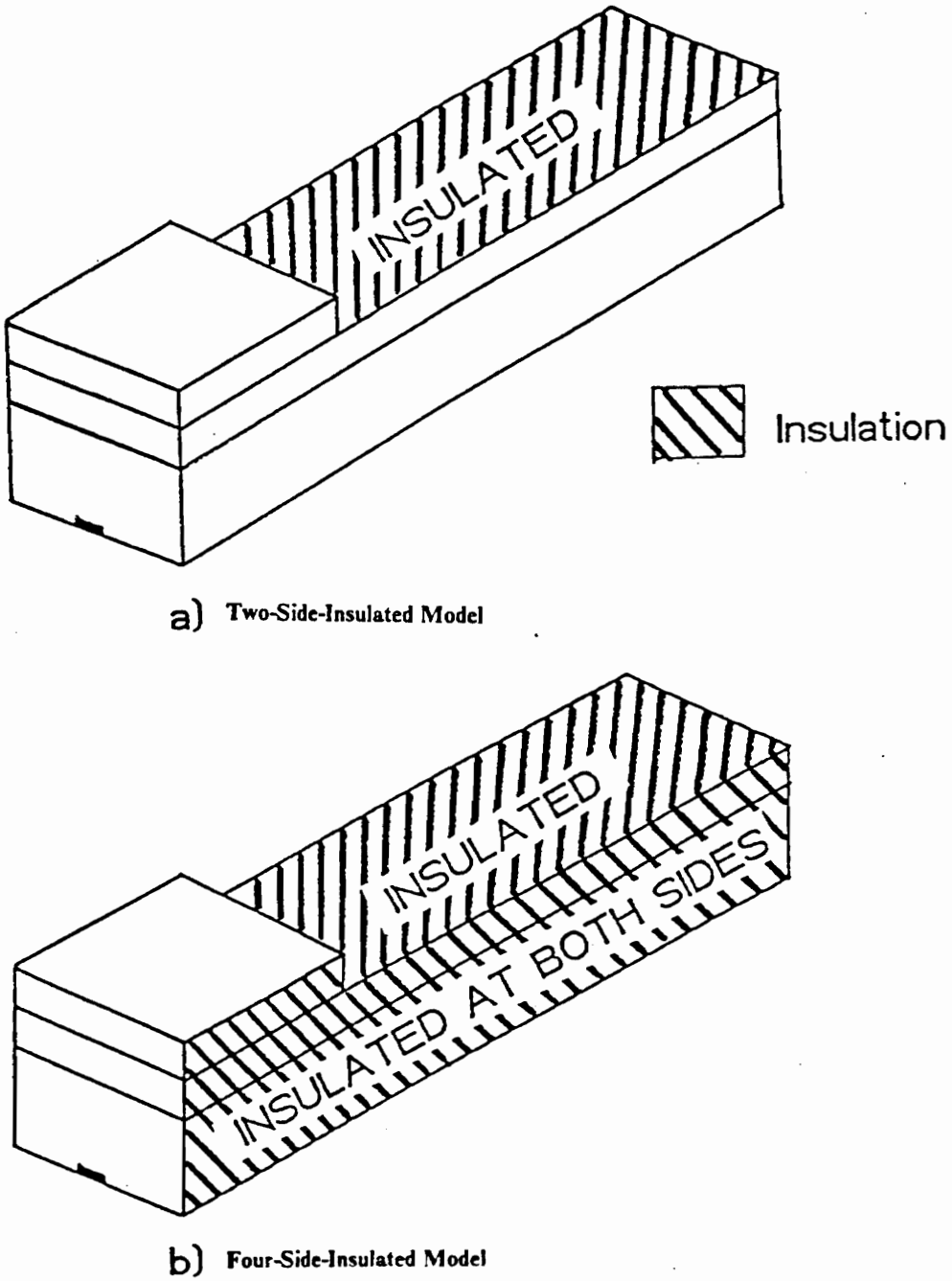

Figure 4. Insulation arrangements for the laboratory-scale pultrusion die.

As a result, the heat lost to the surroundings will only occur through the ends and cooling blocks of the die. This insulation arrangement will certainly reduce the heat loss from the die during the curing process. With these two models it is possible to examine the effect of insulation on the power requirement of the die.

Due to symmetry, only half of the die will be modeled. The plane of symmetry will cut through the center of the die cavity. This plane of symmetry is modeled as an adiabatic surface with zero heat flux. For the insulated surfaces, the heat flux will also be zero.

An estimation of the convection coefficient is required for the free convection surfaces and this will be obtained experimentally. Other thermal properties such as thermal conductivities are obtained from published literature. The thermal conductivities are approximately 42 $W/m°C$ and 57 $W/m°C$ for the steel die and heater platen, respectively [8].

2.5.3. Heat Transfer Model Verification

The performance of the heat transfer models is evaluated by comparing temperatures measured at the die cavity. The die is heated by applying a known amount of power into a prescribed number of the cartridge heaters. A steady-state condition in the die is achieved after several hours. Three test cases are prepared to evaluate the heat transfer models. The heating configurations of these three test cases are listed in Table 1.

The experimental results are obtained by inserting ten thermocouples along the die cavity. The temperatures are measured every 10 minutes until the difference in temperature from the successive measurements is small. This indicates when the steady-state condition of the die is achieved. The temperatures from these three test cases are then compared with three simulated temperatures with the respective heating configurations.

Table 1. Heating configurations of the three test cases.

HEATER NO.	TEST CASE 1 POWER (W)	TEST CASE 2 POWER(W)	TEST CASE 3 POWER(W)
1			
2	59.0		
3	59.0		
4			
5	59.0	85.4	
6			
7	59.0		
8			
9	59.0		85.4
10			
TOTAL =	295.0	85.4	85.4

The heat transfer model itself is checked by comparing the total computed heat loss from the die to the total heat input to the die. Ideally, the total heat loss must equal the total heat input. But with mathematical models, small variations are expected.

2.5.4. Design Optimization

After verification of the heat transfer model, the next step is to formulate the design problem. The design optimization problem here is to synthesize the heating configuration to produce the desired production temperature profile which is formulated as a nonlinear programming problem. Optimization techniques not only can synthesize a design to satisfy a set of design criteria, but can also perform numerical trade-offs against a specified criterion. The design variables associated with the heating configuration are the number of cartridge heaters, power input and location of each cartridge heater.

The primary objective function used to evaluate the performance of the model against the design variables is the minimization of the sum of square error between the desired and synthesized temperature profiles. A secondary objective function, which is the minimization of the power input to the cartridge heaters, will also be examined to see how it will affect the design model. In order to know how sensitive the die is to changes in the design variables, a sensitivity analysis is included in this design optimization study. The sensitivity results give valuable information regarding how the process should be controlled and what kind of controller should be installed. Usually a more sensitive system, requires a more sophisticated controller. For relatively insensitive systems, such as this laboratory-scale die, a simpler control system is appropriate.

2.5.5. Power Requirement Examination

The design optimization program will be an excellent tool to study the effect of insulating the die with respect to the power input to the cartridge heaters. The key here is to use the two-side-insulated temperature profile as the desired temperature profile and let the optimization program come up with a new heating configuration. The optimization program will use the four-side-insulated heat transfer model to synthesize the desired temperature profile. The optimized results, especially the power input to the heaters, should be less than the original power input to the heaters used to generate the desired temperature profiles for all three test cases.

The difference in power input to the die to generate the desired temperature profile and the optimized power input as synthesized by the optimization procedure is calculated. This difference will give an indication of how much the power input to the die can be reduced by further insulating the die.

Chapter III. Pultrusion Die Heat Transfer Model

3.1. General

As mentioned in Section 2.5.1, a steady-state conduction heat transfer solution is required to compute the temperature profile of the laboratory-scale pultrusion die. Assuming that the die is constructed from a linear homogeneous isotropic material, the heat transfer problem is reduced to solving Poisson's equation [9] given in Equation (1).

$$\nabla^2 u = b \qquad [1]$$

where $u =$ the temperature field, and

$b =$ the heat generation term.

The development of Poisson's equation and a listing of associated nomenclature are included in Appendix A. The boundary conditions associated with this heat transfer model for the die are a prescribed boundary temperature, a prescribed flux, and mixed boundary conditions. For the pultrusion die, it is not typical to have an imposed flux on the boundary, except when the boundary is completely insulated. In this case the flux is zero. For this laboratory-scaled die, it will be more

realistic to assume that at the non-insulated boundaries there is some heat transferred from the die to the surroundings. Therefore the non-insulated boundaries are treated with a free convection boundary condition. This free convection boundary condition is a mixed boundary condition because it depends on both boundary temperature and flux.

3.2. Solving Poisson's Equation

There are several ways of solving Equation (1). The commonly used methods are analytical, graphical and numerical approaches.

Analytical approaches give the exact solution of the differential equation. An analytical solution for Equation (1) can be complicated because it involves solving a partial differential equation. A partial differential equation of this kind can be solved using the method of separation of variables. However, the solutions for this method can only be obtained for simple geometries and special boundary conditions. The graphical method requires patience in drawing contour lines such as heat flux lines and isotherms and is not amenable to the design optimization solution.

Numerical methods give an approximate solution of the governing equation at discretized points in the given domain. There are three common numerical methods. These are the finite difference, finite element and boundary element methods. These computational methods are the methods of choice and are widely used in solving complicated potential problems.

The finite difference method involves subdividing the domain into smaller regions, with each region is referenced at the center by a node. The temperature calculated at a node is the average temperature of that region. The finite element method divides the domain into subdomains called finite elements. Each element is represented by an approximation function derived from

interpolation functions. Compatibility and equilibrium at the element nodes and boundaries must be satisfied. The boundary element method requires discretization of the domain and the boundary. In the boundary element method only the boundaries need to be discretized in the absence of distributed sources. The boundary element method involves the transformation of a partial differential equation over a domain into an integration around the boundary. The free space Green's function is used to characterize the solution of the partial differential equation which allows the transformation of the partial differential equation into an integral equation.

Two methods of numerical solution were included in this study. They were the finite difference and boundary element methods. The finite difference model was the initial model. The boundary element model was proposed to provide the modeling flexibility for incorporation into the design optimization program. The results obtained from these two methods were compared before the final method was selected. The formulation used in the finite difference method is briefly mentioned, but more emphasis will be on the boundary element method. Additional development of each of the methods can be found in Appendices B and C, respectively.

3.3. Finite Difference Solution

The initial model was based on a finite difference method for solution as developed by Collie [7]. This involved subdividing the die into small regions where each region was designated by a node at the center. For each node, an energy balance equation was written to include all forms of heat transfer and heat generation involved in the region. After formulation of the finite difference equations for each node, the resulting system of linear algebraic equations is solved simultaneously. The Gauss-Seidel iteration method was used to solve this system of finite difference equations [10]. The rate of convergence is dependent on the initial guesses for the temperature distribution. The

iteration process was repeated until the difference in successive temperatures was less than or equal to a pre-specified convergence value.

3.3.1. Mesh Modeling

The die was previously modeled as a two-side-insulated heat transfer with free convection at both ends and side surfaces. The accuracy of this finite difference method is dependent on the size and distribution of cells in the mesh. A mesh of 128 nodes was found to produce quality results compared to the temperature measured by thermocouples. For this model, a convergence value of 0.001 was selected for the Gauss-Seidel iteration procedure. As mentioned in section 2.5.2., only half the die was modeled. The plane of symmetry is modeled as an adiabatic surface with a zero heat flux. The length of the die was divided into 40 equal segments of 12.5 mm each. The length along the vertical direction was varied to produce unequal sized cells. Smaller cells were located along the heater platen where the temperature measurements were considered crucial. With this mesh, the cartridge heater can be better represented as finely distributed concentrated sources which resulted in higher accuracy. Figure 5 shows the nodal network of the upper half of the die. The two-side-insulated model was also modified to be a four-side-insulated model simply by removing the convection terms associated with both front and back surfaces, refer to Figure 4 for a pictorial view.

3.3.2. Estimations of Convection Coefficient and Thermal Conductivity

The convection heat transfer coefficient depends on the temperature at the surfaces. A simple experimental technique was used to determine the convection coefficient. The convection coefficient can be calculated from the following expression [10]

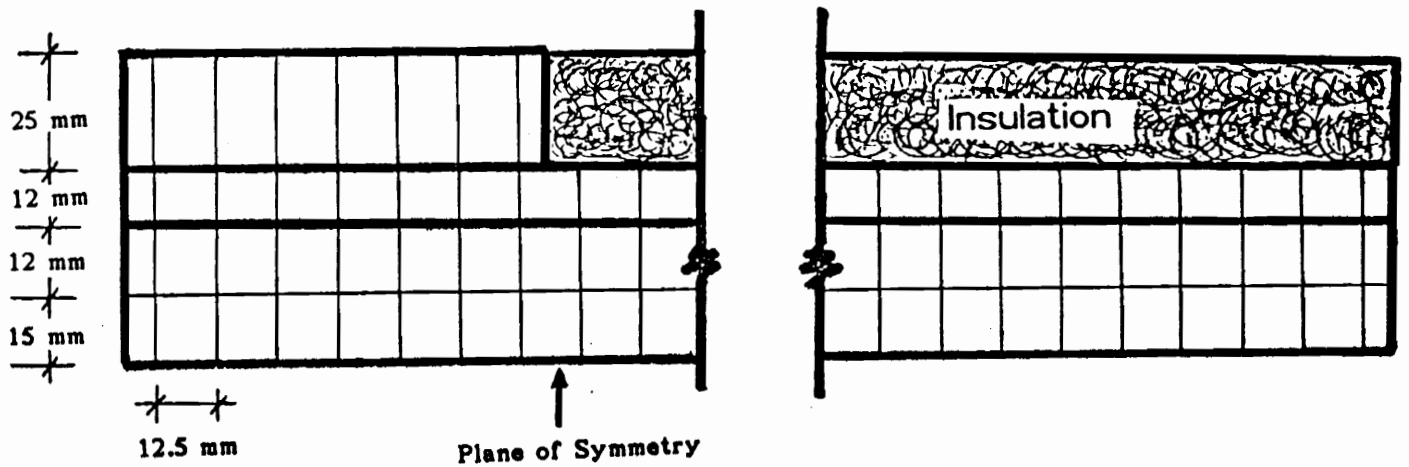

Figure 5. Nodal network of the upper half of the laboratory-scale die.

$$Q = hA(u_s - u_\infty) \qquad [2]$$

where Q = total heat generated by the heaters,

h = convection coefficient,

A = total external surface area,

u_s = average temperature of the die, and

u_∞ = surrounding temperature.

The die was heated up with all ten cartridge heaters at full power until it came to steady state. The average temperature was measured with ten thermocouples inserted along the die cavity every ten minutes. The average temperature was taken as the average surface temperature of the die and was measured to be 230 °*C*. This was an estimate based on assumption that the surfaces of the die were isothermal. With all ten heaters at full power, the total heat generated is 854 watts (averaged 85.4 watts per heater). The air temperature was assumed to be constant and at a value of 22 °*C*. This air temperature was assumed throughout the study. The experiment was carried out without insulation and the total surface area for all six surfaces is 0.207 m^2. With these values, the convection coefficient was calculated to be approximately 20 W/m^2 °*C*. The free convection coefficient for the air is typically in the range of 6 to 30 W/m^2 °*C* [8].

Since the steel die and the heater platen have different thermal conductivities, a value of 42 W/ $m°C$ was used, which is the thermal conductivity of the steel die. Using this convection coefficient and thermal conductivity, the predicted temperature was always low compared to the measured temperature. This indicated that the estimated convection coefficient and the conservative thermal conductivity were not correct for this laboratory-scale die. Adjustment of these values were carried out by trial and error on combinations of the convection coefficient and thermal conductivity close to the experimentally obtained values. After several trials, a convection coefficient value of 17 W/ m^2 °*C* and a thermal conductivity value of 51 W/$m°C$ resulted in better agreement between the predicted and measured temperatures.

Sensitivity analysis was performed on these values by perturbing both the convection coefficient and thermal conductivity. The predicted temperature profile did not change much with a perturbation of 1 or 2 units on the thermal properties used. By studying the effect of these properties individually, the convection coefficient was determined to have more influence on the temperature profile. This is expected, because the convection coefficient influences how much heat is transferred to the surroundings. These two values will be used throughout the study and it should be noted that they are only applicable to this particular die.

3.3.3. Estimation of the Heat Transfer of the Fiber-Resin Mixture

Since the cross-section of the die cavity is small with respect to the cross-section of the die, the heat transfer of the fiber-resin mixture flowing through the die cavity is assumed to be small compared to the total heat transfer of the die. The heat transfer of the fiber-resin mixture flowing through the die cavity can be estimated by heat convection of the following form

$$q_{\text{convection}} = \dot{m} c_p \Delta T \qquad [3]$$

where $\dot{m}$ = mass flow rate,

c_p = specific heat, and

ΔT = change in outlet and inlet temperature.

In order for the assumption to be valid, the internal heat changes for the fiber-resin mixture flowing through the die cavity must be relatively small compared to the total power input to the die.

The mass flow rate can be estimated from the density, the area of the die cavity and the production rate. Equation (3) above can be rewritten as

$$\frac{q_{\text{convection}}}{\Delta T} = A \dot{v} \rho c_p \qquad [4]$$

where A = area of the die cavity,

$\dot{v}$ = production rate, and

ρ = density of the fiber-resin mixture.

The realistic production rate is 2 to 4 feet per second or 10 to 20 mm per second [1]. For this laboratory-scale die, due to symmetry, only half of the die was modeled. The area for half of the die cavity is 15 mm^2. For glass-fiber reinforced composite materials, the specific heat and density vary from 0.8 to 1.5 KJ/Kg °C and 1240 to 2190 Kg/m^3, respectively, depending on the type of resin [16]. For glass-fiber reinforced with epoxy resin, the average specific heat and density are 1 KJ/Kg °C and 1940 Kg/m^3, respectively. The maximum production rate for this laboratory-scale die is 20 mm per second. With these values, the heat convected to the fiber-resin mixture flowing through the die cavity per unit change of outlet and inlet temperature was calculated to be 0.58 W/°C. This laboratory-scale die is normally operated at a production rate of one-third of the maximum allowable rate which reduces the heat convected to the fiber-resin mixture by one-third which is 0.19 W/°C. Usually, cured composite materials are allowed to cool down as they exit the die, thus the difference in outlet and inlet temperature is frequently kept small. This is justified because the cartridge heaters are normally inserted in the middle portion of the die to produce a temperature gradient with a peak at the center of the die. With 10 cartridge heaters, the possible power input to the die is from 0 to 845 watts. From this calculation, it is shown that the internal heat changes for the fiber-resin mixture is small compared to the total power input to operate the die.

3.3.4. Results

Three test cases were run with the two-side-insulated and four-side-insulated models. The results were compared with temperatures measured at 10 different locations along the die cavity. Figure 6, 7 and 8 show the superimposed temperature profiles of the predicted and measured temperatures for the three data sets. These curves demonstrate that the trends of predicted and measured

temperatures are similar. The maximum difference between predicted and measured temperatures was found in test case 2, where a difference of $7°C$ can be seen at 2.875 *mm* from the entrance of the die. The rest of the test cases exhibited less than $5°C$ temperature difference and some of them were identical to the measured temperatures. Additionally, the percent difference between total heat lost and total heat input was calculated for all three test cases and were 0.3, 0.8 and 0.9 % for test case 1, 2, and 3, respectively.

Figure 9, 10 and 11 show the temperature profiles of the four-side-insulated model for all the three test cases. From figure 9,10 and 11, it can be seen that the power input to the die can be reduced by roughly a factor of 2 or 3 by insulating the sides of the die. There are no experimental results available for comparison with this four-side-insulated model. The developed finite difference models are only valid for this laboratory-scale die with the current set up and the empirically estimated thermal properties.

3.4. Comparison of Finite Difference and Boundary Element Methods

There are several limitations associated with the finite difference method. The solution obtained by this method is an approximate solution over the domain. Only the temperature at the nodes can be computed. If the temperature at other places in the domain or moving of the heat sources is required, reconstruction of the mesh and reformulation of the finite difference equation is required for each change. The formulation of the boundary nodes is difficult especially for non-straight boundaries.

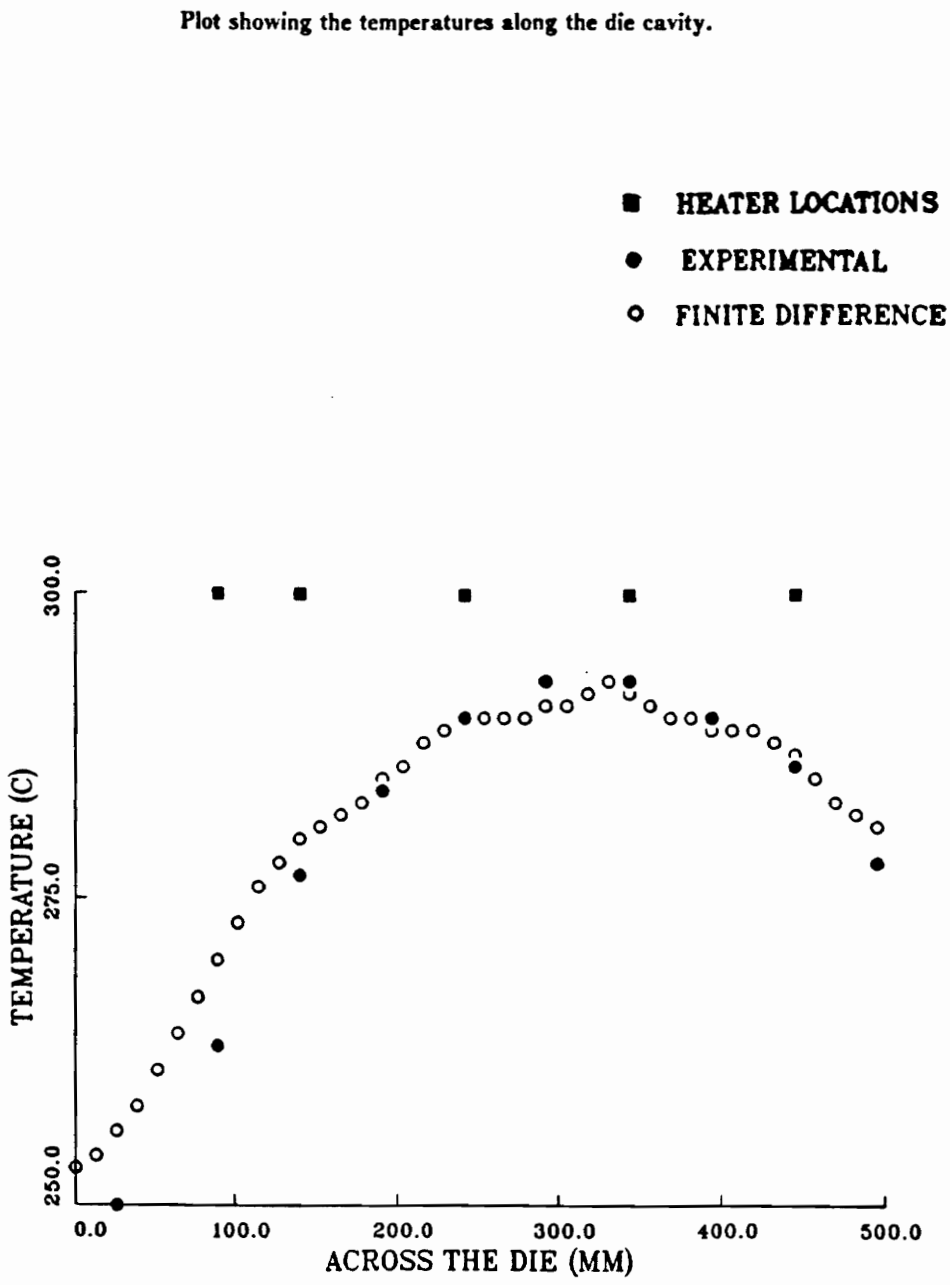

Figure 6. Test Case 1 - Two-side-insulated model and finite difference results.

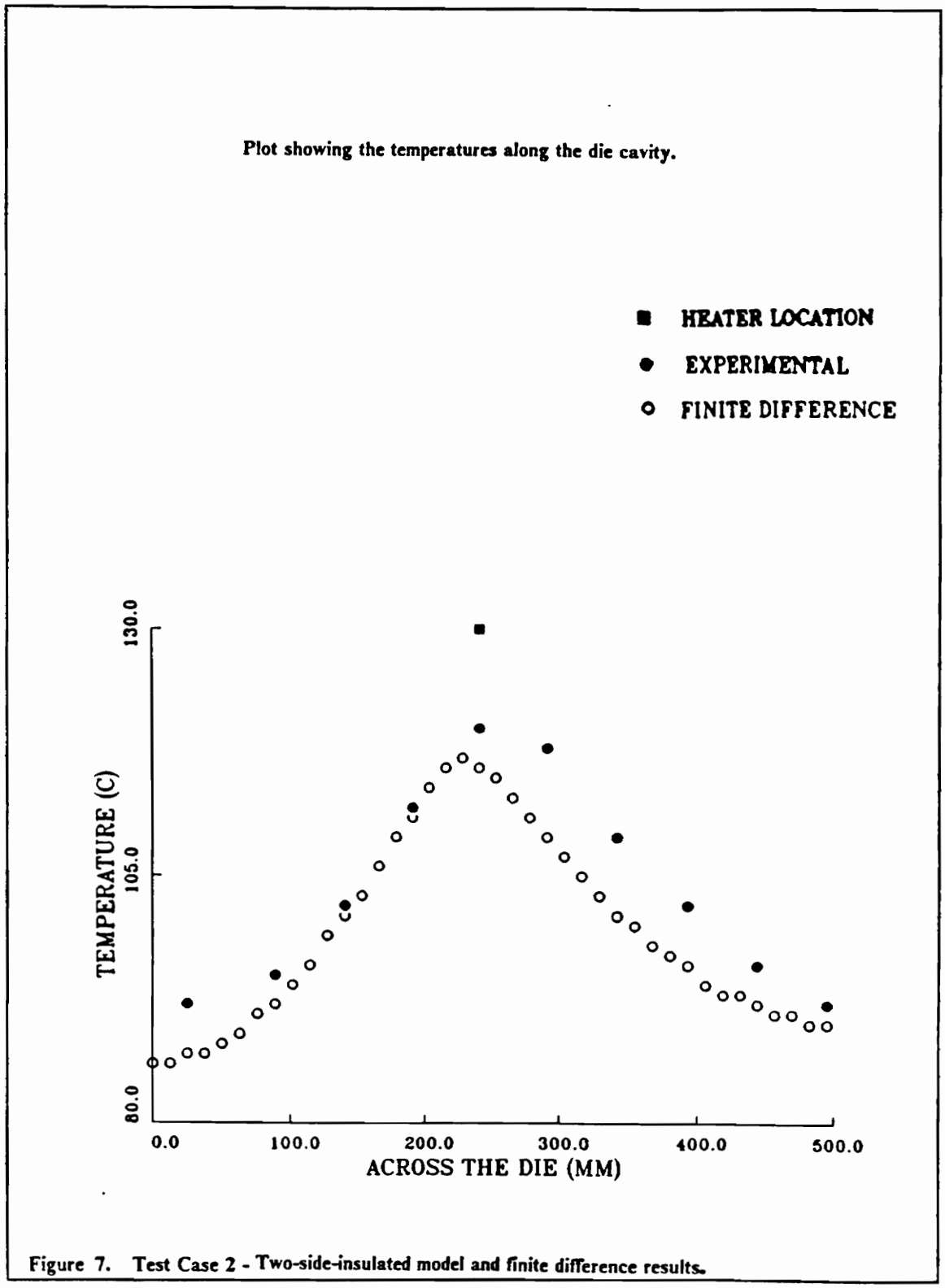

Figure 7. Test Case 2 - Two-side-insulated model and finite difference results.

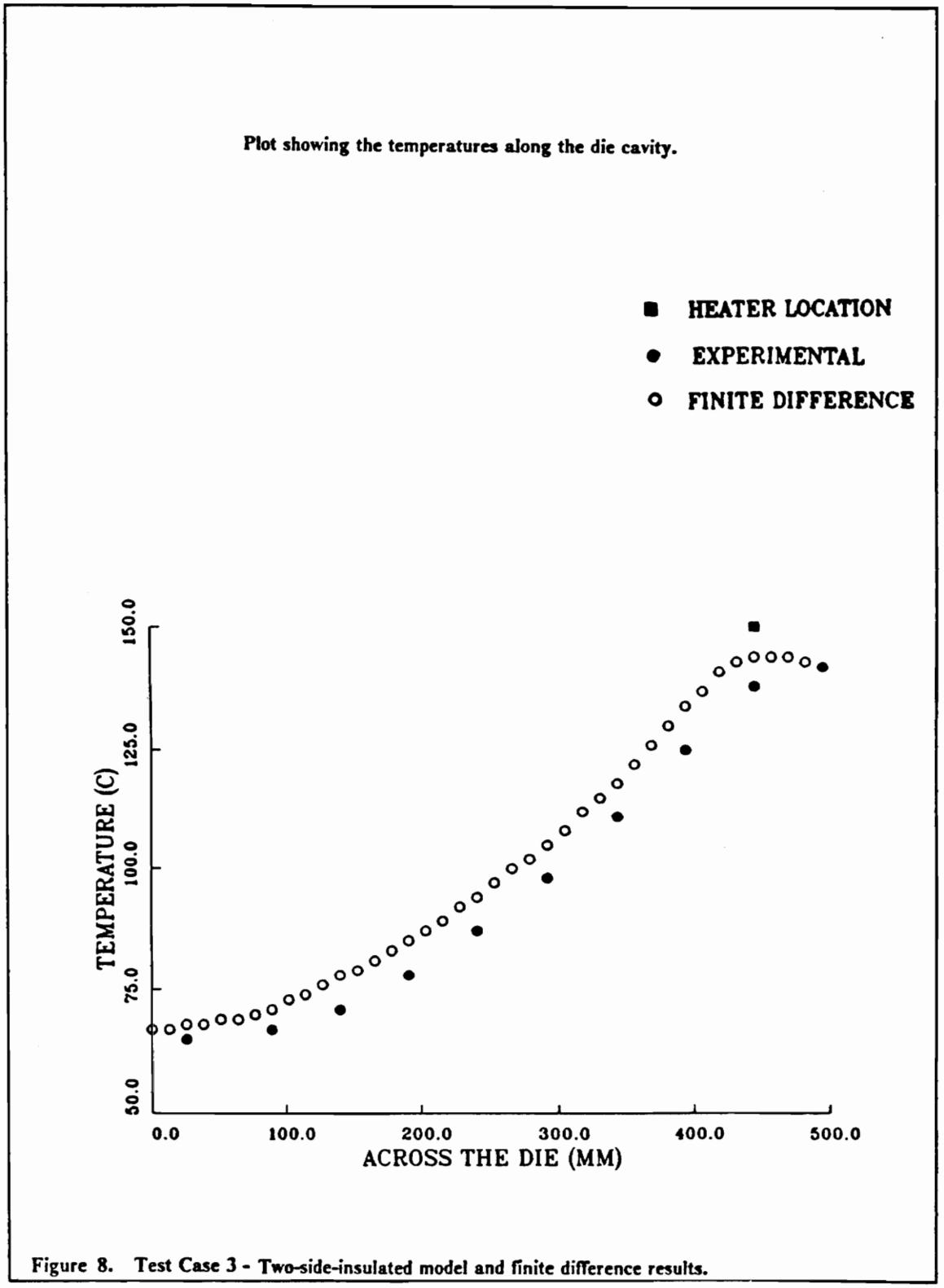

Figure 8. Test Case 3 - Two-side-insulated model and finite difference results.

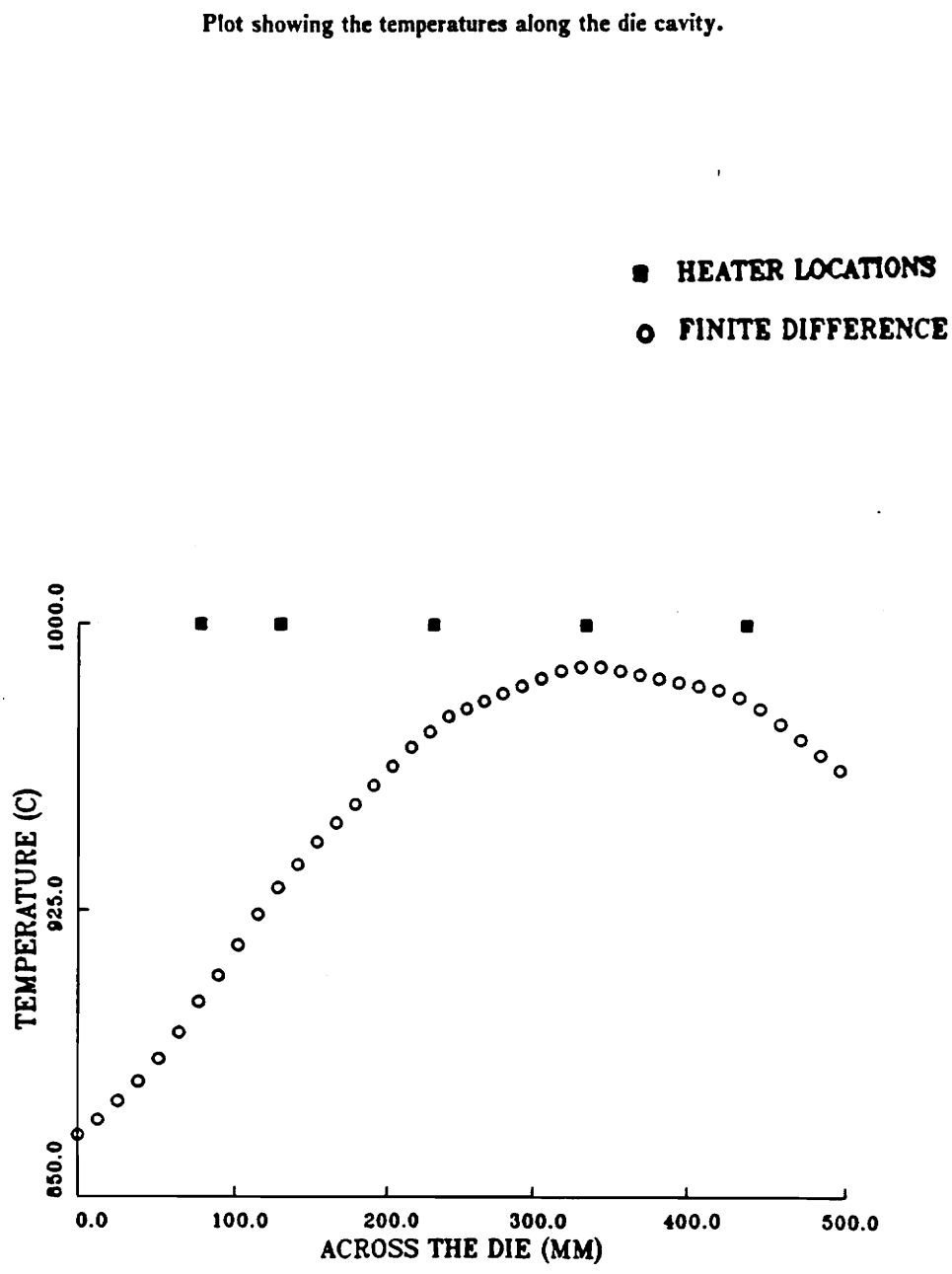

Figure 9. Test Case 1 - Four-side-insulated finite difference model results.

Plot showing the temperatures along the die cavity.

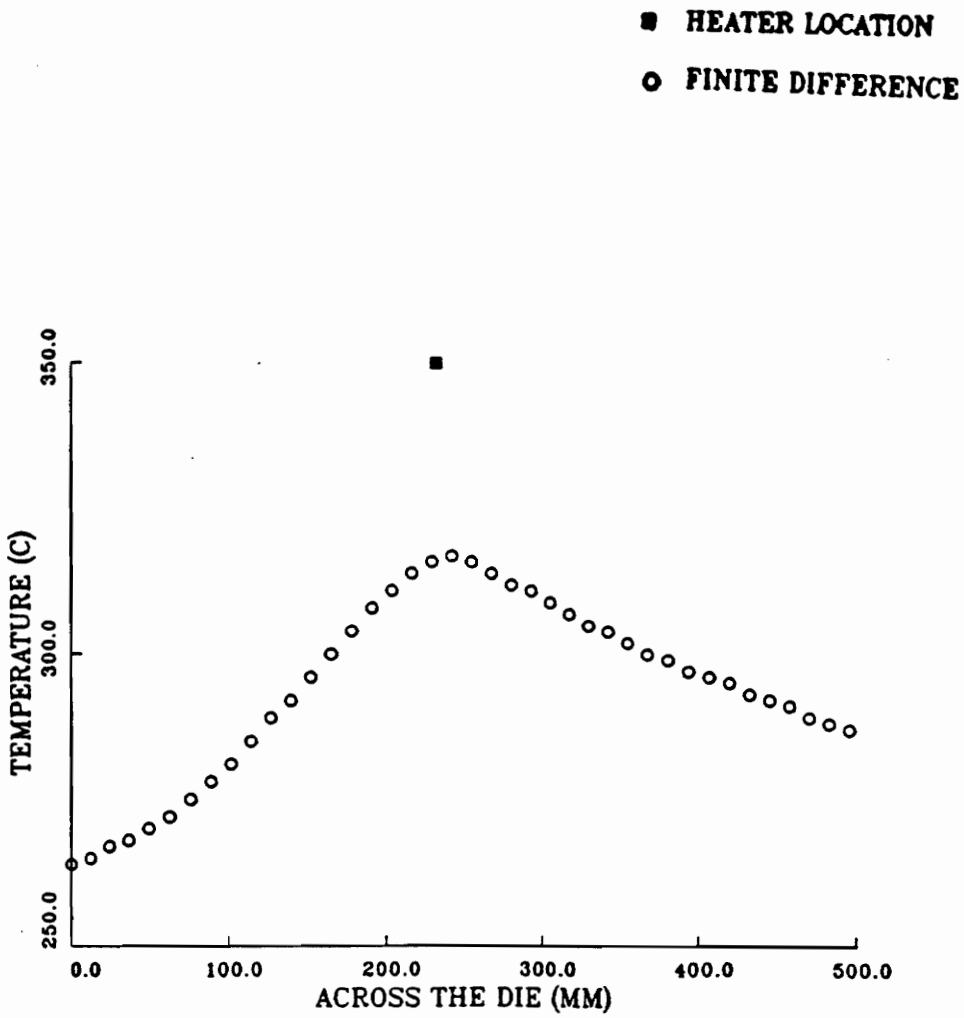

Figure 10. Test Case 2 - Four-side-insulated finite difference model results.

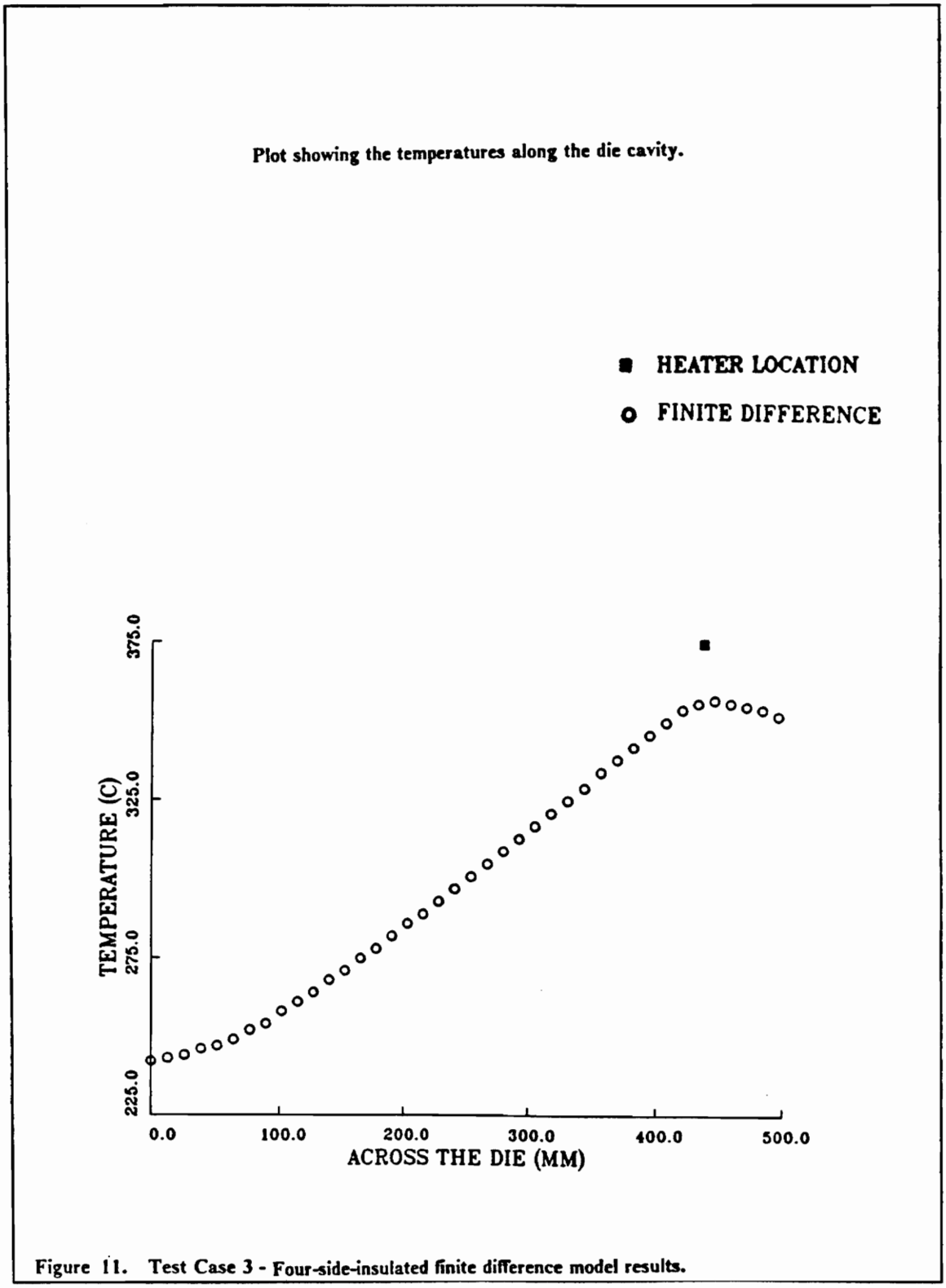

Figure 11. Test Case 3 - Four-side-insulated finite difference model results.

In order to achieve the objective of this study, a more flexible solution method is desired. The solution method must be capable of computing the temperature at any point in the domain. It must allow redistribution of the heat sources without reconstructing the mesh and reformulating the heat transfer equation. Also it is desirable to solve the heat transfer problem directly, not in an iterative fashion.

For this study, the boundary element method is a more flexible numerical solution method than finite differences. The temperature at any point in the domain can be computed. The boundary element method involves the transformation of the partial differential equation over the domain into an integral equation around the boundary and over the domain for the heat sources. For linear problems, such as Poisson's equation, the boundary element method can satisfy the partial differential equation exactly at the boundary and requires less input information than the finite difference and finite element methods. Since problems without distributed sources require discretization only at the boundary, the number of elements required will be fewer and the approximation occurs only at the boundary. The temperature calculated at any point inside the domain is the temperature at that point. This numerical method requires solving the integral equation directly. Therefore, the boundary element method provides a discretized continuum solution. Integral equations for linear steady-state potential flow can be approximated numerically using the Gauss point integration scheme and solved as a set of linear equations. This explicit solution procedure does not required iteration. Although the formulation of the boundary element algorithms are more involved, the computation time in solving a boundary element problem is much less than the finite difference iteration scheme used earlier [7]. As with most numerical schemes, the finer the representation of the boundary, the greater the accuracy.

3.5. Boundary Element Solution

The transformation of the partial differential equation of the domain into an integral equation on the boundary involves two problem solving procedures, an analytical and an approximate solution procedure. The boundary element method combines Green's functions, which comprise the analytical character of the solution, with finite element discretization of the boundaries, which is the approximate procedure. The development of these transformation procedures is included in Appendices C and D. After the unknown boundary values are determined (in this case they are the temperature and heat flux on the boundaries) the temperature at any point in the domain can be calculated.

3.5.1. Boundary Element Shapes

There are three element shapes commonly used in modeling boundary element problems, constant, linear and quadratic elements. Constant elements are straight line segments defined by mid-element nodes. The values of temperature and heat flux are considered to be constant over each element and equal to the value of the mid-element node. As a result, discontinuity can occur from one element to another. Linear elements are also straight line segments, but are defined by two end points. Linear interpolation is required to evaluate the values of temperature and heat flux at any point along the element. Linear elements can be used to model curved boundaries, but will require more elements in order to adequately represent the boundary. Curved boundaries can be effectively modeled by quadratic elements because quadratic elements can follow the curvature of complex geometries. The simplest quadratic element is the three noded element, two end points and one middle point. Computational requirements are increased with increasing element complexity. For this study two kinds of elements will be investigated, constant and linear elements. The adequacy of these element shapes will be tested and final selection will be based on the test results.

3.5.2. Computer Algorithms Development

Two versions of a computer program were written in FORTRAN-77, one with constant and one with linear element models. The programs used Brebbia's [9] basic computer code, which can solve a 2-D general Laplace's equation. The basic program was modified to accommodate the heat transfer analysis for the die design, which involves solving Poisson's equation (i.e., with heat source terms), mixed boundary conditions and a total energy balance analysis.

3.5.2.1. Mixed Boundary Condition Verification

The mixed boundary condition was implemented and verified by comparing the boundary element solutions with the analytical solution of a simple plane wall of unit depth. Figure 12 illustrates the plane wall problem. The analytical solution was calculated using the mixed boundary condition expression. The formulation is listed in Appendix A Equation (A.9). Several comparisons were done by using various numbers of elements for both constant and linear models. Figure 13 shows the comparison between the analytical solution and boundary element solutions. From these simple test cases, the analytical solution can be numerically approximated using finer discretized elements. These tests also showed that there was not much of an advantage of using linear elements rather than constant elements.

3.5.2.2. Heat Source Verification

The heat generation source term has been implemented into the code and verified. Again, the plane wall of unit depth problem was used to verify the boundary element solutions. This time, the plane wall was subjected to distributed heat generation. The heat source term developed in the boundary element formulation is based on a concentrated point source. A distributed heat generation source

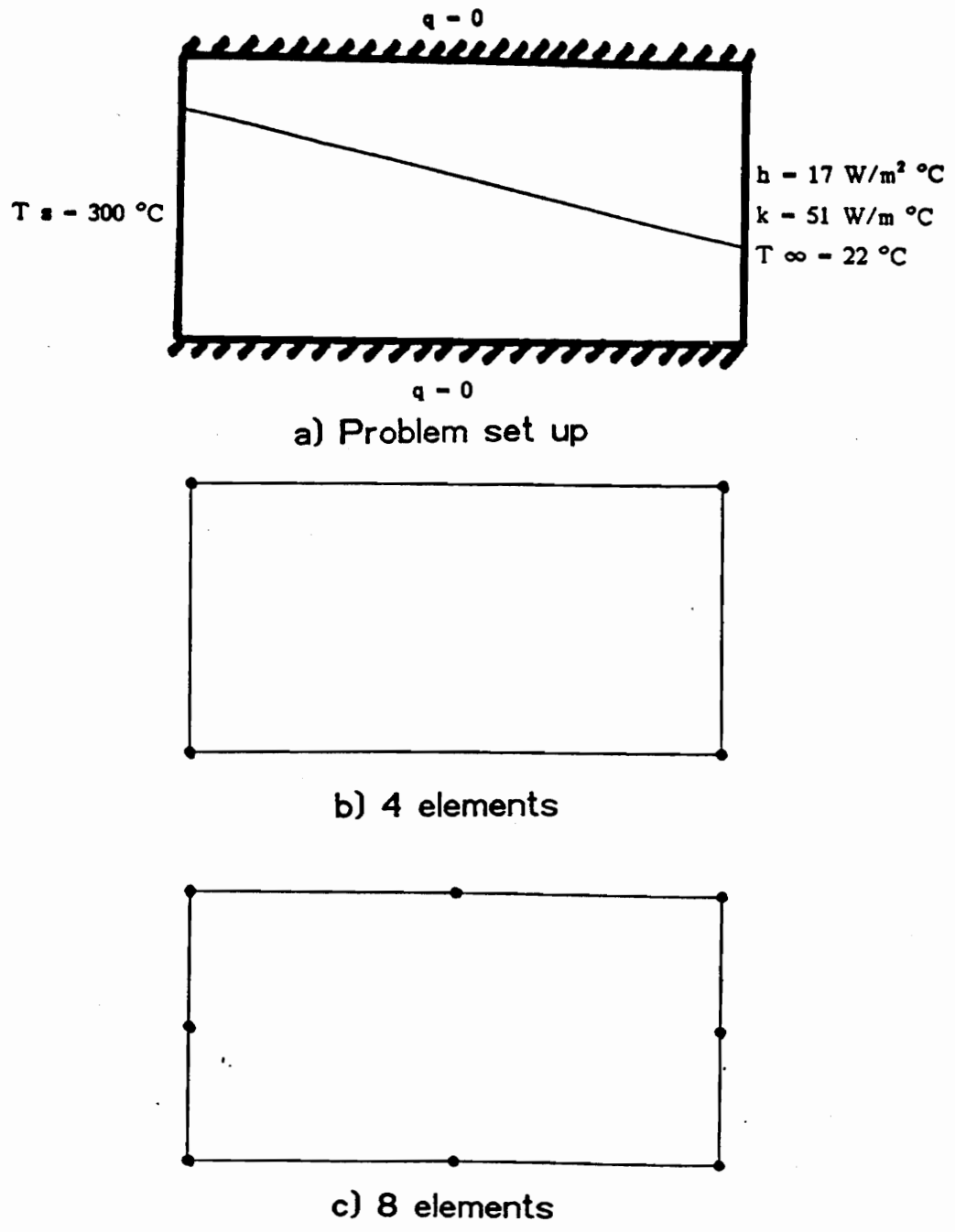

Figure 12. Mixed boundary condition problem set up.

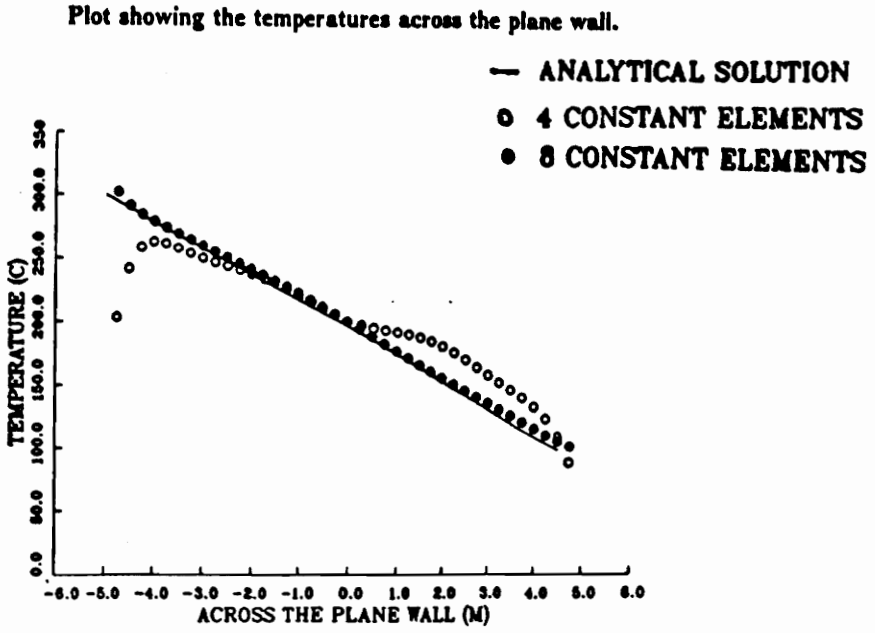

A) CONSTANT ELEMENTS

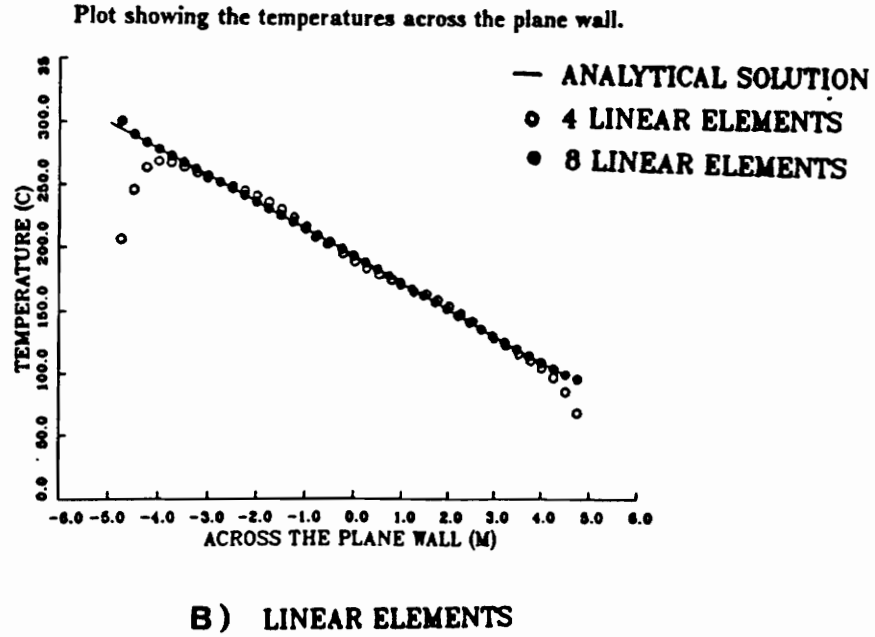

B) LINEAR ELEMENTS

Figure 13. Mixed boundary condition verification.

can be approximated by evenly distributing the heat across the plane wall (Figure 14). The analytical solution is then compared with solutions using various numbers of elements for both constant and linear models. The analytical solution is [8]

$$T(x) = \frac{QL^2}{2k}(1 - \frac{x^2}{L^2}) + T_s \ . \qquad [5]$$

The surface temperature was calculated from the convection equation,

$$T_s = T_\infty + \frac{QL}{h} \ . \qquad [6]$$

The temperature distribution along the wall is obtained by combining Equations (5) and (6) giving

$$T(x) = QL\left[\frac{L}{2K}(1 - \frac{x^2}{L^2}) + \frac{1}{h} \right] + T\infty \ . \qquad [7]$$

where Q is the heat generation term per unit volume, the value used in this example is 100 W/m^3 and L is the thickness of the wall, which is 5 *m*. Figures 15 and 16 compare the results, which as expected, clearly demonstrate that with linear elements less elements are required to achieve more accurate results than with constant elements.

The cartridge heaters used in this study have a diameter of 6 *mm*. The heat source term was developed based on a concentrated point source. Theoretically, this concentrated point source represents an infinitely small point. A check was made on treating the heaters as point sources. Temperature distributions with the source as the original integral over the domain were compared with the source as a concentrated point source. The actual formulation of these source terms is included in Appendix C, Equations (C.23) and (C.25), respectively. In the case of the distributed source, the integral over the domain for Equation (C.23) was carried out using a Gauss 10 point double integration scheme. It was surprising to observe that the results were identical, as shown by a superimposed plot (Figure 17). The temperatures were calculated outside the source points, therefore these calculations did not involve the singularity of the source. This test case

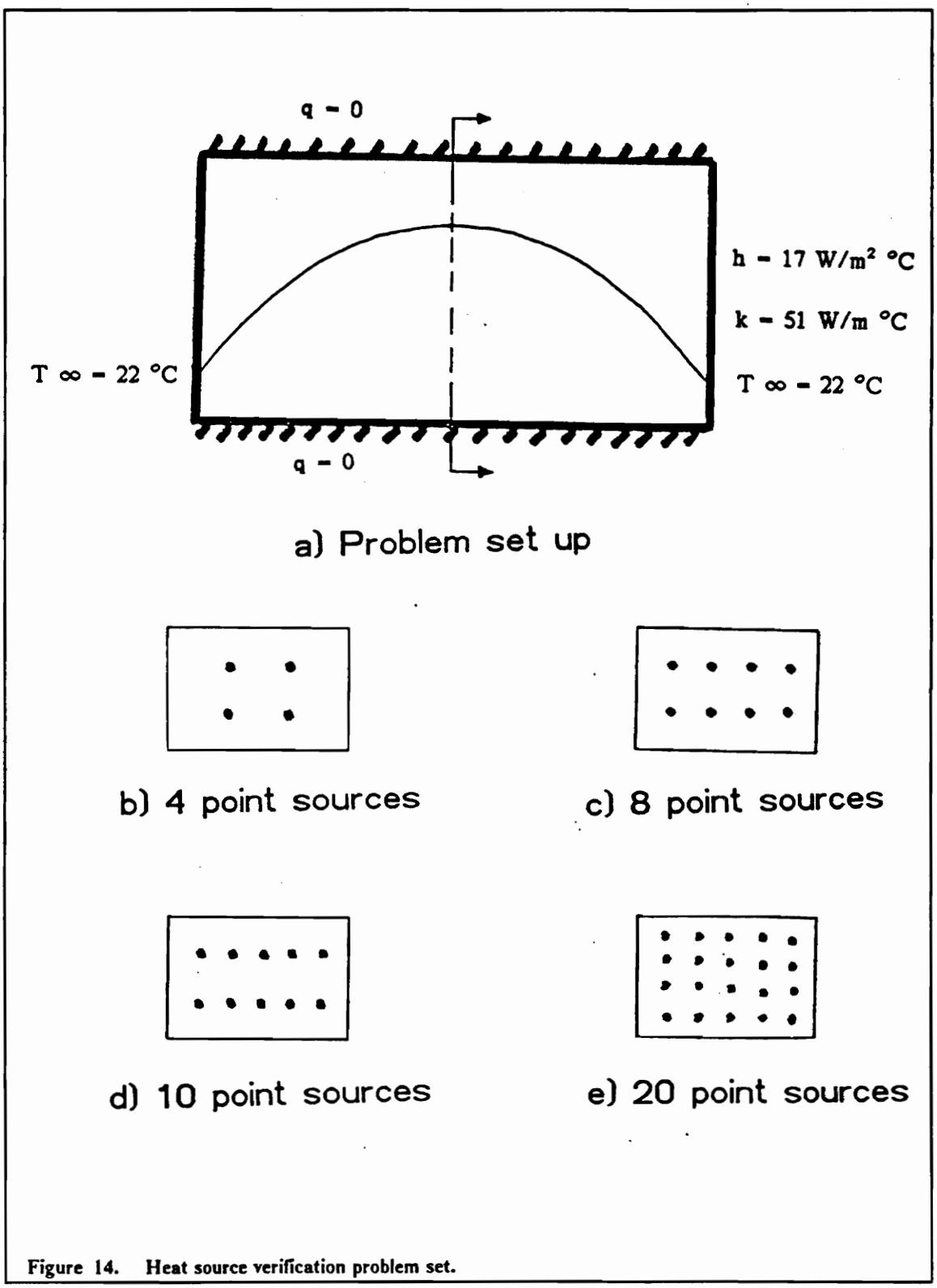

Figure 14. Heat source verification problem set.

Plot showing the temperatures across the plane wall.

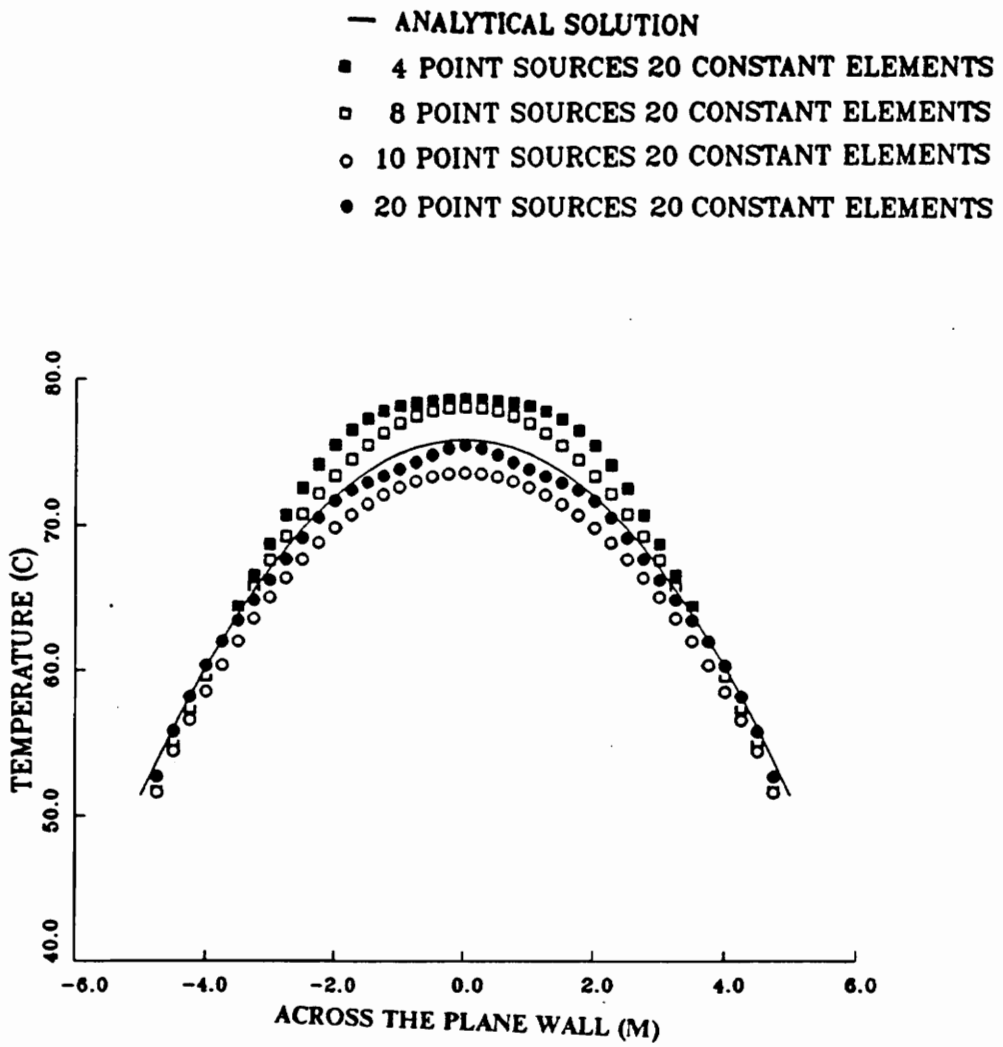

Figure 15. Heat source verification - Constant elements model.

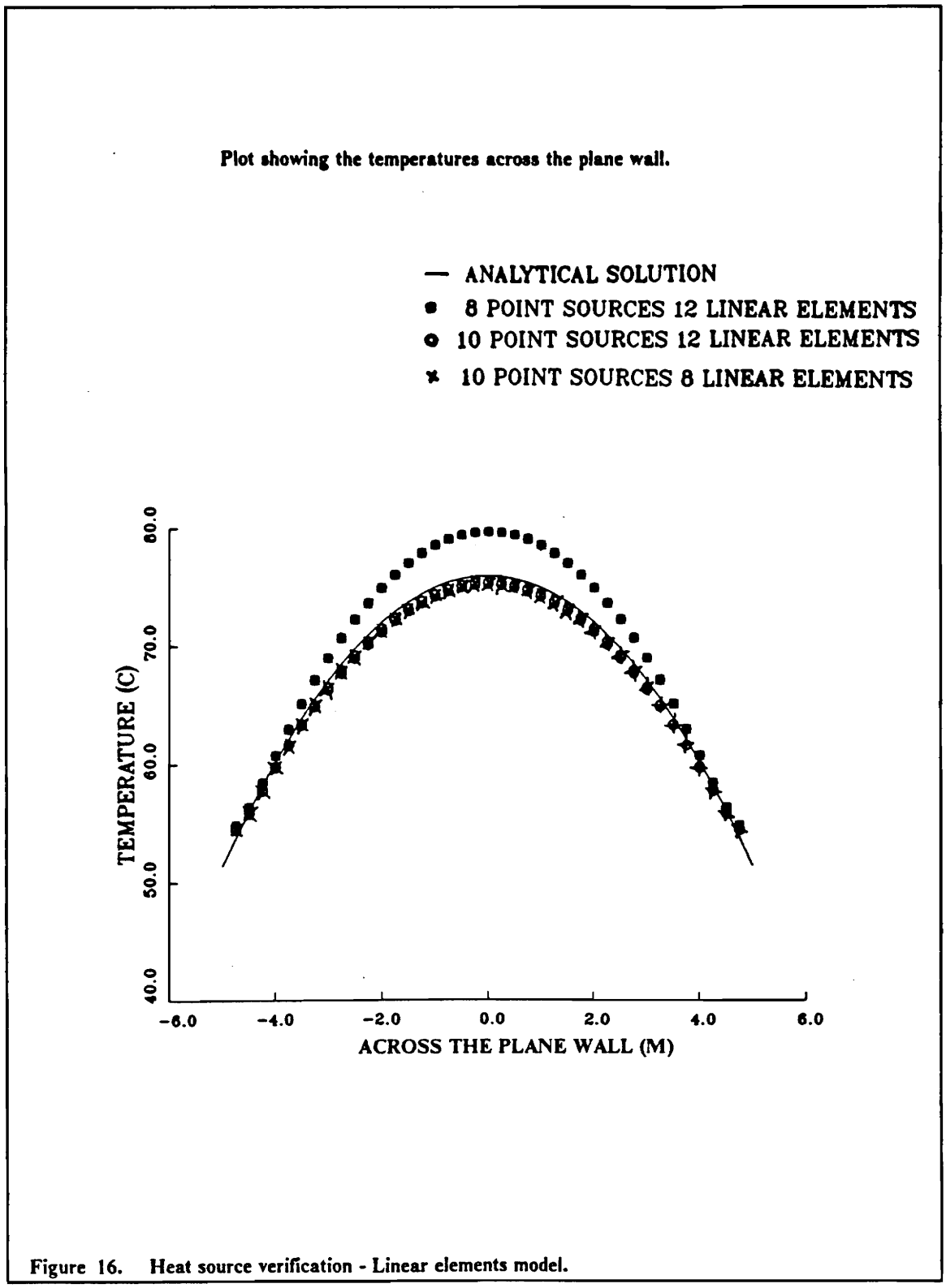

Figure 16. Heat source verification - Linear elements model.

demonstrated that for the purpose of this study, the cartridge heaters could be represented as concentrated point sources.

3.5.3. Die Modeling

The die was modeled with the same element size as the finite difference model except only the boundaries were discretized. Only half of the die was modeled and the plane of symmetry was treated as an adiabatic surface with zero heat flux. The insulated surfaces will have zero fluxes and the free convection surfaces will employ the mixed boundary condition. The internal temperatures calculated are the 39 discrete points along the length of the die cavity and 9 monitoring temperature points alternately spaced along the cartridge heaters. In fact, the monitoring points are coincident with the predrilled holes for the thermocouples. These monitoring temperatures will provide information for process control purposes. After several trials, it was found that two models, one consisting of 86 constant elements and one with 86 linear elements, both predicted a smooth temperature profile in close agreement with the finite difference model.

3.5.4. Results

The boundary element models were then run on the three test cases. Since this is a four-side-insulated model which is completely insulated except at the ends and no experimental results are available, the boundary element results were compared with the finite difference four-side-insulated model. Figures 18, 19 and 20 compare the temperature profiles for all three test cases. The boundary element solutions were run with both constant and linear element models. As expected, the boundary element solutions resulted in higher temperature than the finite difference model because the boundary element method computes the temperature at the point while the temperature at a node in the finite difference method is the average temperature of that

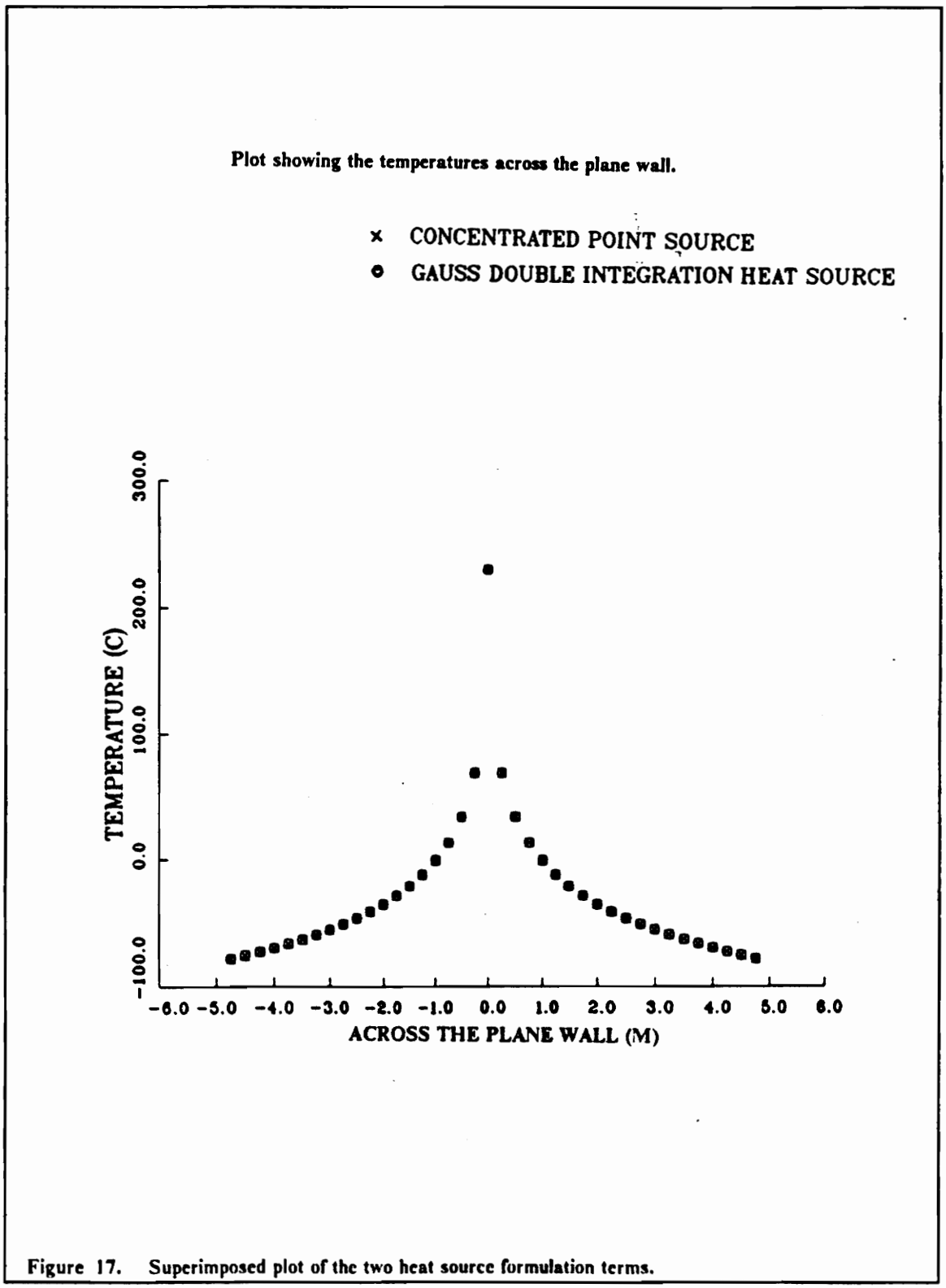

Figure 17. Superimposed plot of the two heat source formulation terms.

mesh region. From these plots, it was also observed that the linear elements predicted a moderate temperature, higher than the finite difference prediction but lower than the constant boundary element model. Table 2 shows the results of the percent difference between total heat lost and the total heat input for the three models and three test cases. The linear elements have the smallest error. From these tests, it was decided that the linear boundary element model would be used in the design optimization method for synthesizing the temperature profile.

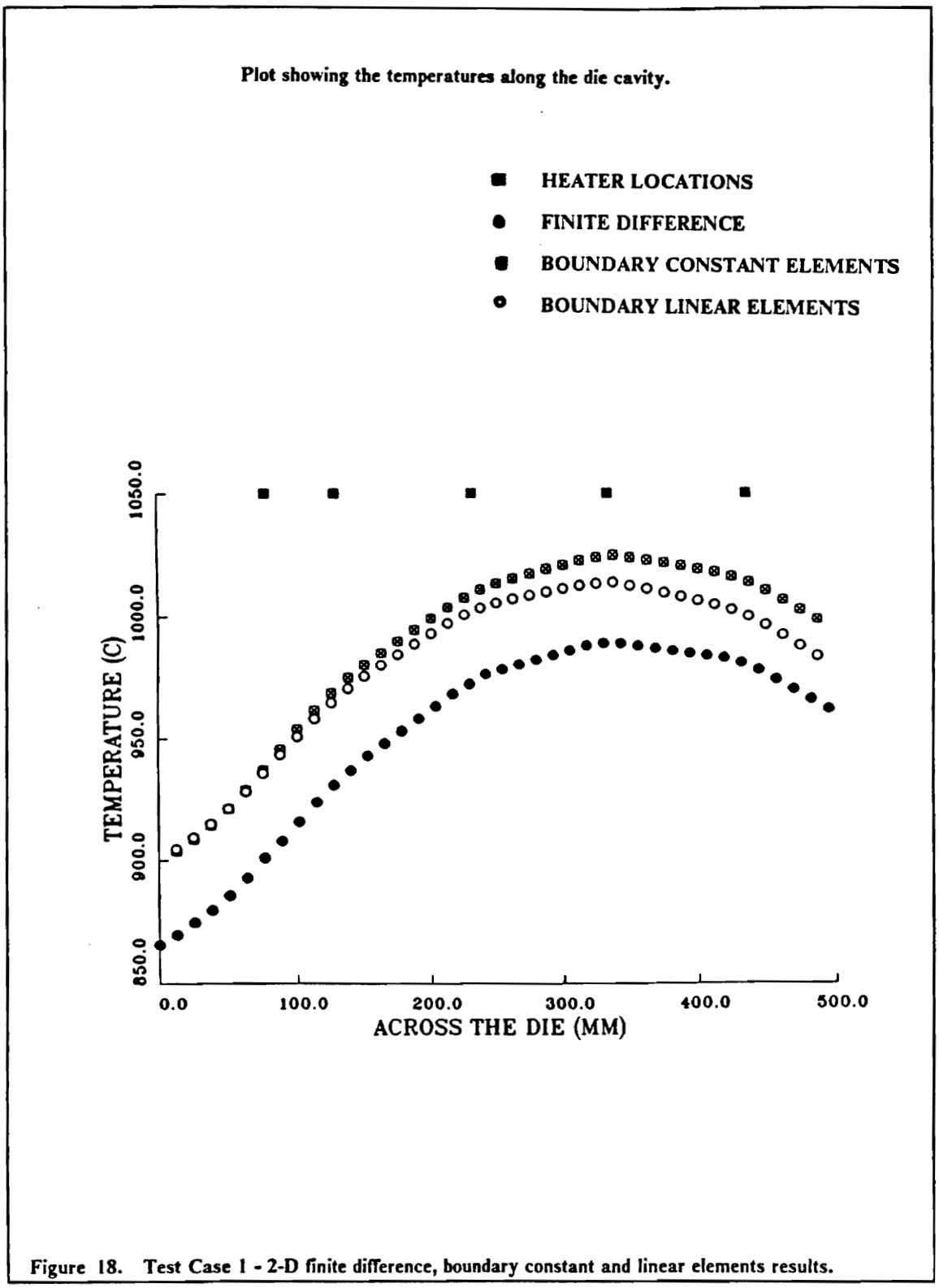

Figure 18. Test Case 1 - 2-D finite difference, boundary constant and linear elements results.

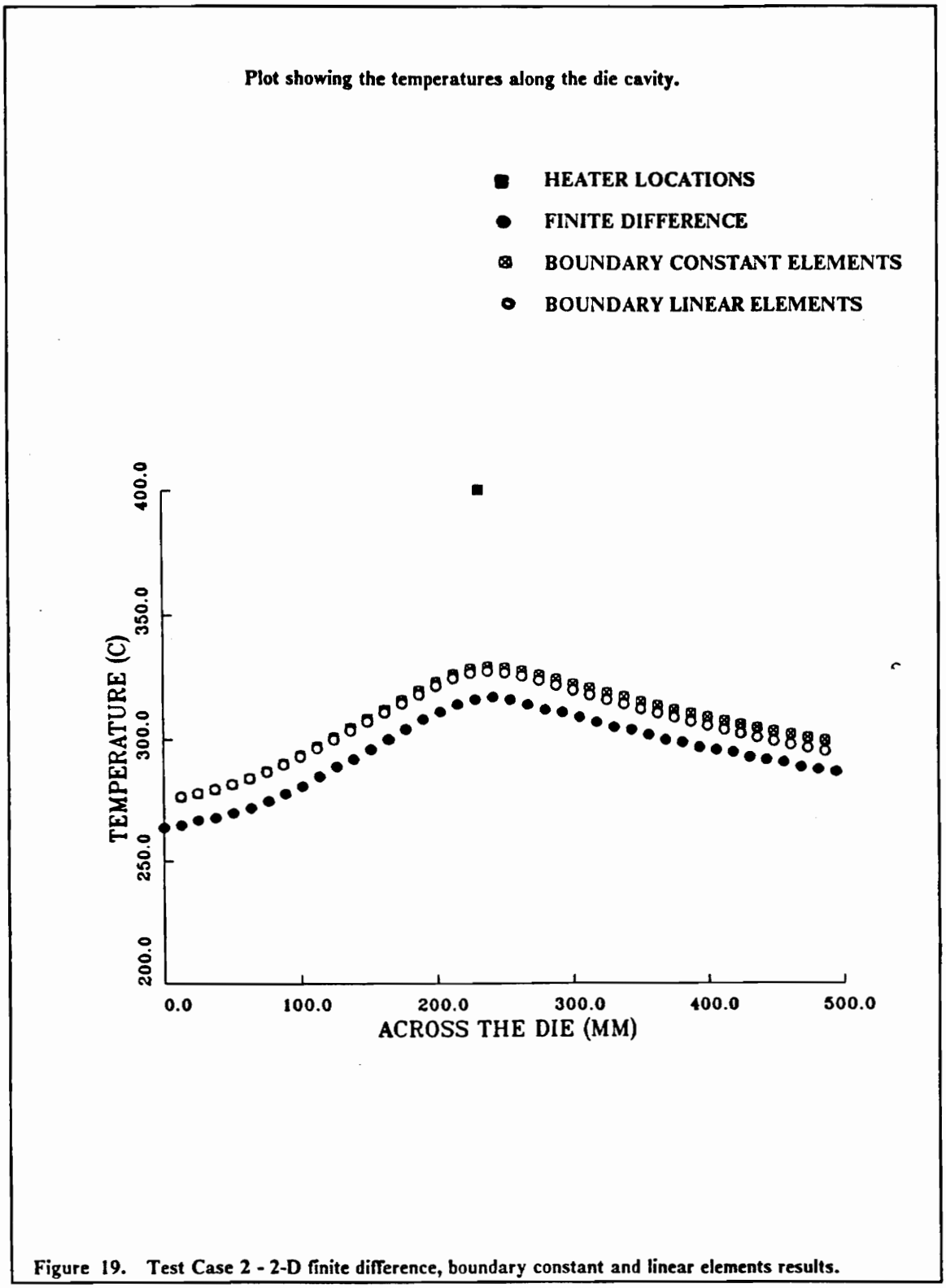

Figure 19. Test Case 2 - 2-D finite difference, boundary constant and linear elements results.

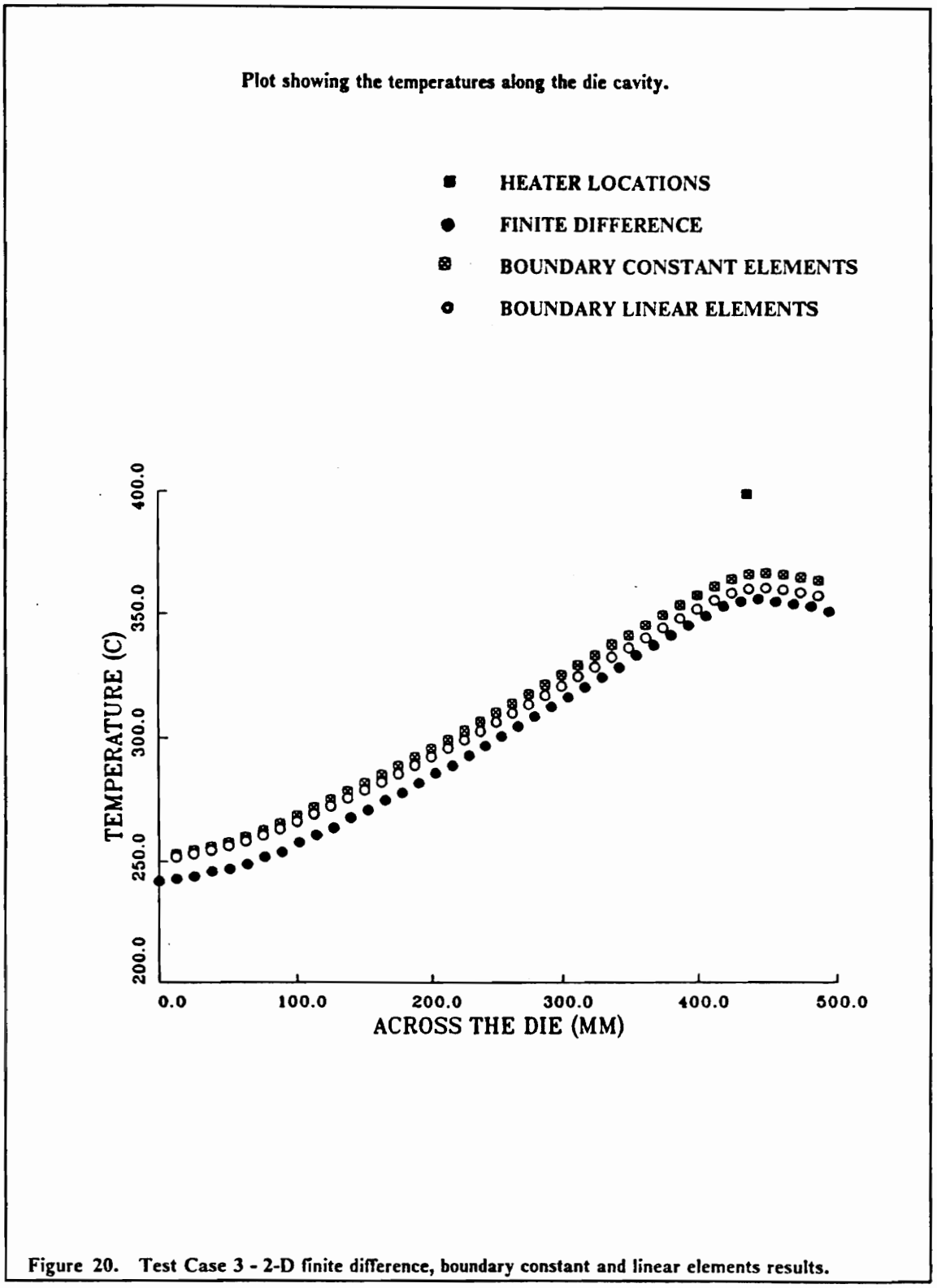

Figure 20. Test Case 3 - 2-D finite difference, boundary constant and linear elements results.

Table 2. Energy balance analysis for comparing the three models.

METHOD	TEST CASE 1 295.00	TEST CASE 2 85.40	TEST CASE 3 85.40	<TOTAL POWER(W)>
FD	293.16 (0.6239%)	84.29 (1.2995%)	84.22 (1.3828%)	<TOTAL POWER(W)> (% OF ERROR)
BCE	295.57 (0.2242%)	85.60 (0.2361%)	85.56 (0.1834%)	<TOTAL POWER(W)> (% OF ERROR)
BLE	294.77 (0.07717%)	85.325 (0.08790%)	85.324 (0.08926%)	<TOTAL POWER(W)> (% OF ERROR)

NOTE : FD = FINITE DIFFERENCE
BCE = BOUNDARY CONSTANT ELEMENT
BLE = BOUNDARY LINEAR ELEMENT

Chapter IV. Design Optimization

4.1. General

The design optimization technique is used to synthesize the heating configuration to produce the desired production temperature profile. The heating configuration includes three variables, which are the number of heaters, power input and location of the heaters. The goal of the design optimization method is to choose the number of heaters, the input power and heater location to minimize the error between the calculated and desired production temperature profile.

4.2. Design Optimization Requirements

A design optimization method is a mathematical process of synthesizing a best design from a set of possible alternative solutions. It normally depends on a numerical method for solution. The cost of using this design method is the requirement of a high performance computational machines

due to the iterative procedures. The procedures here imply that the synthesis of the design will take place over several iterations before an optimum design is obtained to satisfy all the design criteria and constraints.

There are several requirements that need to be defined before the design optimization method can be implemented. Usually the domain of a design problem can be very wide. Therefore, the first step is to narrow the boundaries of the design problem to be optimized. In this study, the boundary of the problem was delineated to examine the heat transfer of the pultrusion die, especially the production temperature profile. A set of design variables is defined to characterize the design. For this pultrusion process study, the design variables are the number of cartridge heaters, the input power and location of each cartridge heater. Design criteria is then prepared and formulated into an objective function to evaluate and select an optimum design. The optimum design either minimizes or maximizes the objective function. If a problem has more then one objective, then one of them will be the primary and the rest are the secondary objectives. This can be done by assigning a heavier weight on the primary and less on the secondary objectives. Design trade-offs are involved here because decisions need to be made on determining the importance of each objective to the design problem. For this pultrusion process study, the objective could be specified as minimizing the error between the desired and computed temperature profiles or minimizing the power input to the heaters. Some of the minor objectives can be formulated into design constraints. For engineering problems, the design variables are usually constrained. In this study, the power input to these particular cartridge heaters has to be greater than zero but less than 85.4 watts. Design constraints will actually reduce the size of the feasible region for the optimization search routines. The constrainted optimization search is now more complicated because the search routines need to check and make sure that the design constraints are not violated.

Generally, design optimization methods are associated with either linear or nonlinear programming techniques. This depends on the functions (i.e., objective and constraints) involved in the design problem. Since the objective and constraint functions in this study are nonlinear, the design problem is a nonlinear programming problem. In addition to the requirements mentioned above,

there are some other independent variables whose values are fixed by outside influences such as the geometry of the pultrusion die, and outer and inner noises [11]. The outer noises represent uncontrollable variation in the design parameter such as the ambient temperature which was treated as 22 °*C*. This value changes according to the environment surrounding the die. The inner noises are unavoidable variation in the design variables such as the wear of the die cavity or fluctuation of the power input to the heaters and the computational error associated with the heat transfer model. The final form of the design optimization method is a system performance model that relate the way the design criteria influence the constrained design variables. This mathematical method offers an inexpensive and faster way of performing design trade-offs to determine a "better" design without using a real system.

4.3. Nonlinear Programming Formulation

Since analytical solutions are not obtainable, the nonlinear programming methods are based on numerical methods for solutions. Usually, an initial design is estimated and improved iteratively until it satisfies the design criteria. Detailed derivations and theory involved in developing a mathematical model are not in the scope of this study. There is a large volume of literature available for design optimization methodologies. In this study, the standard IMSL optimization routines were used [12] and the basic mathematical concepts involved in formulating the IMSL nonlinear programming routines are included in Appendix E.

4.4. Sensitivity Analysis

After an optimum design was obtained, a sensitivity analysis was conducted at the optimum design values. This value gives an indication of how sensitive the pultrusion die is with respect to the changes in the power input to the cartridge heaters. Sensitivity analysis gives information regarding the controllability of the pultrusion die. In addition, the sensitivity of the outer and inner noises can be examined from this sensitivity analysis. A less sensitive system means that the outer and inner noises have less influence on the system. A central difference method was used to compute the sensitivities of the design variables. The principal of first-order variation for a unit change in the independent variable as approximated by a central difference method [13] is

$$\frac{\partial f}{\partial x_i} = \frac{f(x_1, x_i + 1, \ldots, x_n) - f(x_1, x_i - 1, \ldots, x_n)}{2}. \qquad [8]$$

4.5. Design Optimization Modeling

Several alternative models were investigated before a final model was selected. The possible alternative models were based on the way the objective function was defined, the choice of the constraint functions and the treatment of the design variables. For example, the number of the design variables in this study can be 10, which are the power input to each cartridge heater and the locations are fixed at the predrilled holes on the die. Another model using 20 design variables allows the location of each heater to change and move along the length of the die. Two design optimization models were set up based on the two treatments of the design variables as mentioned above.

4.5.1. With 10 Design Variables

The lower and upper bounds for these design variables will be from 0 to 85.4 watts. There will be 20 inequality constraints for the 10 design variables i.e.,

$$g_i(x_i) \equiv x_i \geq 0 \quad \text{for} \quad i = 1 \text{ to } 10 \qquad [9]$$

$$g_{i+10}(x_i) \equiv 85.4 - x_i \geq 0 \quad \text{for} \quad i = 1 \text{ to } 10 \qquad [10]$$

where g_i and x_i are the constraints and design variables, respectively. There were no equality constraints placed on the power. The number of heaters required for a given production temperature profile is determined by the optimization procedures. The program will start with 10 heaters and if only 5 are required, the remaining 5 will be switched off (i.e., have a value of 0 watt).

As an initial investigation, several objective functions were examined. The examined objective functions were to minimize the sum of square error between the desired and predicted temperature profile, to minimize the power input, the sensitivity analysis and any combination of these including the weighted and unweighted factors. The reason for including the sensitivity analysis into the objective function is to examine the sensitivity of the optimum design values to the predicted temperature profile. If the predicted temperature profile is not sensitive to a change in the optimum design values of $\pm$ 1 unit, the inclusion of the sensitivity analysis will have negligible impact on the optimum design values. The primary criterion for the objective function is to minimize the sum of square error of the temperatures, the rest of the design criteria were treated as secondary objectives. By including the secondary objectives both as weighted and unweighted functions, the obtained optimum design values were similar to an objective function with only a primary objective. This also means that the temperature profile (or indirectly the laboratory-scale die) is not sensitive to the changes of power input to $\pm$ 1 watts. The justification for a 1 unit perturbation was chosen due to the limited resolution of the physical instrument to measure power. The

objective function will be formulated as the sum of the square error between the desired and predicted temperature profile of the following form :

$$f(X) = \sum_{i=1}^{n} (T_{di} - T_{pi})^2 \qquad [11]$$

where T_d and T_p are the desired and predicted temperatures at a given point i. In this study, n is equal to 39 points. With only one term in the objective function the computational time, especially in iterative procedures, will be considerably reduced.

4.5.2. With 20 Design Variables

The second model consists of 20 design variables, 10 power inputs and 10 location of the heaters. The lower and upper bounds for the 10 power input variables are the same, but the location of the heaters will be from 0 to 0.5 *m*, which was the length of the die. These heater locations are scaled up by 200 to have the same feasible bound as the power inputs. There are 11 constraints associated with these location variables, which gives a total of 31 inequality constraints. These additional constraints are needed in order to avoid the overlapping and over crossing of the heater locations. The following constraints were imposed :

$$g_{21}(x_{11}) \equiv x_{11} - 0.005 \geq 0 \qquad [12]$$

$$g_{i+21}(x_{i+10}, x_{i+11}) \equiv x_{i+11} - x_{i+10} - 0.01 \geq 0 \quad \text{for} \quad i = 1 \text{ to } 9 \qquad [13]$$

$$g_{31}(x_{20}) \equiv 0.495 - x_{20} \geq 0 \ . \qquad [14]$$

The overlapping of the successive heater locations was eliminated by having a separation of 0.01 *m* between heaters giving a net clearance of 4 *mm* (10 *mm* minus the heater diameter of 6 *mm*).

4.6. Testing Procedures

The same three test cases were used to test the optimization programs. For each test case, there were three runs based on three different convergence rates of 0.1, 0.01 and 0.001. These tests were performed using the temperature profiles generated by the four-side-insulated linear boundary element program as the desired temperature profiles. The optimization programs were to determine the required power input to the die to generate the above desired temperature profiles. The four-side-insulated linear boundary element model used to solve the heat transfer problem was incorporated into the optimization program. Therefore, the total power input to the die to generate the desired temperature profile must equal the optimum design power input values. The purpose of running these tests was to verify the design optimization programs. There will be 9 runs with three test cases and three convergence rates. Since there were two optimization programs based on the two treatments of the design variables, this will give a total of 18 runs.

The second test was performed with the temperature profiles generated by the two-side-insulated finite difference model as the desired temperature profiles. The optimization programs were to synthesize the optimum design values of the heater locations and power input. The synthesized power input will not be the same as the power input to the die for generating the two-side-insulated temperature profiles. In fact, the synthesized input values are going to be less than those obtained for the two-side-insulated model. This provides a way of studying how much power can be saved by further insulation of the die as compared to the two-side-insulated model. As before, there will be 18 runs comprised of three test cases with three different convergence rates in two optimization programs.

Table 3 shows the initial stage of the three test cases used to run the optimization programs. For the 20 design variables model, the 10 extra design variables for the location of the heaters will have an initial stage of zero position.

Table 3. Initial stage of the three test cases used to run the optimization programs.

HEATER NO.	TEST CASE 1 POWER (W)	TEST CASE 2 POWER(W)	TEST CASE 3 POWER(W)
1			
2			
3			
4			
5	50.0	50.0	
6	50.0		
7	50.0		
8	50.0		
9	50.0		50.0
10			
TOTAL =	250.0	50.0	50.0

Chapter V. Results

5.1. General

The results are presented in tabular form. The information included consists of the total power input, the power and location of each cartridge heater, the value of the final objective function, the number of iterations and the results of the sensitivity analysis. The resulting temperature profiles from the three convergence rates are superimposed into a plot and the location of the heaters are also included in the plot. The smaller the convergence rate, the closer the total power converged to the desired power input. The temperature profiles for the three convergence rates were exactly superimposed on top of each other for all three test cases and two optimization programs (Figures 21 to 32). This suggested that all the test runs did converge to the desired result. For this application, there is no apparent practical advantage of using a convergence rate smaller than 0.1. The sensitivity analysis results for all the test runs were very small. It can be concluded that this laboratory-scale die is not sensitive to a change of power in the range of ± 1 watts. The following are the specific results from the test runs as described above.

5.2. *Verification*

This section describes the results obtained from the verification of the optimization programs. The simulated temperature profiles were exactly overlapped with the desired temperature profile for all three test cases and two optimization programs (Figures 21 to 26). This was expected because of the way the objective function was set up to minimize the sum of square error between the simulated and desired temperature profiles. Numerical examination of the results shows small differences, especially in the amount power input to each cartridge heater. This section is divided into two parts according to the type of optimization programs used.

5.2.1. Results of the 10 Design Variables Model

Tables 4, 5 and 6 and Figures 21, 22 and 23 tabulate and show the results of the three test cases for this 10 design variable optimization model.

Test Case 1

Although the desired temperature profile was generated with 5 heaters, the optimum design required all 10 heaters. The total power input to the die was 295 watts and the optimum total power was roughly 295 $\pm$0.7 watts. The power distribution on each cartridge heater varied depending on the convergence rate (Table 4).

Test Case 2

The desired temperature profile was generated by one heater at heater location number 5 with a power input of 85.4 watts. With convergence rate of 0.001, the optimum design values matched the desired power input. The 0.1 and 0.01 convergence rates used 3 heaters at heater number 4, 5 and 6 with a total power of 85.47 watts (Table 5).

Test Case 3

The desired temperature profile was generated by one heater at heater number 9 with a power input of 85.4 watts. All three convergence rates produced an identical result with total power of 85.58 watts at heater number 8,9 and 10 (Table 6).

5.2.2. Results of the 20 Design Variables Model

Tables 7, 8 and 9 and Figures 24, 25 and 26 tabulate and show the results of the three test cases for the 20 design variables optimization model. The simulated temperature profiles for 20 design variables model were identical respectively for all three test cases as the 10 design variables model. Numerical examination of the results show there are some differences especially on the heater locations and power distribution to each heater.

Test Case 1

The optimum results used all 10 available heaters with a different input of power to each of them for the three convergence rates. The scattering of the heater locations were matched up with the initial heater locations except with several more on the beginning and end of the die (Figure 24). The total optimum power for all three convergence rates were 295.01 watts as compared to the desired power input of 295 watts (Table 7).

Test Case 2

Again, the optimum results for all three convergence rates used all 10 heaters, but they were closely concentrated in heater number 5 region and were 10 *mm* apart (Figure 25). These results coincide with the allowable clearance for each successive heater as specified in the design constraints. The results obtained for the three convergence rates were identical with a total power of 85.43 watts as compared to the desired power input of 85.4 watt at heater location number 5 (Table 8).

Test Case 3

For this test case the optimum results used only 9 heaters for convergence rates of 0.1 and 0.01, and 7 heaters for convergence rate of 0.001. These heaters were distributed at the heater location

number 9 where the original heater was located (Figure 26). As before, these heaters were 10 *mm* apart. The total optimum power for convergence rate 0.1 and 0.01 were identical, which was 85.49 watts and 85.46 watts, for the convergence rate 0.001. The desired total power was 85.4 watts.

Table 4. Test Case 1 - Verification with 10 design variables model.

CONVERGENCE RATE	HEATER NO.	POWER (W)	SENSITIVITY ANALYSIS
TEST CASE 1	2	59.0	
	3	59.0	
	5	59.0	
	7	59.0	
	9	59.0	
	TOTAL POWER = 295.0		
0.1	1	26.760	-0.11104
	2	34.837	-0.18572
	3	38.960	-0.21380
	4	22.922	0.85942
	5	47.410	2.5809
	6	28.343	1.2077
	7	22.657	-1.6938
	8	24.280	-2.1539
	9	27.871	-0.30831
	10	21.638	1.8610
	TOTAL POWER = 295.68 % OF ERROR = 0.23 %	OBJ. FUNCT. VALUE = 83.872 NO. OF ITERATIONS = 17	
0.01	1	17.468	0.45151
	2	38.410	-0.33690
	3	51.802	-0.23938
	4	23.609	0.51042
	5	36.933	0.04438
	6	20.877	-0.38006
	7	28.714	-0.24847
	8	35.127	0.45698
	9	33.321	0.04819
	10	9.002	-0.16097
	TOTAL POWER = 295.26 % OF ERROR = 0.09 %	OBJ. FUNCT. VALUE = 20.199 NO. OF ITERATIONS = 24	
0.001	1	8.192	0.02564
	2	46.952	-0.17347
	3	59.717	0.05048
	4	14.094	0.07269
	5	34.242	-0.22078
	6	26.628	0.12213
	7	33.747	0.09140
	8	26.638	0.05471
	9	31.825	-0.22066
	10	13.150	0.09384
	TOTAL POWER = 295.18 % OF ERROR = 0.06 %	OBJ. FUNCT. VALUE = 9.2022 NO. OF ITERATIONS = 31	

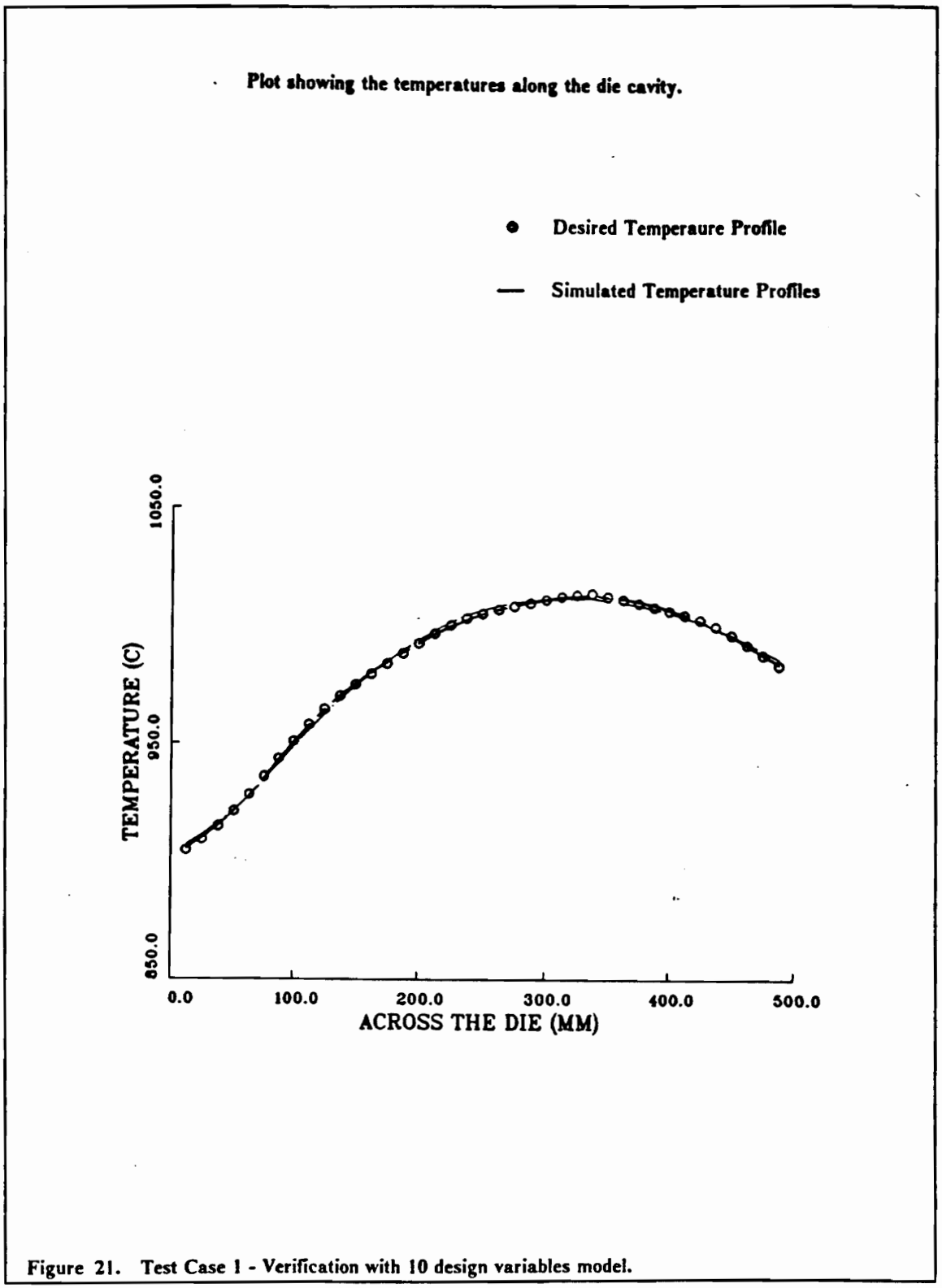

Figure 21. Test Case 1 - Verification with 10 design variables model.

Table 5. Test Case 2 - Verification with 10 design variables model.

CONVERGENCE RATE	HEATER NO.	POWER (W)	SENSITIVITY ANALYSIS
TEST CASE 2	5	85.4	
TOTAL POWER = 85.4			
0.1	4	10.185	4.6389
	5	64.814	4.1748
	6	10.477	6.2387
TOTAL POWER = 85.476		OBJ. FUNCT. VALUE = 13.333	
% OF ERROR = 0.09 %		NO. OF ITERATIONS = 34	
0.01	4	10.184	-0.32425
	5	64.813	-0.89183
	6	10.473	1.10500
TOTAL POWER = 85.470		OBJ. FUNCT. VALUE = 13.315	
% OF ERROR = 0.08 %		NO. OF ITERATIONS = 35	
0.001	5	85.4	0.07762
TOTAL POWER = 85.4		OBJ. FUNCT. VALUE = 0.00035	
% OF ERROR = 0.0 %		NO. OF ITERATIONS = 53	

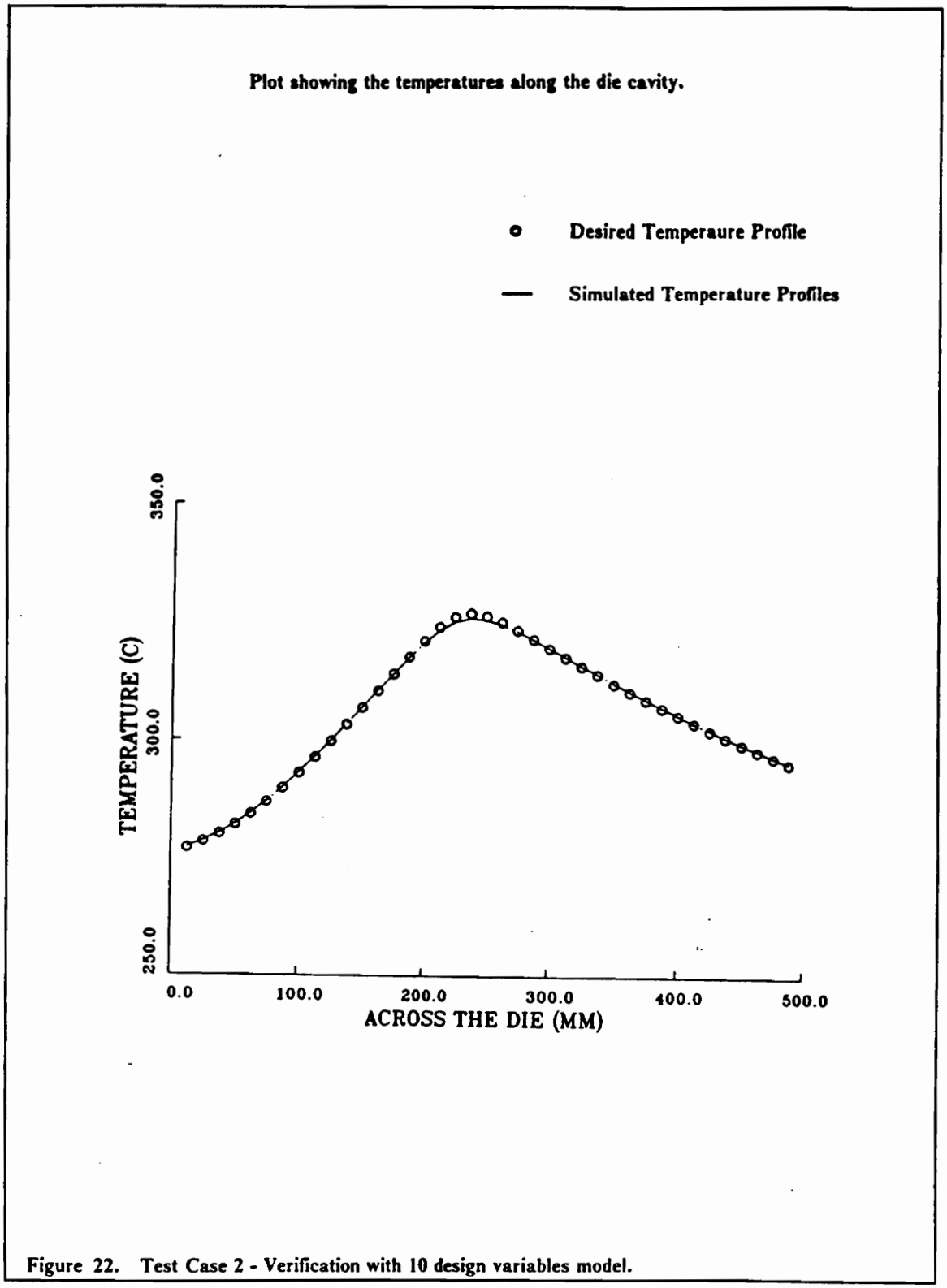

Figure 22. Test Case 2 - Verification with 10 design variables model.

Table 6. Test Case 3 - Verification with 10 design variables model.

CONVERGENCE RATE	HEATER NO.	POWER (W)	SENSITIVITY ANALYSIS
TEST CASE 3	9	85.4	
	TOTAL POWER = 85.4		
0.1	8	7.5951	-0.28648
	9	62.669	-0.44182
	10	15.314	0.39644
	TOTAL POWER = 85.578	OBJ. FUNCT. VALUE = 6.9611	
	% OF ERROR = 0.21 %	NO. OF ITERATIONS = 22	
0.01	8	7.5951	-0.28648
	9	62.669	-0.44182
	10	15.314	0.39644
	TOTAL POWER = 85.578	OBJ. FUNCT. VALUE = 6.9611	
	% OF ERROR = 0.21 %	NO. OF ITERATIONS = 22	
0.001	8	7.5951	-0.28648
	9	62.669	-0.44182
	10	15.314	0.39644
	TOTAL POWER = 85.578	OBJ. FUNCT. VALUE = 6.9611	
	% OF ERROR = 0.21 %	NO. OF ITERATIONS = 22	

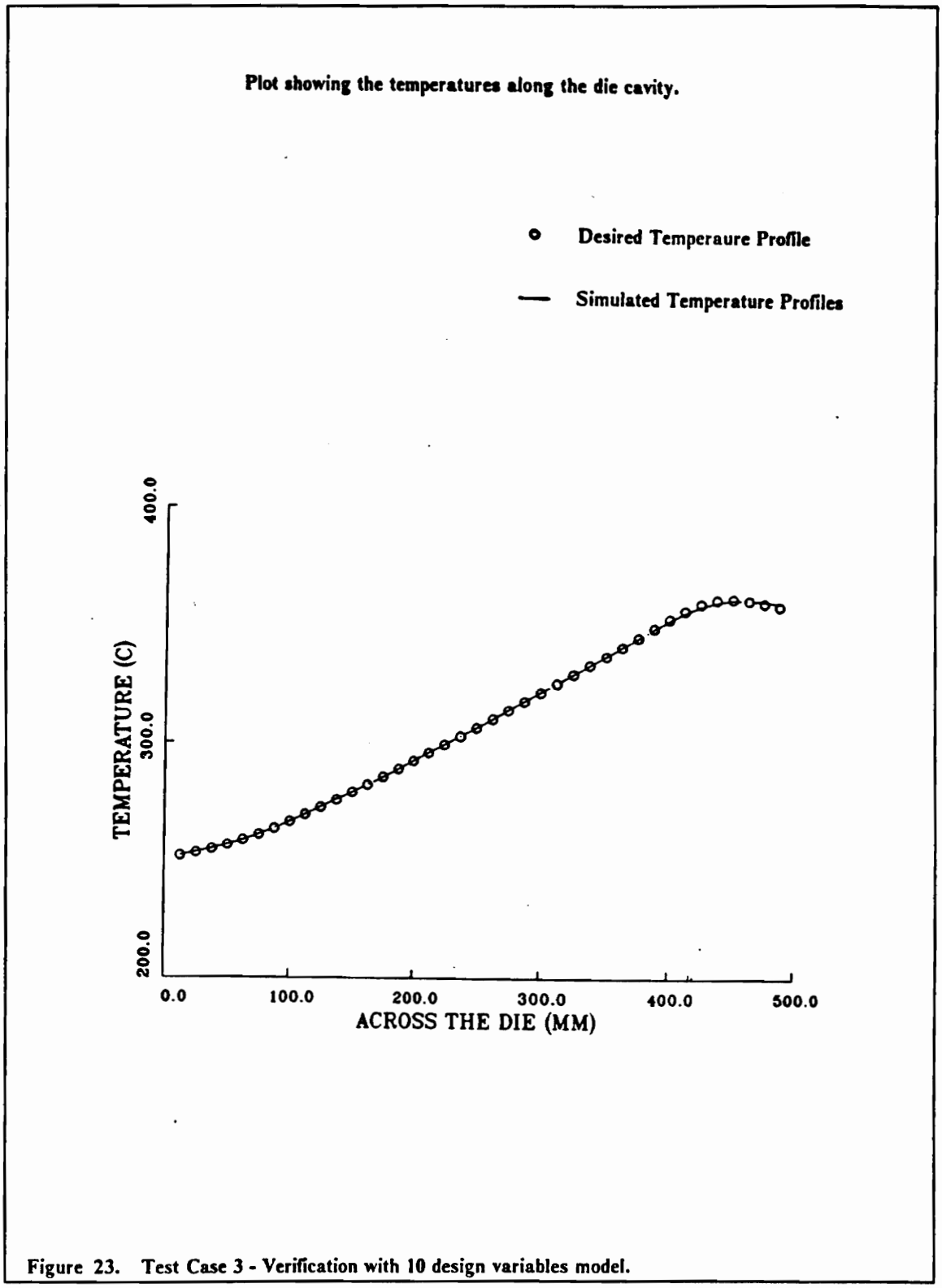

Figure 23. Test Case 3 - Verification with 10 design variables model.

Table 7. Test Case 1 - Verification with 20 design variables model.

CONVERGENCE RATE	HEATER NO.	POWER (W)	LOCATION (MM)	SENSITIVITY ANALYSIS
TEST CASE 1	2	59.0	75.0	
	3	59.0	125.0	
	5	59.0	225.0	
	7	59.0	325.0	
	9	59.0	425.0	
TOTAL POWER = 295.0				
0.1	1	4.4231	46.299	0.26533
	2	4.6334	56.299	0.26770
	3	4.5782	66.299	0.27071
	4	4.4237	76.299	0.27504
	5	53.877	86.299	0.28214
	6	53.673	142.82	0.33009
	7	53.525	239.94	0.33766
	8	53.227	331.82	0.37188
	9	53.240	426.38	0.40863
	10	9.4071	471.39	0.40362
TOTAL POWER = 295.01 OBJ. FUNCT. VALUE = 2.8184				
% OF ERROR = 0.004 % NO. OF ITERATIONS = 21				
0.01	1	4.4224	46.061	0.24958
	2	4.6327	56.061	0.24955
	3	4.5772	66.061	0.24971
	4	4.4222	76.061	0.25024
	5	53.875	86.061	0.25130
	6	53.673	142.82	0.26230
	7	53.530	239.74	0.20041
	8	53.233	331.66	0.17968
	9	53.242	427.19	0.20058
	10	9.4077	464.47	0.19466
TOTAL POWER = 295.01 OBJ. FUNCT. VALUE = 2.7025				
% OF ERROR = 0.004 % NO. OF ITERATIONS = 25				
0.001	1	3.0988	43.076	-0.10548
	2	3.4359	53.076	-0.10612
	3	3.5086	63.076	-0.10672
	4	3.4513	73.076	-0.10735
	5	52.979	84.157	-0.10843
	6	51.975	131.57	-0.11382
	7	58.893	231.36	-0.11907
	8	58.478	333.57	-0.12469
	9	52.004	434.06	-0.12395
	10	7.1843	447.90	-0.12343
TOTAL POWER = 295.01 OBJ. FUNCT. VALUE = 0.05121				
% OF ERROR = 0.004 % NO. OF ITERATIONS = 68				

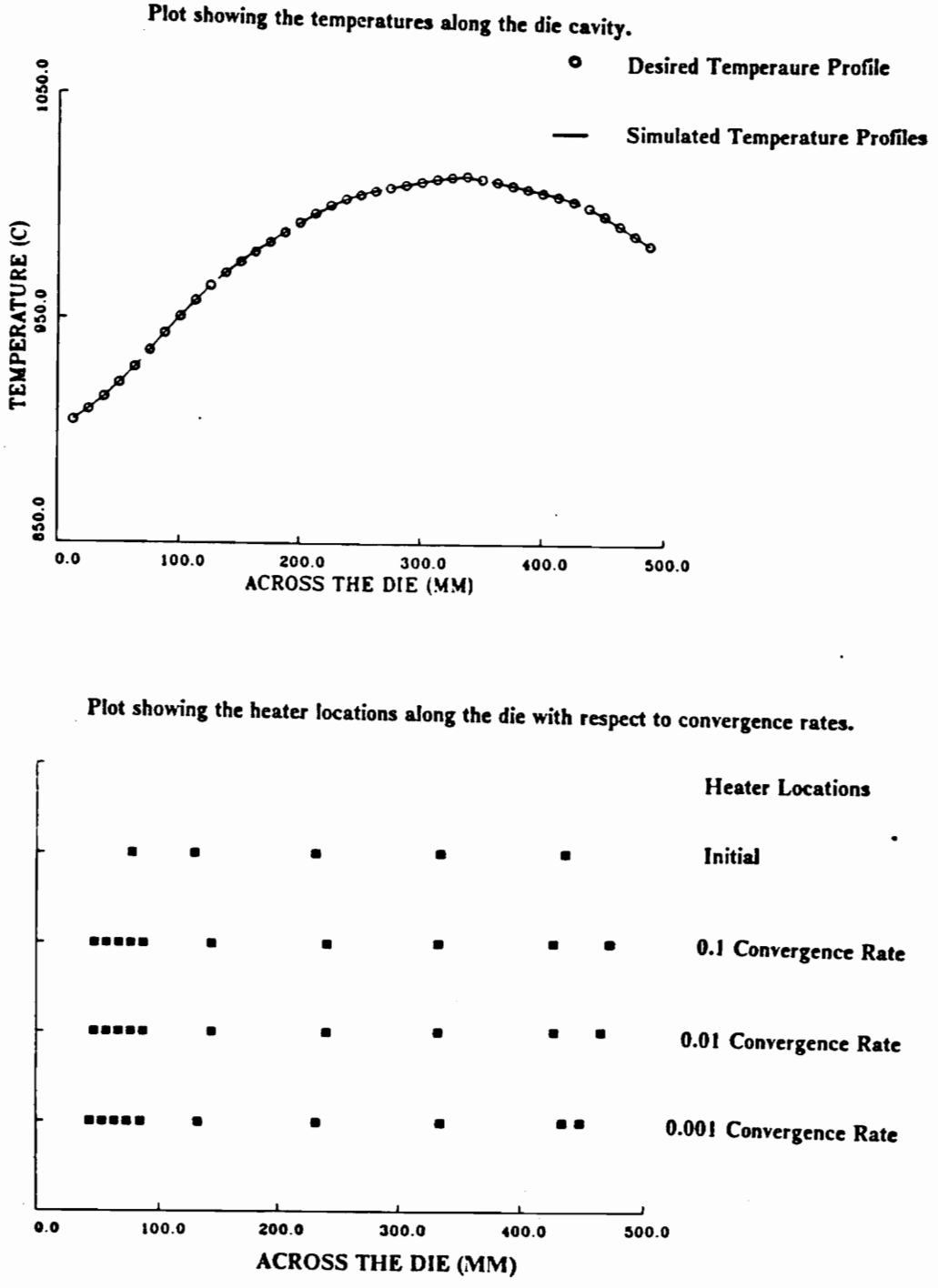

Figure 24. Test Case 1 - Verification with 20 design variables model.

Table 8. Test Case 2 - Verification with 20 design variables model.

CONVERGENCE RATE	HEATER NO.	POWER (W)	LOCATION (MM)	SENSITIVITY ANALYSIS
TEST CASE 2	5	85.4	225.0	
	TOTAL POWER = 85.4			
0.1	1	3.5635	188.98	0.10828
	2	3.6863	198.98	-0.08756
	3	3.7685	208.98	-0.24748
	4	3.8018	218.98	-0.35909
	5	53.155	228.98	-0.41313
	6	3.6642	238.98	-0.40095
	7	3.5935	248.98	-0.31781
	8	3.5077	258.98	-0.17138
	9	3.3966	268.98	0.02125
	10	3.2951	278.98	0.24480
	TOTAL POWER = 85.433		OBJ. FUNCT. VALUE = 4.4232	
	% OF ERROR = 0.04 %		NO. OF ITERATIONS = 11	
0.01	1	3.5635	188.98	0.10828
	2	3.6863	198.98	-0.08756
	3	3.7685	208.98	-0.24748
	4	3.8018	218.98	-0.35909
	5	53.155	228.98	-0.41313
	6	3.6642	238.98	-0.40095
	7	3.5935	248.98	-0.31781
	8	3.5077	258.98	-0.17138
	9	3.3966	268.98	0.02125
	10	3.2951	278.98	0.24480
	TOTAL POWER = 85.433		OBJ. FUNCT. VALUE = 4.4232	
	% OF ERROR = 0.04 %		NO. OF ITERATIONS = 11	
0.001	1	3.5635	188.98	0.10828
	2	3.6863	198.98	-0.08756
	3	3.7685	208.98	-0.24748
	4	3.8018	218.98	-0.35909
	5	53.155	228.98	-0.41313
	6	3.6642	238.98	-0.40095
	7	3.5935	248.98	-0.31781
	8	3.5077	258.98	-0.17138
	9	3.3966	268.98	0.02125
	10	3.2951	278.98	0.24480
	TOTAL POWER = 85.433		OBJ. FUNCT. VALUE = 4.4232	
	% OF ERROR = 0.04 %		NO. OF ITERATIONS = 11	

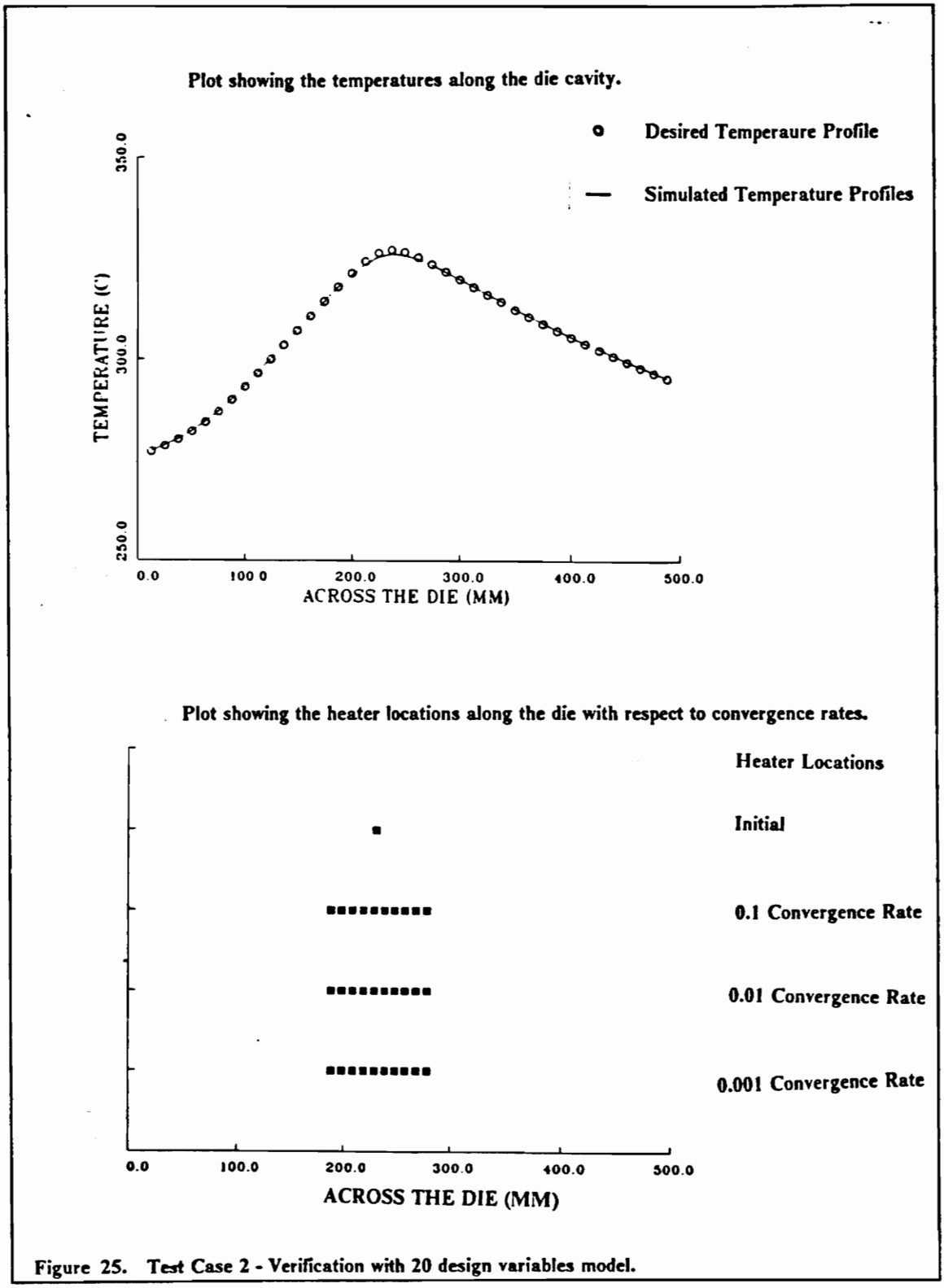

Figure 25. Test Case 2 - Verification with 20 design variables model.

Table 9. Test Case 3 - Verification with 20 design variables model.

CONVERGENCE RATE	HEATER NO.	POWER (W)	LOCATION (MM)	SENSITIVITY ANALYSIS
TEST CASE 3	9	85.4	425.0	
	TOTAL POWER = 85.4			
0.1	2	1.8797	376.22	2.3017
	3	2.2440	386.22	2.0253
	4	2.8997	396.22	1.7787
	5	3.1265	406.22	1.5734
	6	4.8716	416.22	1.4190
	7	5.0660	426.22	1.3247
	8	5.2213	436.22	1.2941
	9	54.713	446.22	1.3164
	10	5.4645	456.22	1.3711
	TOTAL POWER = 85.486		OBJ. FUNCT. VALUE = 4.1500	
	% OF ERROR = 0.10 %		NO. OF ITERATIONS = 17	
0.01	2	1.8797	376.22	2.3017
	3	2.2440	386.22	2.0253
	4	2.8997	396.22	1.7787
	5	3.1265	406.22	1.5734
	6	4.8716	416.22	1.4190
	7	5.0660	426.22	1.3247
	8	5.2213	436.22	1.2941
	9	54.713	446.22	1.3164
	10	5.4645	456.22	1.3711
	TOTAL POWER = 85.486		OBJ. FUNCT. VALUE = 4.1500	
	% OF ERROR = 0.10 %		NO. OF ITERATIONS = 17	
0.001	4	1.9109	392.55	0.17451
	5	2.8253	402.55	0.05803
	6	5.7419	412.55	-0.03433
	7	6.2348	422.55	-0.09452
	8	6.4734	432.55	-0.12093
	9	55.864	442.55	-0.11794
	10	6.4100	452.55	-0.09260
	TOTAL POWER = 85.460		OBJ. FUNCT. VALUE = 1.1908	
	% OF ERROR = 0.07 %		NO. OF ITERATIONS = 40	

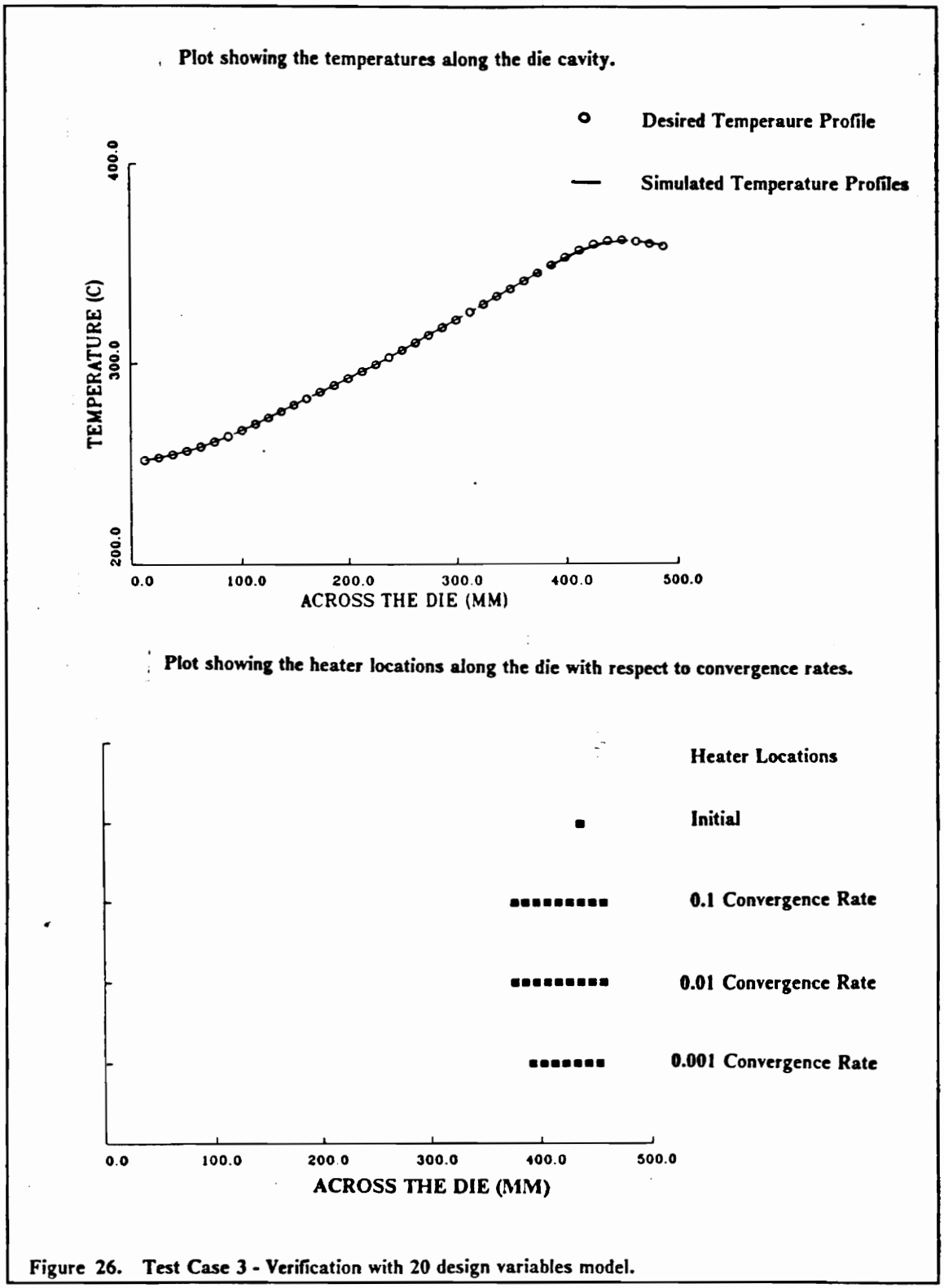

Figure 26. Test Case 3 - Verification with 20 design variables model.

5.3. Power Requirement Examination

This section described the results obtained from the power reduction study. The concept here is to compare the optimum heating configuration obtained from a four-side-insulated boundary element model with a two-sided insulation finite difference model. In this test, the optimization program converged, but the simulated temperature profile did not match the desired temperature profiles except for test case 1 (Figures 27 to 32). The optimization program tried to lower the temperature at the high region to compensate for the temperature at the lower region. But this trade-off was not enough to drive the simulated temperature profile to the desired temperature profile. The conclusion can be drawn from these observations that with a relatively small power input concentrated at a small region, the four-side-insulated model cannot produce the temperatures low enough to match up with the two-side-insulated model. This is due to the fact that the insulated boundary condition prevents heat loss from the die. This also implied that heat sinks as well as sources are required to control temperature profile. This section is divided into two parts according to the type of optimization program used.

5.3.1. Results of the 10 Design Variables Model

Tables 10, 11 and 12 and Figures 27, 28 and 29 tabulate and show the results of the three test cases for the 10 design variable optimization model.

Test Case 1

The two-side-insulated desired temperature profile was generated by 5 heaters with a total of 295 watts. The results obtained form the optimum four-side-insulated model were roughly 79 watts for all three convergence rates. The power was reduced roughly 216 watts. The model using the convergence rate of 0.1 and 0.01 used 9 heaters and the convergence rate of 0.001 used 7 heaters (Table 10).

Test Case 2

The models using the three convergence rates produced identical results for required power. They specified 23.5 watts as compared to 85.4 watts for the total power for the desired temperature profile (Table 11). Only one heater was used, which was heater number 5, the same used by the two-side-insulated model. The power reduction was roughly 62 watts.

Test Case 3

The resulting optimum power was 24.4 watts, which was identical for all the three convergence rates. Only one heater was required at heater location 10, instead of 9, used to generate the desired two-side-insulated temperature profile. The power reduction was roughly 61 watts.

5.3.2. Results of the 20 Design Variables Model

Tables 13, 14 and 15 and Figures 30, 31 and 32 tabulate and show the results of the three test cases for this 20 design variable optimization model. The simulated temperature profiles for the 20 design variables model were the same for all three test cases as with the 10 design variable model. The only exception will be the heater locations and amount of power input to each cartridge heater.

Test Case 1

The optimum results used all 10 available heaters with a convergence rate 0.1 and 8 heaters for both convergence rates of 0.01 and 0.001. The distribution of the heater locations is similar to the initial heater locations with one or more at the beginning and end of the die (Figure 30). The total power for all three convergence rates was 78.7 watts, roughly 216 watts less than the desired power input of 295 watts (Tables 13).

Test Case 2

The optimum results used 5, 3 and 2 heaters for the convergence rates of 0.1, 0.01 and 0.001, respectively. These heater locations were closely concentrated at heater number 5 and were 10 *mm* apart, which coincided with the allowable clearance of the design constraints (Figure 31). The

total power was roughly 23.4 watts for the three convergence rates which was 62 watts less than the desired power input of 85.4 watts at heater location number 5 (Table 14).

Test Case 3

The optimum results used 2 heaters for convergence rate of 0.1 and 0.01, and 1 heater for the model with the convergence rate of 0.001. The heaters were distributed at the heater location number 10 instead of number 9 where the initial heater was located (Figure 32). The total power was roughly 25.4 watts for the three convergence rates which was 60 watts less than the desired total power of 85.4 watts.

Table 10. Test Case 1 - Power examination with 10 design variables model.

CONVERGENCE RATE	HEATER NO.	POWER (W)	SENSITIVITY ANALYSIS
TEST CASE 1	2	59.0	
	3	59.0	
	5	59.0	
	7	59.0	
	9	59.0	
TOTAL POWER = 295.0			
0.1	1	6.8620	0.71302
	2	6.7597	0.28426
	3	6.0389	-0.44065
	4	4.7363	-0.57996
	5	14.605	-0.05029
	6	12.234	0.13892
	7	10.312	0.14295
	8	9.0223	0.14295
	9	8.5020	0.48219
TOTAL POWER = 79.072 OBJ. FUNCT. VALUE = 122.92			
POWER REDUCED = 215.93 NO. OF ITERATIONS = 7			
0.01	2	5.0891	0.15217
	3	12.358	-0.98176
	4	11.105	-0.28918
	5	15.327	0.59446
	6	9.0545	0.51544
	7	6.6764	-0.44257
	8	6.9789	-0.54682
	9	8.9920	-0.10318
	10	3.2067	0.76395
TOTAL POWER = 78.787 OBJ. FUNCT. VALUE = 43.805			
POWER REDUCED = 216.21 NO. OF ITERATIONS = 19			
0.001	3	19.544	-0.16974
	4	12.934	0.16812
	5	11.359	0.06204
	6	5.4953	-0.15401
	7	8.8654	-0.28899
	8	10.115	0.15655
	9	10.342	0.22600
TOTAL POWER = 78.654 OBJ. FUNCT. VALUE = 26.529			
POWER REDUCED = 216.35 NO. OF ITERATIONS = 38			

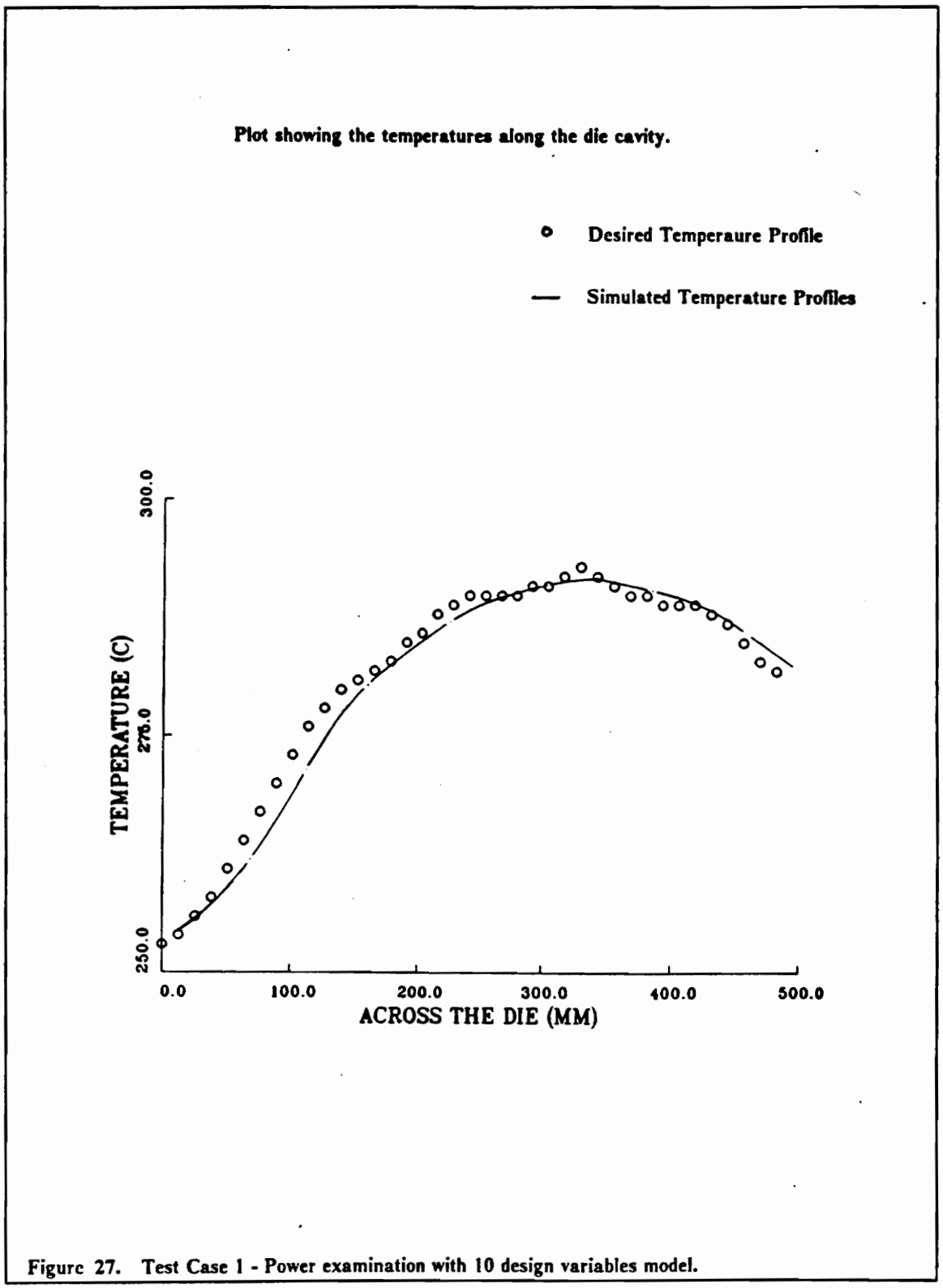

Figure 27. Test Case 1 - Power examination with 10 design variables model.

Table 11. Test Case 2 - Power examination with 10 design variables model.

CONVERGENCE RATE	HEATER NO.	POWER (W)	SENSITIVITY ANALYSIS
TEST CASE 2	5	85.4	
	TOTAL POWER = 85.4		
0.1	5	23.454	0.00007
	TOTAL POWER = 23.454	OBJ. FUNCT. VALUE = 1354.3	
	POWER REDUCED = 61.946	NO. OF ITERATIONS = 3	
0.01	5	23.454	0.00007
	TOTAL POWER = 23.454	OBJ. FUNCT. VALUE = 1354.3	
	POWER REDUCED = 61.946	NO. OF ITERATIONS = 3	
0.001	5	23.454	0.00007
	TOTAL POWER = 23.454	OBJ. FUNCT. VALUE = 1354.3	
	POWER REDUCED = 61.946	NO. OF ITERATIONS = 3	

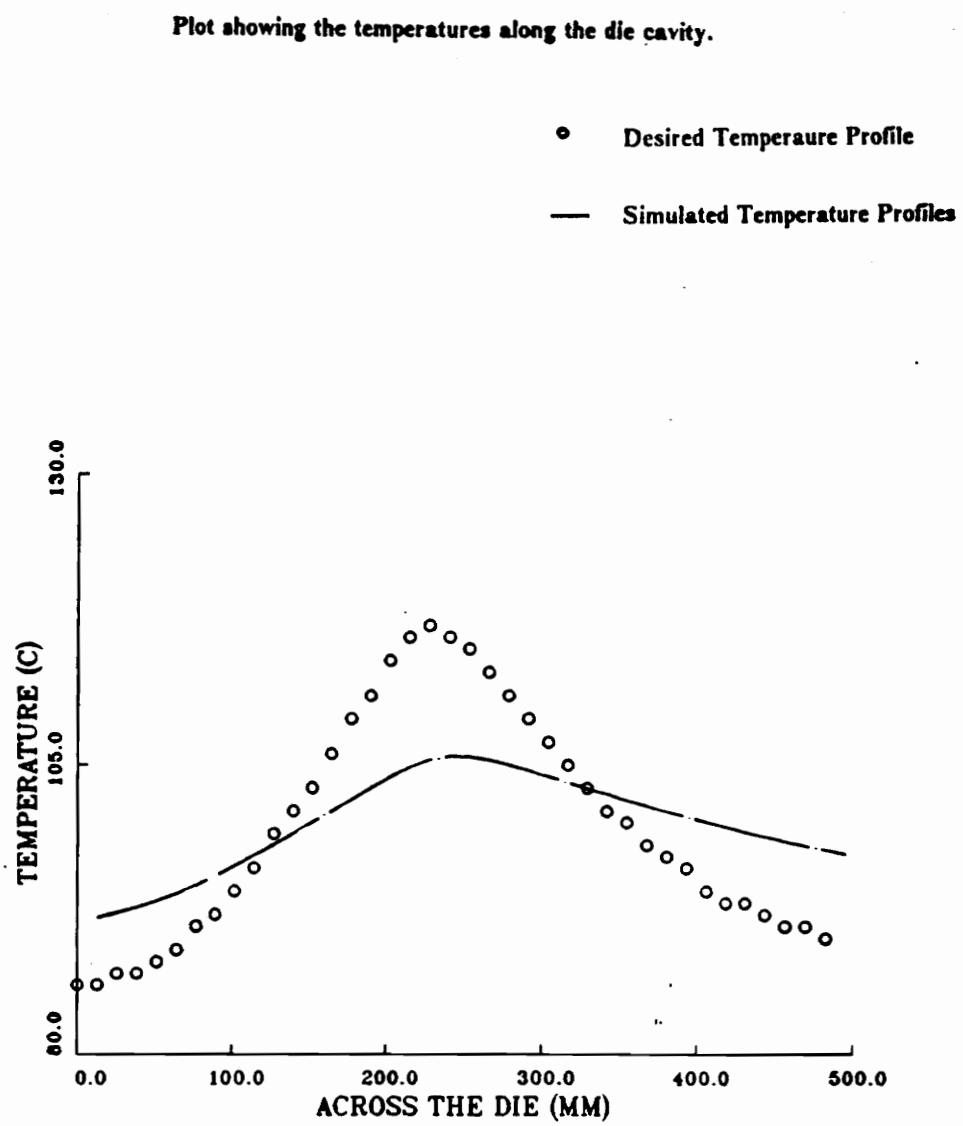

Figure 28. Test Case 2 - Power examination with 10 design variables model.

Table 12. Test Case 3 - Power examination with 10 design variables model.

CONVERGENCE RATE	HEATER NO.	POWER (W)	SENSITIVITY ANALYSIS
TEST CASE 3	9	85.4	
	TOTAL POWER = 85.4		
0.1	10	24.356	-0.88110
	TOTAL POWER = 24.356	OBJ. FUNCT. VALUE = 10297	
	POWER REDUCED = 61.044	NO. OF ITERATIONS = 8	
0.01	10	24.366	-0.14774
	TOTAL POWER = 24.366	OBJ. FUNCT. VALUE = 10297	
	POWER REDUCED = 61.034	NO. OF ITERATIONS = 9	
0.001	10	24.366	-0.14774
	TOTAL POWER = 24.366	OBJ. FUNCT. VALUE = 10297	
	POWER REDUCED = 61.034	NO. OF ITERATIONS = 9	

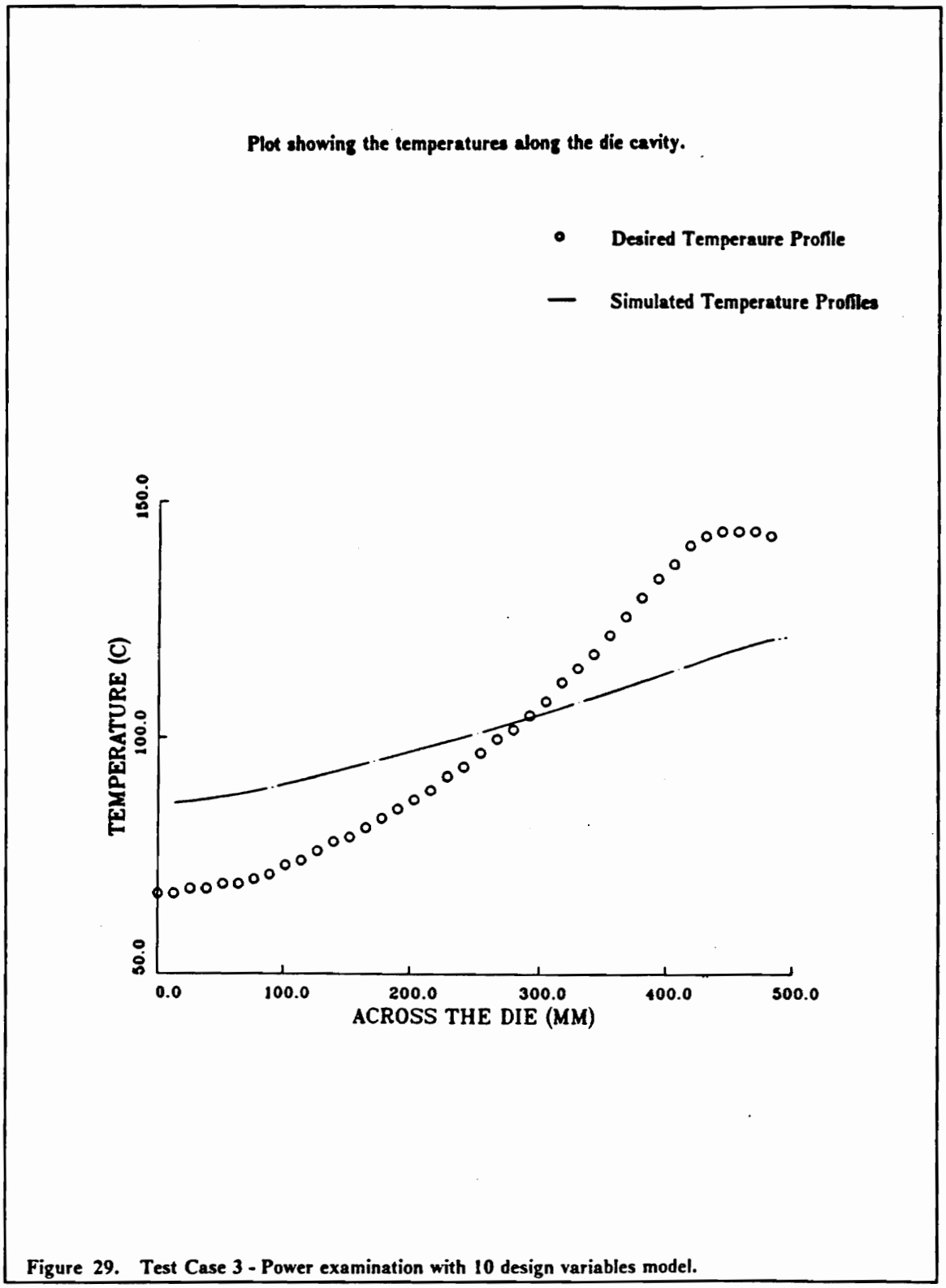

Figure 29. Test Case 3 - Power examination with 10 design variables model.

Table 13. Test Case 1 - Power examination with 20 design variables model.

CONVERGENCE RATE	HEATER NO.	POWER (W)	LOCATION (MM)	SENSITIVITY ANALYSIS
TEST CASE 1	2	59.0	75.0	
	3	59.0	125.0	
	5	59.0	225.0	
	7	59.0	325.0	
	9	59.0	425.0	
TOTAL POWER = 295.0				
0.1	1	5.0770	11.631	5.5542
	2	2.7319	21.631	5.4621
	3	0.0387	31.631	5.3019
	4	0.0114	41.631	5.0762
	5	15.628	140.57	2.0446
	6	15.098	150.57	2.0345
	7	14.870	243.34	1.8238
	8	15.697	330.75	1.8675
	9	15.981	422.43	2.1405
	10	5.6916	443.56	2.1606
TOTAL POWER = 78.674 OBJ. FUNCT. VALUE = 23.504				
POWER REDUCED = 216.33 NO. OF ITERATIONS = 15				
0.01	1	0.3802	99.309	-0.15312
	2	0.1509	109.31	-0.45342
	5	15.683	139.31	-0.86948
	6	15.154	149.31	-0.88075
	7	14.931	242.53	-1.1430
	8	15.755	330.22	-1.1508
	9	16.025	422.91	-0.84126
	10	5.5769	432.91	-0.83368
TOTAL POWER = 78.638 OBJ. FUNCT. VALUE = 21.062				
POWER REDUCED = 216.36 NO. OF ITERATIONS = 25				
0.001	1	0.3793	9.3480	0.48659
	2	0.1503	109.35	0.20079
	5	15.683	139.35	-0.16791
	6	15.155	149.35	-0.16237
	7	14.931	242.82	-0.25720
	8	15.756	329.97	-0.16558
	9	16.025	423.06	0.17661
	10	5.5742	433.06	0.18612
TOTAL POWER = 78.637 OBJ. FUNCT. VALUE = 21.058				
POWER REDUCED = 216.36 NO. OF ITERATIONS = 27				

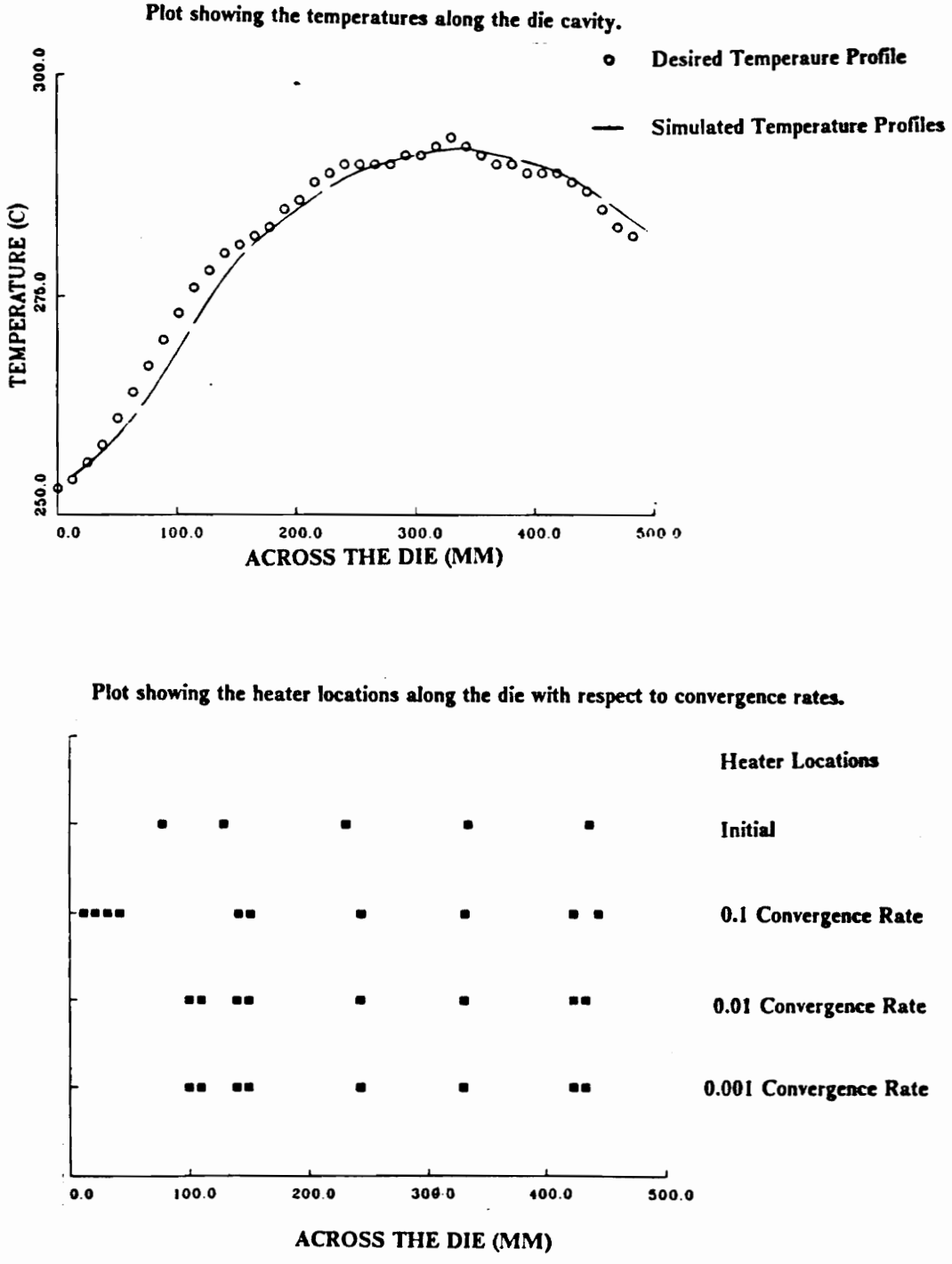

Figure 30. Test Case 1 - Power examination with 20 design variables model.

Table 14. Test Case 2 - Power examination with 20 design variables model.

CONVERGENCE RATE	HEATER NO.	POWER (W)	LOCATION (MM)	SENSITIVITY ANALYSIS
TEST CASE 2	5	85.4	225.0	
TOTAL POWER = 85.4				
0.1	5	16.527	237.78	-0.44325
	6	2.4178	247.78	-0.65304
	7	2.1008	257.78	0.10527
	8	1.5503	267.78	1.7739
	9	0.8334	277.78	4.2368
TOTAL POWER = 23.43 OBJ. FUNCT. VALUE = 1363.2				
POWER REDUCED = 61.97 NO. OF ITERATIONS = 20				
0.01	5	18.875	231.52	0.1804
	6	2.7320	241.52	0.3509
	7	1.8230	251.52	1.3874
TOTAL POWER = 23.43 OBJ. FUNCT. VALUE = 1354.9				
POWER REDUCED = 61.97 NO. OF ITERATIONS = 36				
0.001	5	20.807	234.20	-0.01015
	6	2.6119	244.20	-0.58144
TOTAL POWER = 23.419 OBJ. FUNCT. VALUE = 1351.9				
POWER REDUCED = 61.981 NO. OF ITERATIONS = 46				

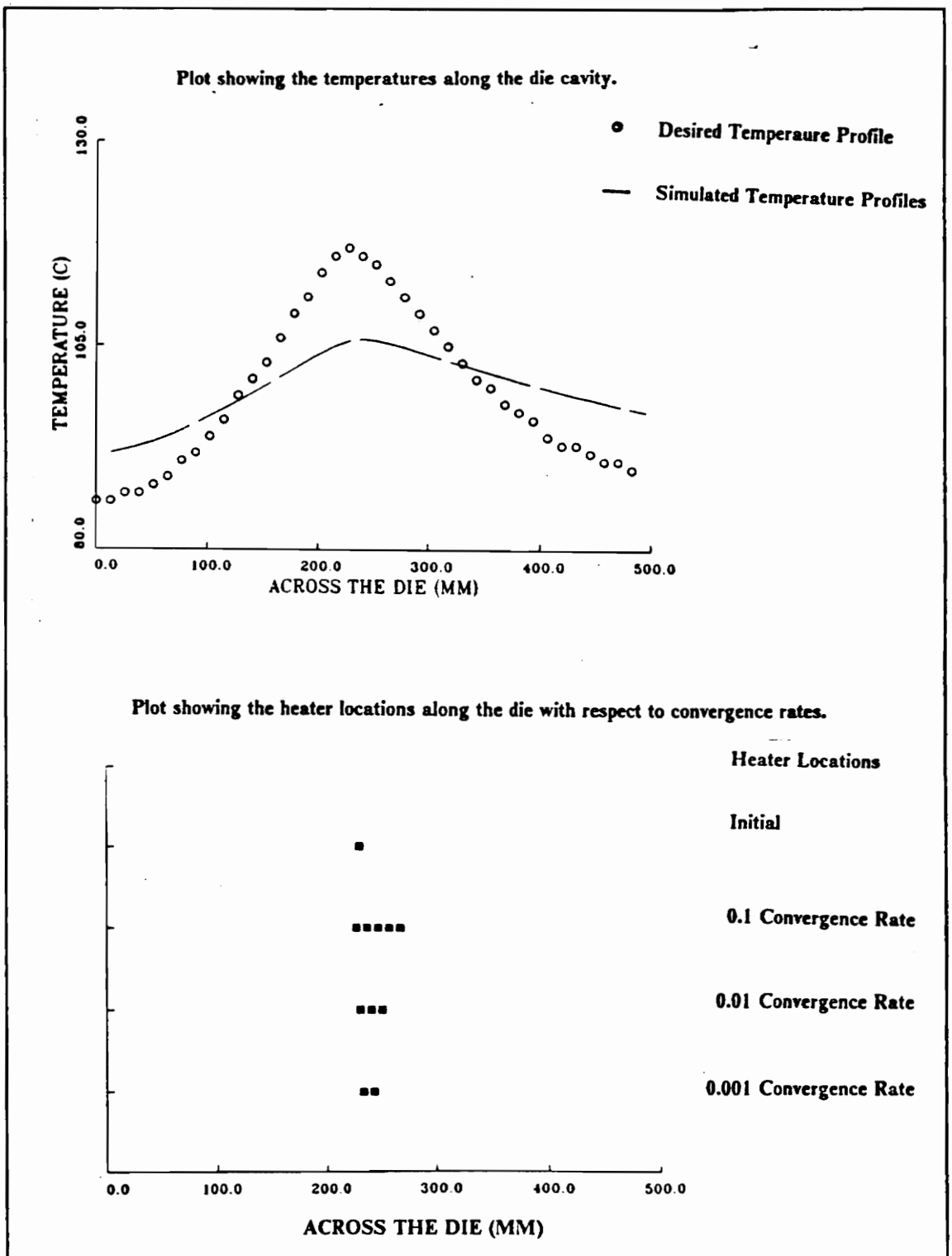

Figure 31. Test Case 2 - Power examination with 20 design variables model.

Table 15. Test Case 3 - Power examination with 20 design variables model.

CONVERGENCE RATE	HEATER NO.	POWER (W)	LOCATION (MM)	SENSITIVITY ANALYSIS
TEST CASE 3	9	85.4	425.0	
	TOTAL POWER = 85.4			
0.1	9	24.184	485.00	0.0467
	10	1.6552	495.00	-1.2379
	TOTAL POWER = 25.839	OBJ. FUNCT. VALUE = 10311		
	POWER REDUCED = 59.561	NO. OF ITERATIONS = 4		
0.01	9	24.184	485.00	0.0467
	10	1.6552	495.00	-1.2379
	TOTAL POWER = 25.839	OBJ. FUNCT. VALUE = 10311		
	POWER REDUCED = 59.561	NO. OF ITERATIONS = 4		
0.001	10	24.494	495.00	-0.5866
	TOTAL POWER = 24.494	OBJ. FUNCT. VALUE = 10280		
	POWER REDUCED = 60.906	NO. OF ITERATIONS = 11		

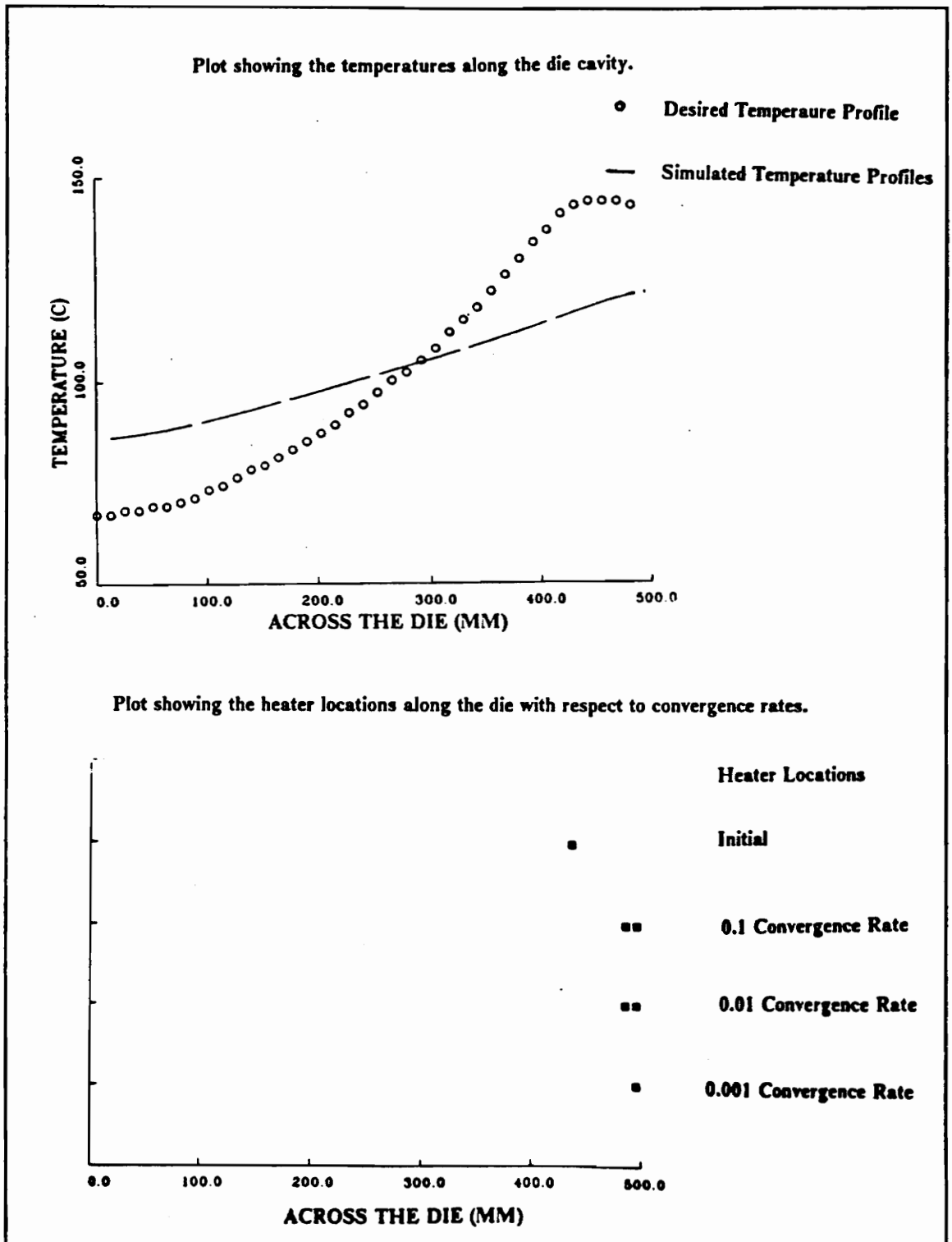

Figure 32. Test Case 3 - Power examination with 20 design variables model.

Chapter VI. Summary and Conclusion

The scope of this study was to design a pultrusion die by determining the heating configuration to generate a given production temperature profile. The heating configuration includes the number of cartridge heaters, power input and location of each cartridge heater. The four investigated parameters, fiber-resin mixture, degree of curing, production temperature profile and pulling speed were found to be interrelated. The production temperature profile was chosen to be the main parameter and can be functionally related to the remaining parameters. A heat transfer model was needed to compute the temperature profile of the laboratory-scale die. This temperature profile was estimated by a 2-D steady-state conduction heat transfer model.

With the heat transfer model as a tool, a design optimization model can be formulated to obtain an optimum heating configuration for a given production temperature profile. Both a finite difference and a boundary element method were investigated and worked well in simulating a production temperature profile. The comparative advantages and disadvantages of these two methods were evaluated for the purposes of supporting the synthesis of the pultrusion die heater configuration. The boundary element method was chosen to solve the problem. The decision was based on the fact that the boundary element method needs less approximation, fewer elements, is a non-iterative solution and the temperature profile can be calculated at any desired point without reconstructing the discrete model or remeshing the domain. The expected temperatures computed

by boundary element method are higher than the finite difference method. It was also found that a distributed source of a small finite dimension (such as the cartridge heater) can be estimated using a concentrated point source. This is much simpler than double integration over the area to model the actual heat source term. Two types of boundary elements were examined, the constant and linear elements. The final model was composed with 86 linear boundary elements. Even though the heat transfer model developed here is only applicable for this particular laboratory-scale die, the code can be easily updated to accommodate changes. The final heat transfer model is a 2-D steady-state conduction heat transfer model with heat sources represented by concentrated point sources.

Using the design optimization method puts the die design one step beyond analysis. The design problem posed for the die design can be stated as follow : for a given temperature profile what is the heating configuration required to generate this desired temperature profile. It also provides a fast and easy way of examining a process by simulation of the system. The optimization method is not only a synthesis tool but also provides an optimum design for the process. Although it took 1 or 2 hours of wall clock time to run a test case on the computer, the obtained results give the users a higher confidence with their system. This 1 or 2 hours is negligible compared the time required to set up and run a real case on a real system.

The nonlinear programming technique successfully synthesized the heating configuration of a given temperature profile. It was found that the optimum design results were dependent on the tightness of the convergence criteria. But these results are possible alternative solutions. Two design optimization programs were developed. Both of them used a 86 linear boundary element model as the conduction heat transfer model. One formulation was developed with 10 design variables and the other with 20 design variables. The 20 design variable program allows the synthesis of the location as well as the input power of the cartridge heaters along the length of the die. Several objective functions were tried. The final objective function was to minimize the sum of square error between the simulated and desired temperature profiles. It was found that the flexible heater location model moved heaters into the same predetermined heater locations used to generate the

temperature profile. The difference between solutions was found in the amount of power input to each cartridge heaters was varied due to the difference in location. The total power input to the die was the same.

The design optimization method also demonstrated that the die was not sensitive to changes in power input to the die in the magnitude of $\pm$ 1 watt. This can be explained from the geometry and mass of the die. The die was constructed from massive steel blocks and has a die blocks to die cavity ratio of 6:1. Therefore, a slight change in power will not change the temperature profile much and at steady state the heat transfer in the die should be stable. With a less sensitive die, the task of controlling the die is eased. The computed temperatures at the nine monitor points are very useful in implementing a feedback control system. These monitor temperatures can be visualized as the desired monitor temperatures because they were computed at the optimum heating configuration for the desired temperature profile. Since the die was found to be insensitive, these monitor temperatures should not change much throughout the process.

Using the results from the numerical heat transfer analysis, it was found that with a four-side-insulated model, the power input to the die can be cut down a factor of 2 to 3 times as compared to two-side-insulated model. This finding should be verified by experimental results.

For this particular die, when comparing the four-side-insulated and two-side-insulated models, the simulated temperature profile can not be matched up with the desired temperature profile. This is due to the design of the die itself. The additional insulation prevents heat loss to the surroundings and forces the heat in the die to be more evenly distributed. This also implies that heat sinks as well as sources are required to control the temperature profile.

In conclusion, the design optimization techniques can be used to design this laboratory-scale die by synthesizing the production temperature profile to produce an optimum heating configuration. Conclusions to the specific objectives are :

1. The temperature profile in a pultrusion process can be simulated using a conduction heat transfer model.

2. The design optimization method successfully synthesized the heating configurations to generate a given temperature profile.

3. The insulated model did cut down the consumption of power input to the die by a factor of approximately 2 to 3 times as compared to the partially insulated model.

Chapter VII. Recommendations

The die design as performed in this study is an initial stage of the pultrusion process design. At this stage, the heating configuration for a given production temperature profile can be synthesized using design optimization techniques. Additional design flexibility can be introduced into the design model to change the geometry dimensions (i.e., the length and cross section) of the die. Changing the size and/or shape of the die will change the heat transfer in the die and will influence the production temperature profile. This recommendation is suggested only if redesigning of a die is desired.

The computed monitor temperatures can be fed back to a controller and the controller will maintain the power input to the cartridge heaters so that the required production temperature profile will always be obtained. This is called a process feedback control system. If desired, an integrated process and properties feedback control system can be implemented. This means that a non-destructive measuring method is required to measure the pultruded properties while the process is still taking place. This information can be fed back to the controller and the controller can decide how to maintain the production temperature profile to produce the desired composite material properties. Since the die itself is relatively insensitive to small changes in input power, the temperatures calculated at the monitor points do not vary much during the process. The conclusion can be drawn that a less sophisticated controller is sufficient for this die. The incoming

raw material might not be uniform and consistent throughout the process. Therefore, the raw material can be fed to the controller and the controller can make the required adjustment on the process in order to produce the product with desired composite properties.

A 3-D heat transfer model of the die should be considered. It can be used to verify the 2-D model and also can provide a way of modeling the die cavity and the material passing through the die cavity. Additional complexities are introduced with a 3-D model, in this case the boundary elements would be surface patches.

The current heat transfer model considered only the heat generated by the heaters. The next logical step is to examine the coupling effect between the heaters and the thermosetting resin reactions. If it turns out that the effect is significant, then this effect must be included in the heat transfer model. Similar to the heaters, the endothermic and exothermic reactions from the resin should be modelled as heat generation terms in the heat transfer model. The endothermic reaction would represent a heat sink in the heat transfer model. The improved model would not only give a better understanding of the heat coupling effect, but the relation between the fiber-resin mixture and degree of curing can be better understood. Finally, the effects of the pulling speed can be analyzed and incorporated into the heat transfer model. The development of a more complete heat transfer model will provide the basis for more representative design trade-offs, which will give a more realistic and reliable simulation of the pultrusion process. This will allow better die design.

Bibliography

[1] Leonard, L. 1988. *Continuous Processing: Pultrusion Sets the Pace.* Advances Composites, July/August 1988, pp. 28-35.

[2] Sumerak, J. E. 1985. *Understanding Pultrusion Process for the First Time.* 40th. Annual Conference, Reinforced Plastics/Composites Institute, The Society of the Plastics Industry, Inc. Jan. 28-Feb. 1, 1985.

[3] McQuarrie, T. S. 1981. *High-Speed Pultrusion Polyester Resins and Process.* U.S. Patent 4,252,696, Feb. 24, 1981.

[4] Price, H. L. and S. G. Cupschalk. 1984. *Pulling Force and Its Variation in Composite Materials Pultrusion.* American Chemical Society, Advances in Chemistry Series, NO. 206 - Polymer Blends and Composites in Multiphase Systems, C. D. Han editor, chapter 18.

[5] Tulig, T. J. 1985. *A Heat Transfer and Reaction Model for Pultrusion.* Presented at American Institute of Chemical Engineers Annual Meeting, Chicago, Illinois, November 1985.

[6] Kershaw, J. A., T. J. Tulig and G. I. Yamashita. 1986. *Pultrusion Processing of Epoxies into Advanced Composite Structures.* Paper NO. EM86-711, Fabricating Composites' 86, The Society of Manufacturing Engineers, Dearborn, Michigan. September 8 - 11, 1986.

[7] Collie, Jeffrey C. and Teck W. Awa. 1989. *Measuring and Predicting Temperature Distribution in a Pultrusion Die.* FIBER-TEX' 89 - Proceedings of the 3rd. Conference on Advanced Engineering Fibers and Textile Structures for Composites. Edited by J. D. Buckley, NASA Conference Publication 3082, Washington D.C.

[8] Holman, J. P. 1986. *Heat Transfer.* 6th. Edition. McGraw-Hill Book Company, New York, U.S.A.

[9] Brebbia, C. A. and J. Dominguez. 1989. *Boundary Elements : An Introductory Course.* Computational Mechanics Publications, Southampton, U.K. and McGraw-Hill Book Company, New York, U.S.A.

[10] Incropera, F. P. and D. P. DeWitt. 1981. *Fundamentals of Heat Transfer.* John Wiley & Sons, Inc., New York, U.S.A.

[11] Sandgren, E. *Structural Design Optimization for Latitude by Nonlinear Goal Programming.* School of Mechanical Engineering, Purdue University, West Lafayette, Indiana.

[12] International Mathematical Subroutine Library. 1987. *Math/Library : FORTRAN Subroutines for Mathematical Applications.* IMSL, INC., Texas, U.S.A.

[13] Moore, R. E. 1975. *Mathematical Elements of Scientific Computing.* Holt, Rinehart and Winston, Inc., U.S.A.

[14] Pina, H.L.G. 1984. *Heat Transfer Applications.* Boundary Element Techniques in Computer Aided Engineering. Edited by C. A. Brebbia, NATO ASI Series, Southampton, U.K., pp. 111 - 125.

[15] Brebbia, C. A. 1980. *Fundamentals of Boundary Elements.* New Developments in Boundary Element Methods. Edited by C. A. Brebbia, Proceedings of the Second International Seminar, University of Southampton, U.K., March 1980. Computational Mechanics Publications, Southampton, U.K., pp. 3 - 33.

[16] Owens-Corning Fiberglas Corporation. 1974. *An Introduction to Fiberglas-Reinforced Plastics/Composites.* Owens-Corning Fiberglas Corporation, Fiberglas Tower, Toledo, Ohio.

[17] Reklaitis, G. V., A. Ravindran and K. M. Ragsdell. 1983. *Engineering Optimization : Methods and Applications.* John Wiley & Sons, Inc., New York, U.S.A.

Appendix A. Heat Transfer Formulation

Heat transfer is the prediction of energy transfer due to the existence of a temperature gradient. The mode of heat transfer that governs the flow of heat from a high temperature region to a low temperature region through a solid medium is called conduction.

A.1. Heat Conduction Formulation

The basic equations of heat conduction in solids can be formulated from an energy balance. The time rate of increase in internal energy per unit volume is equal to the net sum of energy conducted into the unit volume plus heat generated by heat sources in the unit volume. The energy balance equation is [14],

$$\rho c \frac{\partial u}{\partial t} = \nabla q + r \qquad [A.1]$$

where $\rho(x)$ = specific weight,

$c(x)$ = specific heat,

$u(x,t)$ = temperature field (a function of spatial coordinate x and time t),

$q(x,t)$ = heat flux (or heat transfer rate), and

$r(x,t)$ = heat source (a function of spatial coordinate x and time t).

The heat flux is proportional to the normal temperature gradient and in engineering application this relation is known as Fourier's Law of heat conduction [14]

$$q = k\nabla u \qquad [A.2]$$

where k = thermal conductivity.

Substituting Equation (A.2) into Equation (A.1) to get the following expression :

$$\rho c \frac{\partial u}{\partial t} = \nabla(k\nabla u) + r \ . \qquad [A.3]$$

For a steady-state problem, when the temperature is independent of time, Equation (A.3) can be reduced to

$$\nabla(k\nabla u) + r = 0 \ . \qquad [A.4]$$

A.2. Poisson's Equation

Equation (A.4) above assumes that the solid is homogeneous and that isotropic, and the thermal conductivity and the heat source terms are independent of temperature. With these assumptions, Equation (A.4) becomes a linear problem of the form

$$\nabla^2 u = b \qquad [A.5]$$

where $b = \frac{-r}{k}$.

This partial differential equation has the form of Poisson's equation. The Laplacian operator, ∇^2 (i.e., $\nabla^2 = (\frac{\partial^2}{\partial x^2} + \frac{\partial^2}{\partial y^2})$ for the 2-D case), and b is normally known as the source term. By letting $b = 0$ (i.e., no heat sources),

$$\nabla^2 u = 0 \text{ in domain } \Omega. \qquad [A.6]$$

This partial differential equation is a Laplace's equation, which is the homogenous form of Poisson's equation, and governs many engineering problems known as potential problems.

A.3. Boundary Conditions

The boundary conditions associated with this kind of differential equation are :

a) Prescribed boundary temperature

$$u = \bar{u} \text{ on } \Gamma_1 \qquad [A.7]$$

where $\bar{u}$ = the prescribed temperature function, and

Γ_1 = the boundary of the domain Ω where this temperature is enforced.

This is the forced boundary condition.

b) Prescribed flux

$$q = \frac{\partial u}{\partial n} = \bar{q} \text{ on } \Gamma_2 \qquad [A.8]$$

where $\bar{q}$ = the prescribed flux function,

$\frac{\partial u}{\partial n}$ = derivative of the temperature u with respect to the normal, and

Γ_2 = the boundary of the domain Ω where this flux is applied.

This is the natural boundary condition.

c) Mixed Boundary Condition

The mixed boundary condition is the combination of both boundary temperature and flux conditions. Equation (A.9) is the free convection equation at the surface when both boundary temperature and flux are unknowns.

$$-kq = h(u_s - u_\infty) \text{ on } \Gamma_3 \qquad [A.9]$$

where h = the convection coefficient,

u_s = the average surface temperature of the die,

u_∞ = the surrounding temperature, and

Γ_3 = the boundary of the domain Ω where this boundary condition is prescribed.

Appendix B. Finite Difference Formulation

The finite Difference method determines the temperatures at discretized points in the domain. Therefore, the location of these points must first be identified by subdividing the domain into smaller regions. The center of each small region is called the node, except on the boundaries where the nodes are on the outside surfaces of the regions. The entire node system is known as nodal network or mesh [9], Figure B-1. Each node represents a certain region and the temperature computed at each node is the average temperature of that region. These finite difference equations were formulated from an energy balance equation on the cell. For steady-state conditions, there is no energy stored or released from the unit depth mesh. Therefore, the energy equation at a node says that the heat generated at the node must equal the heat conducted and convected out of the mesh. The are two type of nodes, the boundary and the interior nodes. Figure B-2a shows the formulation of an interior node with a square mesh. At the boundary node, appropriate boundary conditions must be applied. Figure B-2b shows the finite difference equation of a boundary node subjected to free convection. Finite difference equations with heat generation terms are easy to formulate. The heat generation term can be simply added to the left hand side of Equation (B.1) on Figure B-2a.

After formulating the finite difference equations, the resulting system of linear equations is solved simultaneously. The Gauss-Seidel iteration method can be used to solve this system of finite

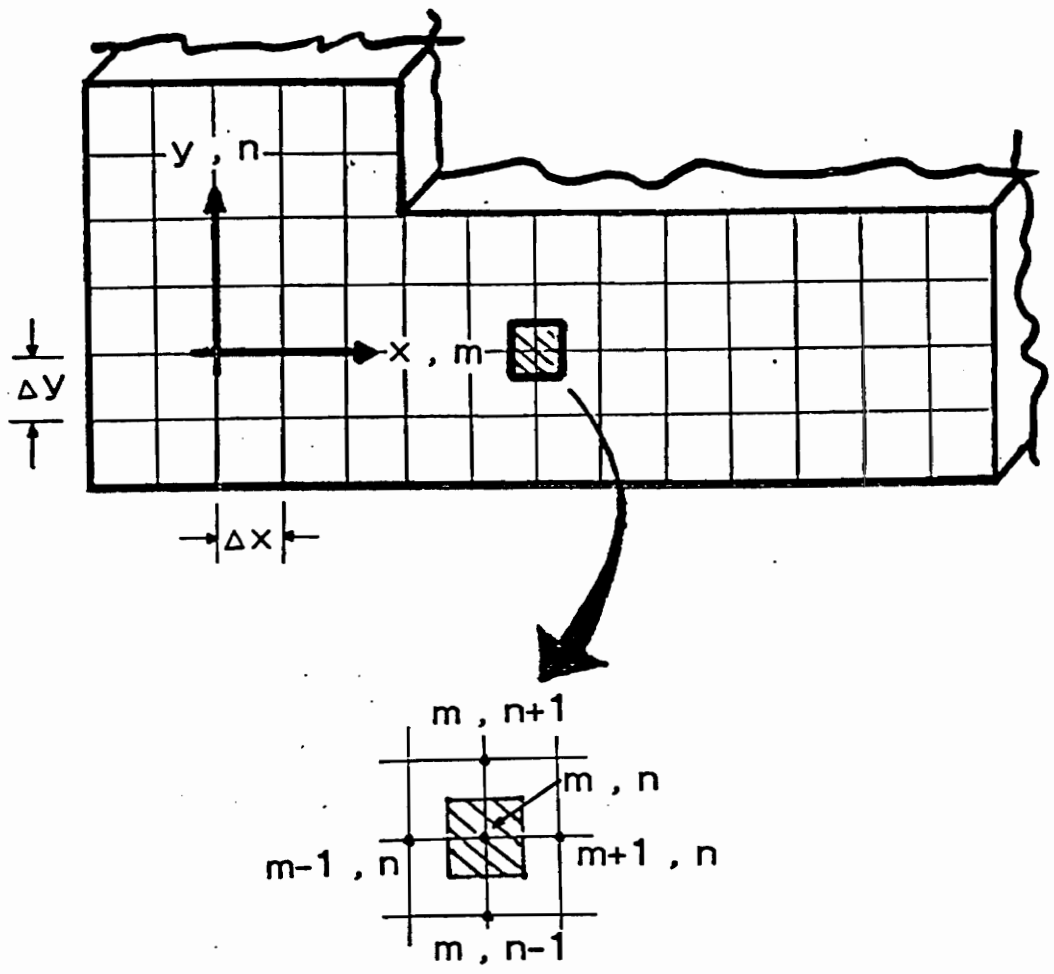

Figure B-1. Definition of a difference mesh.

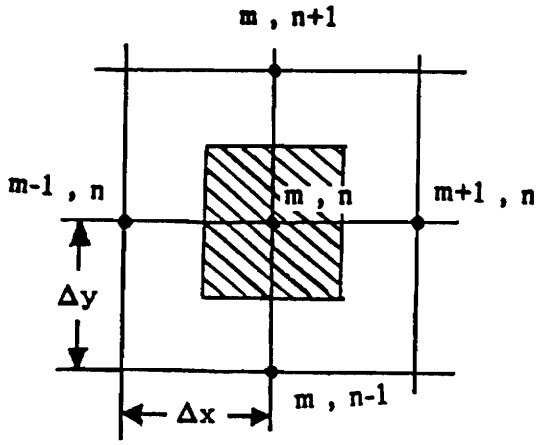

$$T_{m,n+1} + T_{m,n-1} + T_{m+1,n} + T_{m-1,n} - T_{m,n} = 0 \qquad [B.1]$$

a) Interior node

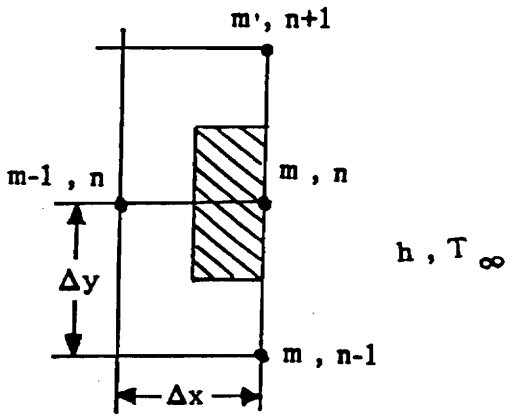

$$(2T_{m-1,n} + T_{m,n+1} + T_{m,n-1}) + \frac{2h\Delta x}{k} T_{\infty} - 2(\frac{h\Delta x}{k} + 2)T_{m,n} = 0 \qquad [B.2]$$

b) Boundary node

Figure B-2. Diagrams and formulas of the boundary and interior nodes.

difference equations [10]. The explicit form of the finite difference equations for each node is written with respect to that node. This method requires a set of initial guess temperature for all of the nodes. The iteration process was repeated until the difference in successive temperatures was less than or equal to a pre-specified convergence value. The temperature profile in the die is produced by inserting heat sources at the appropriate cells The heat source in this model represents power input from the cartridge heater to the appropriate node.

Appendix C. Boundary Element Formulation

The boundary element method is a method of representing a governing partial differential equation in an integral form. The boundary element method involves a transformation of the governing partial differential equation over the domain to an integral equation over the domain and on the boundary and numerical solution for the boundary integral equation.

C.1. Boundary Integral Formulation

There are many ways to reduce the partial differential equation to the boundary integral equation. One method for use is the weighted residual method. Let R be a residual error term defined by $R = \nabla^2 u - b$ [9]. The residual error is the error associated with the solution of the governing partial differential equation. The task here is to seek a weighting function with continuous derivatives up to second order. This differential equation can be solved by applying the property of orthogonality, by forcing R and w to be orthogonal to each other, and requiring the integral of these two functions over the domain Ω to be equal to zero. The objective of this procedure is to minimize the error distribution over the domain. The mathematical expression for this minimization procedure is

$$\int_{\Omega} R w d\Omega = 0 \text{ in } \Omega$$

or

$$\int_{\Omega} (\nabla^2 u - b) w d\Omega = 0 \text{ in } \Omega. \qquad [C.1]$$

This equation also can be rearranged as

$$\int_{\Omega} (\nabla^2 u) w d\Omega = \int_{\Omega} b w d\Omega \ . \qquad [C.2]$$

The integral in Equation (C.1) can be transformed from an integral over the domain to an integral over the boundary by applying Green's Second Identity as shown below

$$\int_{\Omega} (\nabla^2 u) w d\Omega - \int_{\Omega} (\nabla^2 w) u d\Omega = \int_{\Gamma} (\frac{\partial u}{\partial n} w - u \frac{\partial w}{\partial n}) d\Gamma \ . \qquad [C.3]$$

Replacing $\frac{\partial u}{\partial n}$ with q and substituting Equation (C.2) into Equation (C.3).

$$\int_{\Omega} b w d\Omega - \int_{\Omega} (\nabla^2 w) u d\Omega = \int_{\Gamma} (q w - u \frac{\partial w}{\partial n}) d\Gamma \ . \qquad [C.4]$$

C.2. Fundamental Solution

It is required to look for a particular type of weighting function called a fundamental solution which will satisfy the original governing differential equation in a finite linear space. Consider a fundamental solution u^* in an infinite domain that satisfies Laplace's equation and represents the temperature field generated at a source point 'i',

$$\nabla^2 u^* = \Delta^i \qquad [C.5]$$

where Δ^i is a Dirac Delta function which is infinity at $x = x^i$ and zero elsewhere and u^* is the fundamental solution or a free space Green's function for Laplace's equation [15]. This fundamental solution u^* depends only on the distance between two points, the source point 'i' at which the singularity occurred, the Dirac Delta function, and the field point, any point under consideration, which is the variable involved in the differential equation. For a two dimensional domain, the fundamental solution for Laplace's equation is

$$u^* = \frac{1}{2\pi} \ln\left(\frac{1}{r}\right) \qquad [C.6]$$

where r is the distance between the source point 'i' and the field point. The integral of a Dirac Delta function, Δ^i is equal to 1 at the point source location and zero elsewhere. The multiplication of an integral of a Dirac Delta function, Δ^i in domain Ω with another function is equal to the value of the function at the source point 'i',

$$\int_\Omega u(\Delta^i) d\Omega = u^i$$

or

$$\int_{\Omega} u(\nabla^2 u^*)d\Omega = u^i \quad . \qquad [C.7]$$

Replacing u^* as the weighting function w in Equation (C.4) and substituting Equation (C.7) into (C.4)

$$\int_{\Omega} bu^* d\Omega - u^i = \int_{\Gamma} (qu^* - uq^*)d\Gamma$$

or

$$u^i = \int_{\Gamma} uq^* d\Gamma - \int_{\Gamma} qu^* d\Gamma + \int_{\Omega} bu^* d\Omega \quad . \qquad [C.8]$$

Note $q^* = \frac{\partial u^*}{\partial n}$. Splitting Γ into two terms Γ_1 and Γ_2 (i.e. $\Gamma = \Gamma_1 + \Gamma_2$) and applying the boundary conditions into Equation (C.8) gives

$$u^i = \int_{\Gamma_1} \bar{u}q^* d\Gamma_1 + \int_{\Gamma_2} uq^* d\Gamma_2 - \int_{\Gamma_1} qu^* d\Gamma_1 - \int_{\Gamma_2} \bar{q}u^* d\Gamma_2 + \int_{\Omega} bu^* d\Omega$$

or

$$u^i = \int_{\Gamma_1} (\bar{u}q^* - qu^*)d\Gamma_1 + \int_{\Gamma_2} (uq^* - \bar{q}u^*)d\Gamma_2 + \int_{\Omega} bu^* d\Omega \quad . \qquad [C.9]$$

The mixed boundary condition on Γ_3, required in solving heat transfer problem, will be handled differently, in Section C.4.

The above integral equation is only applicable when point 'i' is in the domain. Since the Green's function is the free space (infinite domain) Green's function, there are no boundary conditions

enforced on it. Therefore, a method of reducing the problem from an infinite domain to a finite linear space is required. In order to consider point 'i' on the boundary, Equation (C.8) is rewritten as

$$c_i u^i = \int_\Gamma uq^* d\Gamma - \int_\Gamma qu^* d\Gamma + \int_\Omega bu^* d\Omega \qquad [C.10]$$

before the boundary conditions are applied. Note that c_i is equal to 1 when point 'i' is in the domain. The c_i term depends on the shape of boundary and the general expression is

$$c_i = \frac{\theta}{2\pi} \qquad [C.11]$$

where θ is the internal angle of the shape curve in radians. For a smooth surface, c_i is found to have a value of -1/2. The following shows the concept involved in solving c_i value as shown by Brebbia [9]. For the 2-D case, consider point 'i' is on the boundary but the domain itself is surrounded by a semicircle around point 'i' with a radius ξ which is taken to be near zero. Integration of the first integral on the right hand side of equation (C.8) is -1/2 as shown below

$$\lim_{\xi \to 0} \{\int_{\Gamma_\xi} uq^* d\Gamma\} = \lim_{\xi \to 0} \{ - \int_{\Gamma_\xi} u \frac{1}{2\pi\xi} d\Gamma\} = \lim_{\xi \to 0} \{ - u \frac{\pi\xi}{2\pi\xi} \} = - \frac{1}{2} u^i \qquad [C.12]$$

and Γ_ξ has a value of $\pi\xi$ which is the perimeter of a semicircle. Contrarily, integration of the second integral of the right hand is equal to zero.

$$\lim_{\xi \to 0} \{\int_{\Gamma_\xi} qu^* d\Gamma\} = \lim_{\xi \to 0} \{\int_{\Gamma_\xi} q \frac{1}{2\pi} \ln(\frac{1}{\xi}) d\Gamma\} = \lim_{\xi \to 0} \{q \frac{\pi\xi}{2\pi} \ln(\frac{1}{\xi}) d\Gamma\} = 0 \ . \qquad [C.13]$$

There is no integration required for the third term because it is the integration of the heat source term on the domain. As a result, the c_i term accounts for the effect of the boundary when the point

'i' is on the boundary. For each new source point 'i', there will be a new integral equation. Figure C-1 shows the relation between field points and both boundary and internal source points.

C.3. Element Discretization

Equation (C.10) involves u and q on the boundary and b the source distribution over the domain. There are two kinds of discretization required here. They are the discretization on boundary for the integrals involving u and q, and the discretization over the domain for the integral of b. For the ease of discussion, these two kind of discretizations are separated into two parts: discretization of u and q and discretization of b.

C.3.1. Discretization of u and q

The following is the boundary integral portion of the right hand side Equation (C.10) contains the u and q terms,

$$\int_\Gamma uq^* d\Gamma - \int_\Gamma qu^* d\Gamma \quad . \qquad [C.14]$$

Discretization here involves dividing of the boundary into N distinct segments called elements. Over a single element, the functions of u's and q's can be represented by their nodal values with their associated interpolation functions. For linear elements, the functions of u's and q's can be defined in terms of homogeneous coordinate ζ of the following form:

$$u(\zeta) = \Phi_1 u^1 + \Phi_2 u^2 \quad \text{and} \quad q(\zeta) = \Phi_1 q^1 + \Phi_2 q^2 \qquad [C.15]$$

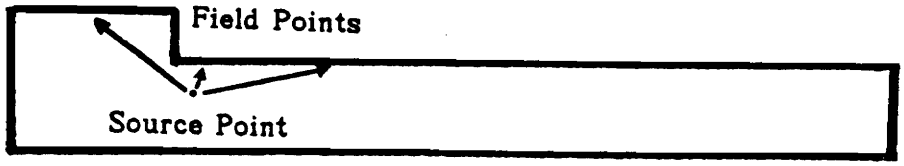

a) Interior Point 'i'

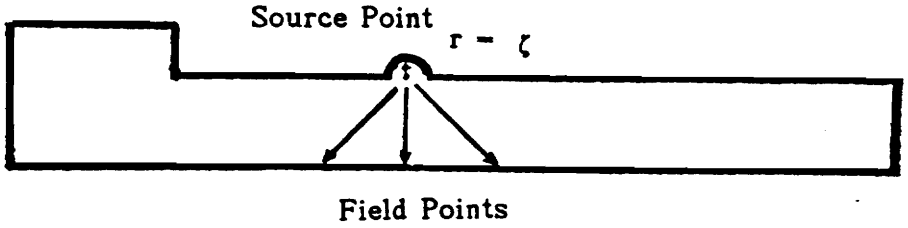

b) Boundary Point 'i'

Figure C-1. Relation between field points and source points.

where Φ_1 and Φ_2 are the two interpolation functions, i.e.,

$$\Phi_1 = (1-\zeta)/2 \quad \text{and} \quad \Phi_2 = (1+\zeta)/2 \quad . \qquad [C.16]$$

Figure C-2a shows the homogeneous coordinate ζ. Substituting Equation (C.15) into Equation (C.14)

$$\int_\Gamma [\Phi_1 u^1 + \Phi_2 u^2] q^* d\Gamma - \int_\Gamma [\Phi_1 q^1 + \Phi_2 q^2] u^* d\Gamma \quad . \qquad [C.17]$$

Equation (C.17) can be rewritten in vector form as

$$\int_\Gamma [\Phi_1 \Phi_2] q^* d\Gamma \begin{Bmatrix} u^1 \\ u^2 \end{Bmatrix} - \int_\Gamma [\Phi_1 \Phi_2] u^* d\Gamma \begin{Bmatrix} q^1 \\ q^2 \end{Bmatrix}$$

or

$$[h_1^{ij} h_2^{ij}] \begin{Bmatrix} u^1 \\ u^2 \end{Bmatrix} - [g_1^{ij} g_2^{ij}] \begin{Bmatrix} q^1 \\ q^2 \end{Bmatrix} \qquad [C.18]$$

where h's are

$$h_1^{ij} = \int_{\Gamma_j} \Phi_1 q^* d\Gamma \quad \text{and} \quad h_2^{ij} = \int_{\Gamma_j} \Phi_2 q^* d\Gamma \qquad [C.19]$$

and g's are

$$g_1^{ij} = \int_{\Gamma_j} \Phi_1 u^* d\Gamma \quad \text{and} \quad g_2^{ij} = \int_{\Gamma_j} \Phi_2 u^* d\Gamma \quad . \qquad [C.20]$$

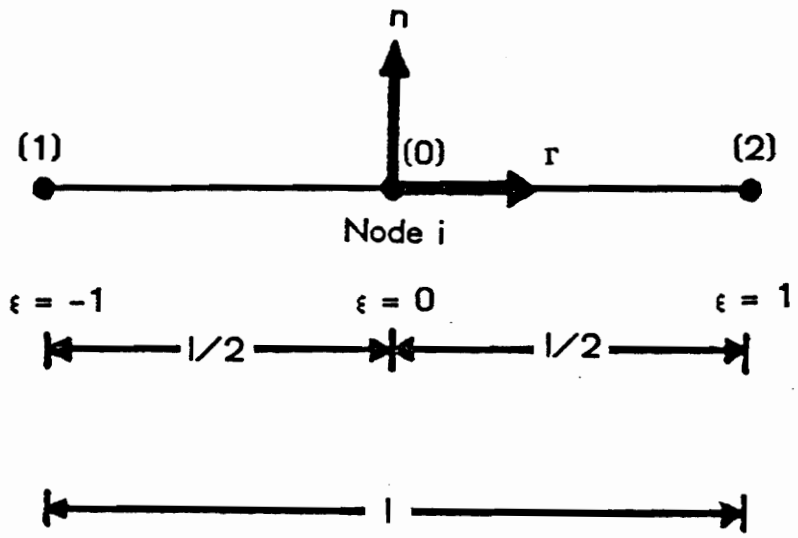

a) Element Coordinate System

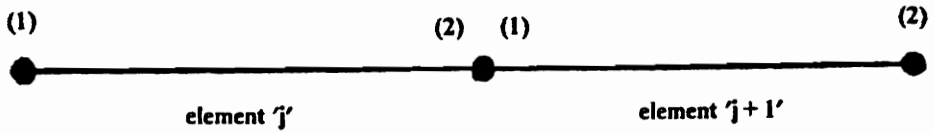

b) Relationship of two adjacent elements

Figure C-2. Element coordinate system and relationship of two adjacent elements.

A linear element is represented by 2 nodes. Node 2 of element 'j' is the same as node 1 of element 'j + 1'. The potential for u^2 of element 'j' is the same as potential for u^1 of element 'j + 1'. But for some boundary points, the fluxes are not unique, especially for the corner points. Therefore, the fluxes are arranged in a $2n$ array (i.e., 2 flux values per element). Figure C-2b shows the relationship of two adjacent elements. The following is the expression of the discretization for the boundary integral of a given field point 'i' is

$$\sum_{j=1}^{N} \hat{H}^{ij} u^j - \sum_{j=1}^{2N} G^{ij} q^j \qquad [C.21]$$

where $\hat{H}^{ij}$ is the sum of h_i^j term of element 'j' plus the h_i^{j-1} term of element 'j-1'. These integrals involve regular and singular integration. For the regular part, when the field points do not coincide with elements containing the source point, these integrals can be evaluated using a Gauss numerical integration scheme. The scheme used in this study is a Gauss 4 points integration scheme. When the field points are coincident with the source points, singular integrals will occur due to the singularity in the fundamental solution. A more sophisticated scheme is necessary and there are many schemes available. The method used in this study is the homogeneous coordination transformation. Detail description on solving the singularity integral with the coordinate transformation scheme is included in the Appendix D.

C.3.2. Discretization of b

The following is the source integration in the right hand side of Equation (C.10).

$$\int_{\Omega} bu^* d\Omega \ . \qquad [C.22]$$

This integral of the heat source term involves integration in the domain and on the boundary. Usually, this type of integration can be done using a Gauss numerical integration scheme having the following form

$$B^i = \int_{\Omega} bu^* d\Omega = \sum_{e=1}^{M} \left(\sum_{k=1}^{r} w_k (bu^*)_k \right) \Omega_e \qquad [C.23]$$

where $e =$ the different cells,

$M =$ the total number of cells in domain Ω,

$w_k =$ the integration weights,

$r =$ the number of Gauss points used, and

$\Omega_e =$ the area of the cell e.

The script 'i' designates a boundary node and B^i is the result of the heat source distribution on the boundary node 'i'. The process of integrating this type of boundary and domain integral can be very difficult especially when the heat source term, b is in the form of a complex function. If b is a simple function such as a concentrated point source, then no numerical evaluation of the integral b over the domain is required. For a single concentrated point source at internal point 'l', b can be represented by

$$b = P^l \Delta^l \qquad [C.24]$$

where P^l is the magnitude of the point source at internal point 'l' and Δ^l is the Dirac Delta function having the integral value of 1 at the point 'l' and zero elsewhere. Substituting Equation (C.24) into Equation (C.23) gives

$$B^l = \int_{\Omega} P^l \Delta^l u^* d\Omega = P^l u^{*l} \qquad [C.25]$$

where u^{*l} is the value of the fundamental solution applied at point 'l'. Therefore, for any number of M concentrated point sources at internal point 'l', the integration of the source over the domain yields the simple summation

$$B^l = \sum_{l=1}^{M} P^l u^{*l} \quad . \qquad [C.26]$$

C.3.3. Element Discretization formulation

The following expression results from combining the discretized elements together

$$c_i u^l = \sum_{j=1}^{N} \hat{H}^{ij} u^j - \sum_{j=1}^{2N} G^{ij} q^j + B^l$$

or

$$-c_i u^l + \sum_{j=1}^{N} \hat{H}^{ij} u^j + B^l = \sum_{j=1}^{2N} G^{ij} q^j \quad . \qquad [C.27]$$

Assuming the fundamental solution is applied at each node successively (i.e. point 'i' can vary from 1 to N), a system of equation can be obtained. Equation (C.27) can be rearranged as

$$\sum_{j=1}^{N} H^{ij} u^j + B^i = \sum_{j=1}^{2N} G^{ij} q^j \qquad [C.28]$$

where H^{ij} is defined as $\{ \hat{H}^{ij}$ when $i \neq j$ else $\hat{H}^{ij} - c_i$ when $i = j \}$.

This equation also can be written in the matrix form

$$HU + B = GQ \qquad [C.29]$$

where G is an $N \times 2N$ matrix and H is an $N \times N$ matrix and U is a vector of length N and Q is a vector of length $2N$. B is a vector of length N and the components of the G and H matrices and B vector are all known coefficients. As long there is only one unknown per node after the boundary conditions are applied, Equation (C.29) can be rearrange into a general linear form

$$AX = F \qquad [C.30]$$

where X is an N vector of unknowns u and q, A is a $N \times N$ matrices of the G and H coefficients of the unknowns u and q boundary values and F is the product of known u and q values with the corresponding coefficients of the G and H matrices plus the B term.

C.4. Applying Mixed Boundary Conditions

The expression for the free convection boundary condition (i.e., Equation (C.9)) needs to be rearranged and substituted into Equation (C.29). First, solve for U_s

$$U_s = U_\infty - \frac{k}{h} Q \qquad [C.31]$$

and substitute Equation (C.31) into Equation (C.29) for the appropriate U components.

$$H[U_\infty - \frac{k}{h} Q] + B = GQ$$

or

$$HU_\infty + B = [G + \frac{k}{h} H]Q \quad . \qquad [C.32]$$

Designate $\hat{G} = G + \frac{k}{h} H$. Therefore Equation (C.29) can be written as

$$HU_\infty + B = \hat{G}Q \quad . \qquad [C.33]$$

This means that for a boundary element involving a free convection boundary condition, U_∞ the surrounding temperature is known and Q the heat flux is unknown. Replacement of G with $\hat{G}$ is required. With this convention, the boundary element formulation can handle three type of boundary conditions: u prescribed, q prescribed and mixed.

C.5. Internal Points Calculation

Once the unknown u and q boundary values are computed by Equation (C.29), the values at internal point 'i' can then be calculated using Equation (C.27) with $c_i = -1$ for internal point 'i'. The resulting equation is

$$u^i = \sum_{j=1}^{2N} G^{ij} q^j - \sum_{j=1}^{N} \hat{H}^{ij} u^j - B^i \quad . \qquad [C.34]$$

The two integrals are computed using the same techniques except the fundamental solution is acting on internal point 'i'. No singularity is involved in these internal points calculations.

Appendix D. Singularity Integration

The following is a short development describing the singularity integration performed on the singular integrals of the G and H matrices as derived in Section C.3.1. In the boundary element analysis, $\hat{H}^{ii}$ term is equal to zero because the normal to the boundary, n, and the element coordinate are always orthogonal to each other.

$$h_1^{ii} = \int_{\Gamma_i} \Phi_1 q^* d\Gamma = \int_{\Gamma_i} \Phi_1 \frac{\partial u^*}{\partial r} \frac{\partial r}{\partial n} d\Gamma = 0 \ . \qquad [D.1]$$

A similar result is obtained for the h_2^{ii} term. As a reminder, Φ's are the interpolation functions.

The integral G^{ii} requires a special integration scheme.

$$g_1^{ii} = \int_{\Gamma_i} \Phi_1 u^* d\Gamma = \frac{1}{2\pi} \int_{\Gamma_i} \Phi_1 \ln(\frac{1}{r}) d\Gamma \ . \qquad [D.2]$$

The homogeneous coordinate transformation scheme is employed to remove the singularity that occurs in Equation (D.2) above. The element coordinate is changed to a homogeneous coordinate ζ from -1 to +1 (see Figure C-2a on Appendix C) and Equation (D.2) is rewritten as

$$g_1^{il} = \frac{1}{2\pi}\int_{-1}^{1} \Phi_1 \ln(\frac{1}{r})\frac{J(\zeta)}{2}d\zeta \qquad [D.3]$$

where $J(\zeta)$ is an one-dimensional Jacobian scalar, i.e. a differential length for derivative of Γ with respect to ζ

Make the following substitution for $\ln(\frac{1}{r})$

$$\ln(\frac{1}{r}) = \ln(\frac{1}{\hat{r}}) + \ln(\frac{\hat{r}}{r}) \quad . \qquad [D.4]$$

Rewrite Equation (D.3) as

$$g_1^{il} = \frac{1}{2\pi}\int_{-1}^{1} \Phi_1 \ln(\frac{\hat{r}}{r})\frac{J(\zeta)}{2}d\zeta + \frac{1}{2\pi}\int_{0}^{1} \Phi_1 \ln(\frac{1}{\hat{r}})J(\zeta)d\hat{\zeta} \quad . \qquad [D.5]$$

The first term on the right-hand side of Equation (D.5) is a regular integral which can be calculated numerically using Gaussian quadrature rules with $\Phi_1 = (1-\zeta)/2$ and $\hat{r} = (1+\zeta)/2$. The second term on the right-hand side of Equation (D.5) is a singular integral and it can be calculated numerically using logarithmic Gaussian quadrature rules with $\hat{r} = \hat{\zeta}$ and $\zeta = 2\hat{\zeta} - 1$ on the interval [0,1] with the singularity at $\hat{\zeta} = 0$. The g_2^{ij} term can be evaluated numerically using the same scheme as g_1^{il} with appropriate substitution of $\Phi_2 = (1+\zeta)/2$ for Φ_1 term.

Appendix E. Design Optimization Formulation

A design optimization method is highly dependent on mathematical modeling formulations which frequently rely on numerical method for solution. Iterative procedures are required to solve for the numerical solution.

E.1. Standard Design Optimization Model

The standard design optimization model is to find an n-vector $X = (x_1, x_2, ..., x_n)$ design variables to minimize an objective function of the form

$$f(X) = f(x_1, x_2, ..., x_n) \qquad [E.1]$$

subject to m_e equality constraints

$$g_j(X) \equiv g_j(x_1, x_2, ..., x_n) = 0 \quad \text{for} \quad j = 1 \text{ to } m_e \qquad [E.2]$$

and the m_i inequality constraints

$$g_j(X) \equiv g_j(x_1, x_2, \ldots, x_n) \geq 0 \quad \text{for} \quad j = m_e + 1 \text{ to } m \ . \qquad [E.3]$$

There will be a total of $m = m_e + m_i$ constraints. The design variables are subject to a bound of $x_{il} \leq x_i \leq x_{iu}$ where x_{il} and x_{iu} are the lower and upper bounds for the design variables x_i. The number of independent equality constraints m_e, must be less than the number of the design variables n, otherwise, the system of equations is overestimated. This can happen either due to the existence of dependent constraints or an inconsistent formulation. The redundant constraints due to linearly dependency can be easily resolved, but the formulation inconsistency will require more caution. If the number of equality constraints is equal to number of design variables, then this is not a design optimization problem, instead it is a problem of solving a system of equations . There is no restriction on the number of the inequality constraints m_i. Due to the formulation of the inequality constraints "$\geq$", the constraint is said to be active when the equality is satisfied. Scaling the objective and constraint functions is often important to the success of the problem formulation. Scaling will only change the objective and constraint values but not the optimum design results.

E.2. Optimization Searching Scheme

There are several methods developed to search for the optimum design for a nonlinear programming problem. They are the linearization of the problem, sequential linear programming, successive quadratic programming, constrained steepest descent method, constrained Quasi-Newton Methods and others [17]. The code developed in the IMSL library is based on a successive quadratic programming method.

This method requires that all the functions involved are continuously differentiable so that quadratic approximation of Lagrangian functions and linearization of the constraints can be done [12]. The general form is to minimize

$$\frac{1}{2} d^T B_k d + \nabla f(x_k)^T \qquad [E.4]$$

subject to

$$\nabla g_j(x_k)^T d + g_j(x_k) = 0 \quad \text{for} \quad j = 1 \text{ to } m_e \qquad [E.5]$$

$$\nabla g_j(x_k)^T d + g_j(x_k) \geq 0 \quad \text{for} \quad j = m_e + 1 \text{ to } m \qquad [E.6]$$

bounded by

$$(x_l - x_k) \leq d \leq (x_u - x_k) \qquad [E.7]$$

where B_k is a positive definite approximation of the Hessian. By definition, the problem must be convex and a unique global solution must exist. The x_k is the current iterate and d_k is the current iterate solution. The next x_{k+1} value is determined by a line search of the form of

$$x_{k+1} = x_k + \lambda d_k \quad \text{where} \quad \lambda \in (0,1] \ . \qquad [E.8]$$

The iterative procedure will be terminated once the objective function reached a certain convergence value.

Vita

The author, Teck Wah Awa was born in Seremban, Negeri Sembilan, Malaysia on September 23, 1962. He received his Malaysia Certificate of Education in 1979. The author went to Canada in 1980. He attended Park Avenue Academy, Toronto, Ontario, Canada and completed his Ontario Secondary School Honor Graduation Diploma in 1981 and received his Bachelor of Science Degree in Agricultural Engineering in 1985 from University of Guelph, Guelph, Ontario, Canada. In Fall 1986, the author returned to North America and enrolled at Virginia Polytechnic Institute and State University. He graduated with a Master Degree in Agricultural Engineering in June 1988. After working for a short time, he decided to enroll as a graduate student in the Mechanical Engineering Department in January 1989 and finished his Master Degree in Mechanical Engineering in February 1991.